NASA CR-167856
SSS-R-82-5218

ADDITIONAL EXTENSIONS TO THE NASCAP COMPUTER CODE, Volume II

P.R. Stannard
I. Katz
M.J. Mandell

S-CUBED

Prepared for
National Aeronautics and Space Administration
Lewis Research Center

Contract NAS3-22536

NASA CR-167856
SSS-R-82-5218

ADDITIONAL EXTENSIONS TO THE NASCAP COMPUTER CODE, Volume II

P.R. Stannard
I. Katz
M.J. Mandell

S-CUBED

Supported by
AIR FORCE GEOPHYSICS LABORATORY
Hanscom Air Force Base, MA. 01731

Prepared for
National Aeronautics and Space Administration
Lewis Research Center

Contract NAS3-22536

1. Report No. NASA CR-167856	2. Government Accession No.	3. Recipient's Catalog No.
4. Title and Subtitle ADDITIONAL EXTENSIONS TO THE NASCAP COMPUTER CODE, VOLUME II		5. Report Date February 1982 6. Performing Organization Code
7. Author(s) P. R. Stannard, I. Katz, M. J. Mandell		8. Performing Organization Report No. SSS-R-82-5218
9. Performing Organization Name and Address S-CUBED P. O. Box 1620 La Jolla, CA 92038		10. Work Unit No. 11. Contract or Grant No. NAS3-22536
12. Sponsoring Agency Name and Address National Aeronautics and Space Administration Lewis Research Center 21000 Brookpark Road, Cleveland, OH 44135		13. Type of Report and Period Covered Contractor Report 9/9/1980 - 12/22/1981 14. Sponsoring Agency Code 5532

15. Supplementary Notes

Project Manager, James C. Roche, NASA-Lewis Research Center, Cleveland, OH

16. Abstract

This report is concerned with application and validation of the NASCAP (NASA Charging Analyzer Program) computer code. Particular attention is given to comparison of the actual response of the SCATHA (Spacecraft Charging AT High Altitudes) P78-2 satellite with theoretical (NASCAP) predictions. Extensive comparisons for a variety of environmental conditions confirm the validity of the NASCAP model.

A summary of the capabilities and range of validity of NASCAP is presented, with extensive reference to previously published applications. It is shown that NASCAP is capable of providing quantitatively accurate results when the object and environment are adequately represented and fall within the range of conditions for which NASCAP was intended.

Three-dimensional electric field effects play an important role in determining the potential of dielectric surfaces and electrically isolated conducting surfaces, particularly in the presence of artificially imposed high voltages. A theory for such phenomena is presented and applied to the active control experiments carried out in SCATHA, as well as other space and laboratory experiments.

Finally, some preliminary work toward modeling large spacecraft in polar earth orbit is presented. An initial physical model is presented including charge emission. A simple code based upon the model is described along with code test results.

17. Key Words (Suggested by Author(s))	18. Distribution Statement
NASCAP Spacecraft Charging SCATHA Computer Simulation	Publicly available (no restrictions on provision to domestic or foreign requesters)

19. Security Classif. (of this report)	20. Security Classif. (of this page)	21. No. of Pages	22. Price*
UNCLASSIFIED	UNCLASSIFIED	165	

* For sale by the National Technical Information Service, Springfield, Virginia 22161

TABLE OF CONTENTS

TABLE OF CONTENTS (Continued)

TABLE OF CONTENTS (Continued)

LIST OF FIGURES

LIST OF FIGURES (Continued)

LIST OF FIGURES (Continued)

LIST OF TABLES

LIST OF TABLES (Continued)

ACKNOWLEDGMENTS

We would like to acknowledge the cooperation of our colleagues at Air Force Geophysics Laboratory and NASA/Lewis Research Center for providing material used in this report. L. Gedeon and N. J. Stevens performed many of the SSPM simulations discussed in Sections 2.9 and 3.2. Section 2.12, concerning the Helios spacecraft, is based on work performed by A. Rubin and M. Tautz. In addition, figures were provided by J. C. Roche, J. V. Staskus, and C. K. Purvis as noted in the text, and raw SCATHA environment data was provided by A. Rubin, J. Fennel (Aerospace Corporation), D. Nichols and E. Whipple (UCSD), and R. Strangeway (Lockheed).

SUMMARY

This report is concerned with application and validation of the NASCAP (NASA Charging Analyzer Program) computer code. Particular attention is given to comparison of the actual response of the SCATHA (Spacecraft Charging AT High Altitudes) P78-2 satellite with theoretical (NASCAP) predictions. Extensive comparisons for a variety of environmental conditions confirm the validity of the NASCAP model.

A summary of the capabilities and range of validity of NASCAP is presented, with extensive reference to previously published applications. It is shown that NASCAP is capable of providing quantitatively accurate results when the object and environment are adequately represented and fall within the range of conditions for which NASCAP was intended.

Three-dimensional electric field effects play an important role in determining the potential of dielectric surfaces and electrically isolated conducting surfaces, particularly in the presence of artificially imposed high voltages. A theory for such phenomena is presented and applied to the active control experiments carried out in SCATHA, as well as other space and laboratory experiments.

Finally, some preliminary work toward modeling large spacecraft in polar earth orbit is presented. An initial physical model is presented including charge emission. A simple code based upon the model is described along with code test results.

1. INTRODUCTION

This report describes a portion of the work performed by Systems, Science and Software on Contract NAS3-22536, "Additional Extensions to the NASCAP Computer Code". The report covers work in which the NASCAP computer code was used in conjunction with supplementary analytical models to analyze the charging effects of the natural space environment and charged particle emitters on the SCATHA spacecraft and to analyze the combined effects of this environment and of the charged condition of the spacecraft on the scientific instruments of SCATHA. This work is part of a series of analyses designed to assist in the interpretation of the data collected by the SCATHA spacecraft, and to validate and verify the NASCAP computer code as a modeling tool for analysis of spacecraft charging. The development of a validated code for the analysis of spacecraft charging is one of the goals of the joint NASA/Air Force Spacecraft Charging Investigation program.

Much of the material contained in this report was originally prepared for monthly progress reports during the contract year. This document consolidates those reports and includes additional material to provide a unified and comprehensive description of the SCATHA modeling effort. It is assumed that the reader is familiar with the capabilities and general features of the NASCAP computer code, which is described in detail in References 1-3. Reference 4 provides a summary of the capabilities of the NASCAP program. The first description of the SCATHA model was presented at the 1978 Spacecraft Charging Technology Conference[5] and much previous work has been presented in the 1980 annual report, "Analysis of the Charging of the SCATHA (P78-2) Satellite.[6]

The results of the validation study of the NASCAP model using SCATHA data are presented in detail in Chapter 2. This work was presented at the AIAA 20th Aerospace Sciences Meeting, Orlando, FL,

January 11-14, 1982, AIAA-82-0269, and is authored by P. R. Stannard and I. Katz, S-CUBED, La Jolla, CA; L. Gedeon and J. C. Roche, NASA-Lewis Research Center, Cleveland, OH; and A. G. Rubin and M. F. Tautz, Air Force Geophysics Laboratory, Hanscom Air Force Base, MA. In Chapter 3, as a complement to the validation effort, the applicability of the code to realistic charging problems and its limitations are discussed.

Chapter 4 discusses the response of surfaces on SCATHA and other spacecraft to active control by ion and electron beams. A theory is presented which explains surface potential measurements from SCATHA during space charge limited electron beam operations.

In Chapter 5 we report on work carried out modeling the charging of large space structures in polar orbit. A preliminary physical model of charging, including the effects of beam emission, is presented. A simple code designed to implement this model is described, along with test results.

Finally, in Chapter 6 we discuss what conclusions are to be drawn from these studies.

2. VALIDATION OF THE NASCAP MODEL USING SATELLITE DATA

2.1 INTRODUCTION

The NASA Charging Analyzer Program is a computer code designed to model spacecraft charging in a plasma environment of the type encountered at geosynchronous altitudes. The SCATHA (Spacecraft Charging AT High Altitude) (P78-2) satellite was launched in early 1979, specifically to monitor charging activity and material response, and to observe the plasma environment in this region. The wealth of data collected by SCATHA has provided an opportunity to validate the NASCAP model by comparing the observed response of the satellite to NASCAP's numerical simulations. In addition, a simulation has been made of data collected by the Helios satellite. This is discussed in Section 2.13.

In order for a computer model of spacecraft charging to accurately reproduce experimental results at least two conditions must be satisfied:

1. The physical model on which the computer code is based must contain all of the essential processes and mechanisms responsible for spacecraft charging.
2. The values of the input parameters that characterize these physical processes must accurately reflect the situation observed experimentally.

In this chapter we provide an overview of the validation of NASCAP using data collected by SCATHA. We briefly describe the physical model employed by the NASCAP code and then go on to describe in detail the standard techniques used in numerical simulations. We enumerate and discuss each of the simulations carried out, and what conclusions we can draw from them. Finally we summarize the present status of the validation effort and discuss the insights that have been gained into the mechanisms of spacecraft charging as a result of this study.

2.2 THE NASCAP PHYSICAL MODEL

NASCAP and its physical basis have been described at length elsewhere.[1-4] Briefly the model provides for a three-dimensional, finite element representation of a spacecraft within 16 x 16 x 32 cubic cells. The spacecraft is assumed to charge due to the accumulation of electrons and ions from the surrounding plasma, with energies in the 0-50 keV range. Fluxes of particles with energies greater than ~50 keV that are able to penetrate the materials are assumed to be negligible by comparison, and the deposition of charge within spacecraft materials is neglected. Collection is assumed to be orbit-limited. This is a very good approximation for sufficiently convex objects with dimensions much smaller than the Debye length of the ambient plasma.[7] (A typical geosynchronous orbit plasma with a density of 10^6 m^{-3} and a temperature of 1 keV has a Debye length of ~235 m.) In addition to the collection of primary electron and ion currents other surface mechanisms (viz. secondary electron emission, backscatter and photoemission) are also included. State of the art descriptions for the variation of these processes with incident particle energy and angular distribution are incorporated into the model. The most recent set of values for the parameters characterizing these descriptions has been compiled from the literature for many different materials. This same standard set of so-called "Material Properties" is used in all the simulations done under this contract. The distribution of incident particle energies and angles may be specified by choosing from a number of possible representations of the surrounding plasma's spectrum and its angular distribution function. The spectrum may be Maxwellian, double Maxwellian, or described by a set of tabulated spectral data points. The angular distribution function may be isotropic, or a loss-cone/gain-cone type of anisotropic form (i.e., showing depletion or enhancement symmetrically about the magnetic field direction).

NASCAP translates this charge collection algorithm into potentials via a resistive-capacitive electrical model of the

satellite. In addition, NASCAP takes into account the three-dimensional character of the satellite's electric field and the role it can play in limiting the emission of low energy secondary and photoelectrons. Space charge effects within the sheath are neglected however, since the fields due to this effect are negligible by comparison to those due to surface charging.

NASCAP does adequately represent this description of the physical processes responsible for spacecraft charging as confirmed by numerous comparisons with laboratory experiments.[8,9] The question that still remains to be answered is whether the mechanisms incorporated into NASCAP are sufficient to explain charging phenomena observed in space. In the remainder of this paper we describe the NASCAP simulations of SCATHA results that have been made, and discuss what they tell us about the validity of the assumptions built into the NASCAP model for the conditions encountered in space.

2.3 SIMULATION METHODOLOGY

Each of the simulations described below was carried out using the standard set of material properties tabulated in Reference 5. This set represents our best estimates of quantities such as secondary emission yields drawn from the literature. For simulations involving a full model of the SCATHA spacecraft, the "One-grid" model, also described in Reference 5, was used (Figure 2.1). Representations of plasma spectra measured on board SCATHA by the SC9 detector were used in all simulations. These were constructed using the same standard fitting procedures in each case. Both single and double Maxwellian fits were made.

Double Maxwellian fits to SC9 spectra are noticeably better than the single Maxwellian fits. This reflects the deviation of the observed spectra from pure Maxwellian forms. Experimentally observed values and both fits are compared in Figure 2.2 for a Day 87 environment. Moment fitting becomes rather involved for a double

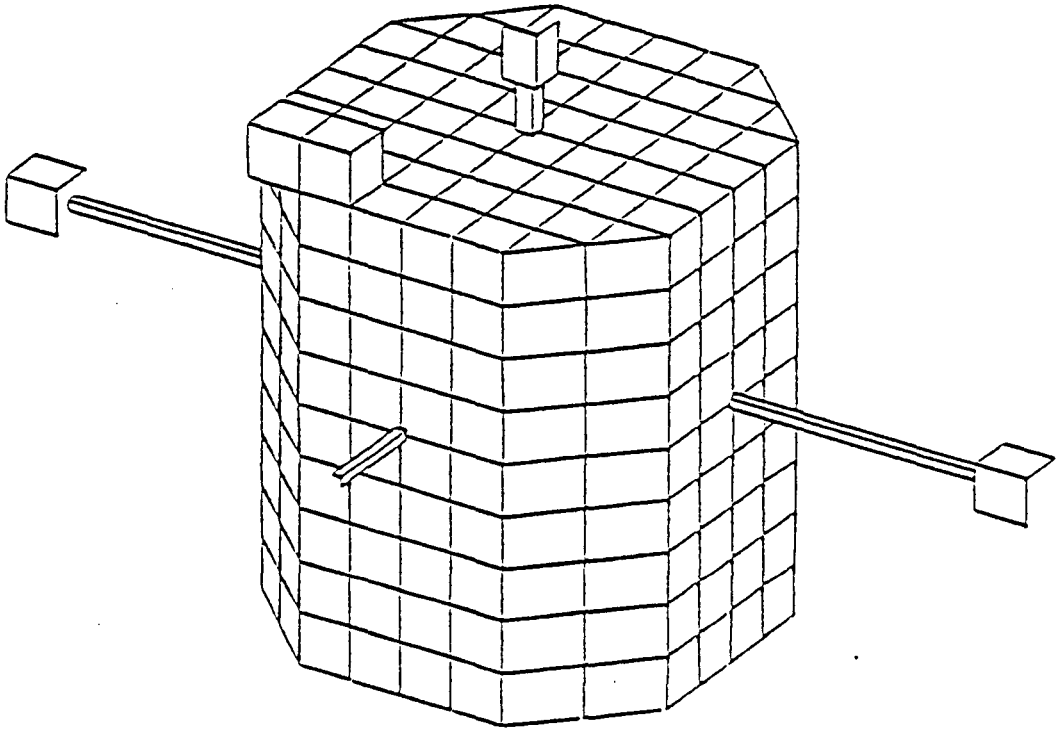

Figure 2.1. SCATHA "One-Grid" NASCAP representation.

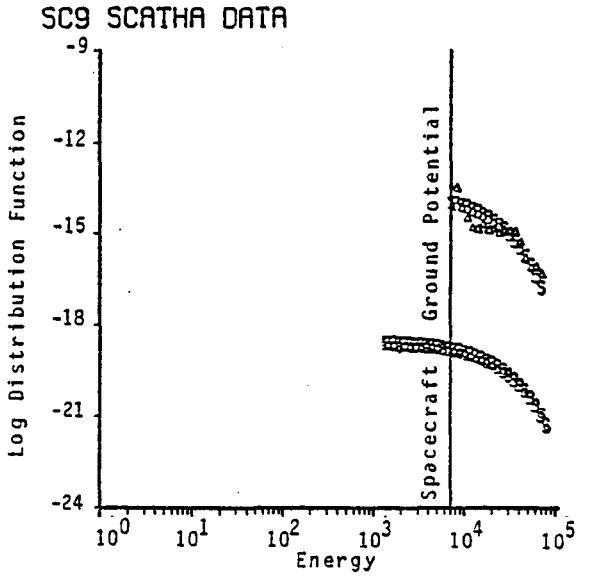

Figure 2.2a. Comparison of single Maxwellian fits (S) with observed ion (Δ) and electron (◇) distribution functions.

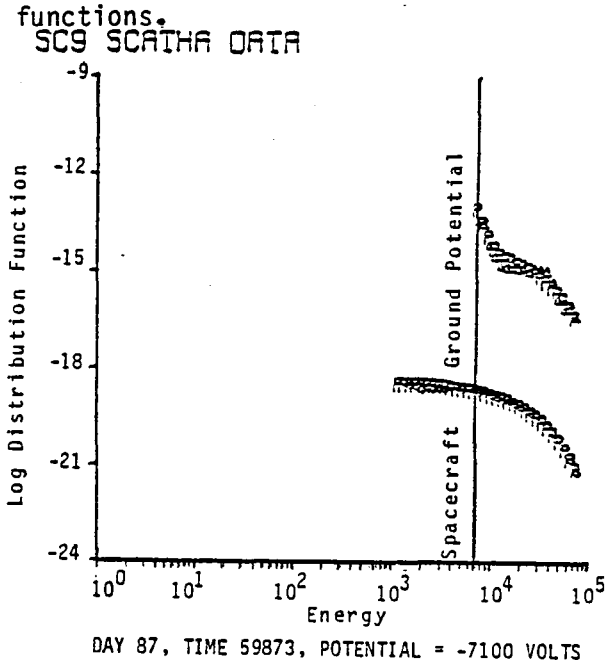

Figure 2.2b. Comparison of double Maxwellian fit (P) with observed ion (Δ) and electron (◇) distribution functions.

Maxwellian when the cutoff and spacecraft potential are non-zero. When the spacecraft is charged, repelled particles with energies at infinity less than the spacecraft potential in eV, never reach the detector and so are not measured. For a negative spacecraft this creates an information "gap" in the electron spectrum observed between zero and the spacecraft potential in eV. Much better fits are obtained using a simple least squares procedure. A range of choices for densities and temperatures, within physically reasonable bounds, are tested until the best fit (in a least squares sense) is found. Representations found in this way have usually been remarkably close fits to experiment. The information gap is filled in simply by extrapolating the fit made to the data actually measured. In many cases (particularly for ions) noise in the low energy channels forced us to ignore data below a cutoff of several hundred volts. A standard value of 500 eV above the energy of the lowest energy particles arriving at the surface was finally chosen as the minimum possible to guarantee physically reasonable parameters in the resulting fits. (Using all of the data sometimes leads to components of the double Maxwellian with densities in the range typical of liquid metals!).

Both single and double Maxwellian fits made using these procedures suffer from a deficiency derived from the original data. The electron densities tend to be as much as a factor of ten higher than the ion densities. This unphysical result is thought to be due to a systematic error in the calibration of the SC9 electron detector.[10] To correct for this the electron densities are normalized to the overall ion density so that the plasma is neutral. This would be a trivial operation if all the ions were actually protons but as shown by Kaye, et al.,[11] O^+ often dominates the ion composition.

If all the incident ions were O^+, the count rate would be reduced by a factor of $(m_O/m_H)^{1/2}$ compared to a proton plasma at the same temperature. The processing of raw SC9 data assumes that all ions are protons and so the ion density is underestimated by the same

factor. This does not affect the calculation of ion fluxes by NASCAP because in translating from distribution functions it too assumes an all proton plasma (i.e., the errors cancel out). However in normalizing the electron densities the underestimation of ion density must be taken into account. If α is the fraction of O^+ in the plasma then the electron densities are normalized by multiplying the initial (large) values by the fraction g:

$$g = \frac{N_{total}^{ion}}{N_{total}^{electron}\,(1-0.75\alpha)}$$

The values of α for the relevant SC9 collection period are estimated from data provided by SC8,[11] which are accurate only to within a factor of two. For periods where no SC8 data has been supplied α is assumed to be 0.5 (a typical value).

The angular distribution of the plasma velocities was assumed to be isotropic in all cases except for the simulation made specifically to test the NASCAP anisotropic formulation, described below.

Using these established techniques for obtaining the NASCAP input parameters a number of comparisons between simulations and observed behavior have been made. We now discuss each of these in detail.

2.4 SIMULATIONS OF SPACECRAFT GROUND POTENTIAL

The SC9 detector on board SCATHA is a high resolution device. It is capable of resolving incoming particles with energies of up to 80 keV, differing in energy by 13 percent or less. A plot of the measured incoming ion spectrum shows a distinct discontinuity at the minimum energy for positively charged particles to reach a negatively charged spacecraft. This minimum is the "structure" potential and is assumed to represent the overall potential of the spacecraft. It is known only to within the resolution of the instrument ($\pm$13 percent).

A series of simulations have been carried out to compare NASCAP predictions for the satellite underlying ground conductor potential with the observed SC9 structure potential. The standard procedure described above was used in all cases. We discuss these in turn.

2.5 DAY 146 (1979): SUNLIGHT CHARGING

The period 1797-3600 UT on Day 146 of the SCATHA mission has been simulated to test the ability of the NASCAP code to predict spacecraft ground potentials in sunlight. During this time the satellite was illuminated by the sun only on the sides, leaving the top and bottom in shadow (Figure 2.1). SC9 data collected were fit to a double Maxwellian form using the procedure described above. Table 2.1 shows that the environment was very stable during the entire period, and so just one set of typical parameters (at 1797 UT) were chosen for the simulation.

The abundant emission of photoelectrons will prevent sunlit surfaces from acquiring a negative charge unless positive fields, due to highly negative neighboring surfaces, inhibit their escape. Surfaces in shadow with an effective secondary yield smaller than unity will begin to charge negatively, however. As the spacecraft rotates such surfaces will charge and discharge as they move periodically in and out of the sunlight. NASCAP is able to model this behavior successfully. If the timescale for charging is much longer than the period, for the purposes of a ground potential calculation, we can average the illumination of each cell over a rotation. For most SCATHA surfaces this is true at one rotation per minute.

With these factors in mind the numerical simulation of ground charging was carried out using the so-called "SPIN" option, which averages the illumination in the way described above. This caused all of the cells on the side of the spacecraft initially to remain neutral. However, the kapton SSPM on the top and the white paint on the bottom remained in shadow and began to charge. As their

TABLE 2.1. DOUBLE MAXWELLIAN FITS TO PLASMA SPECTRA OBSERVED BY SC9 ON DAY 146, 1979, 1797-3600 UT

Time	NE1	TE1	NE2	TE2	NI1	TI1	NI2	TI2
1797	1.8+05	1.4	2.5+05	8.0	1.6+04	0.8	2.2+05	16.0
1828	1.6+05	1.2	3.0+05	8.0	4.8+04	1.4	2.1+05	18.0
1859	1.5+05	0.9	2.5+05	8.0	3.4+04	1.3	1.8+05	16.0
2045	1.2+05	0.7	4.3+05	8.0	1.1+05	2.7	2.0+05	17.0
2510	2.0+05	0.9	2.6+05	8.0	6.3+04	1.9	2.2+05	16.0
2882	1.1+05	0.8	3.2+05	7.0	7.5+04	1.5	2.3+05	15.0
3130	1.0+05	0.9	4.0+05	7.0	8.0+04	2.9	2.3+05	16.0
3378	1.5+05	1.1	6.1+05	8.0	2.6+04	1.3	3.4+05	13.0
3595	1.2+05	0.8	5.6+05	9.0	2.6+04	1.0	3.0+05	14.0

NE1, NE2, NI1, NI2 - First and second component electron and ion densities respectively in m^{-3}.

TE1, TE2, TI1, TI1 - First and second component electron and ion temperatures respectively in keV.

potentials decreased their associated electric fields became sufficiently strong to limit the photoemission from the side cells and they, along with the spacecraft ground, gradually acquired small negative potentials. This mechanism for sunlight charging has been discussed by Mandell.[12] A ground potential of -22 V is predicted. The SC9 ion spectra and SC10 measurements[13] both indicate a ground potential in the -100 V range.

The simulation clearly shows that the NASCAP model is capable of predicting a negative ground potential for the satellite in sunlight, as observed. No free parameters were involved in this comparison. Quantitative agreement is reasonable given the considerable uncertainty in the particle densities measured by SC9. The calculation also shows that the photocurrent in the absence of field limiting exceeds the incident electron current by an order of magnitude (6×10^{-6} A m^{-2} versus 8×10^{-7} A m^{-2}). Hence negative charging in sunlight is a purely three-dimensional electric field related phenomenon.[14] Our understanding of this type of charging behavior is derived primarily from NASCAP studies.

2.6 SIMULATION OF DAY 87 (1979)

In this, and the remaining examples, charging takes place in eclipse. The period chosen on Day 87, 1979 was the eclipse that began at ~59800 sec UT. Some of the double Maxwellian fits to the SC9 data made using the standard procedure are shown in Table 2.2. The entry into eclipse preceded the onset of a magnetic substorm, and as can be seen to some extent from Table 2.2, the environment fluctuated wildly during this time. This conclusion is also supported by the rapid changes in ground potential indicated by both the SC9 ion data and the spectrogram of the period. Because of these rapid changes in environment this period is a difficult case for a comparison between calculated ground potentials and those observed experimentally.

TABLE 2.2. DOUBLE MAXWELLIAN FITS TO PLASMA SPECTRA OBSERVED BY SC9 ON DAY 87, 1979, 59800-62000 UT

Time	NE1	TE1	NE2	TE2	NI1	TI1	NI2	TI2
59813	8.0+05	1.5	7.4+04	7.0	3.5+05	3.5	1.3+05	28.0
59853	2.2+04	5.1	1.2+05	11.0	2.1+04	0.6	3.7+04	16.0
59873	2.1+04	4.7	2.9+05	12.0	3.7+04	1.0	9.6+04	14.0
59933	6.7+05	1.8	3.5+05	9.0	1.1+05	1.7	3.2+05	10.0
59973	1.0+06	2.9	2.5+05	9.0	0	-	5.5+05	4.0
60013	1.5+05	1.6	2.2+05	10.0	7.6+04	2.0	8.0+04	29.0
60493	1.8+05	1.8	2.7+05	7.0	1.0+05	1.8	1.8+05	16.0
61033	1.8+05	3.9	1.0+05	15.0	7.4+04	1.5	1.0+05	19.0
61513	4.4+05	1.7	3.7+05	9.0	2.0+05	2.2	1.7+05	23.0
62033	3.3+05	3.7	1.5+05	9.0	0	-	3.0+05	4.0

SC9 samples the environment over a span of 20 seconds. This is a much longer timescale than that associated with many of the fluctuations in both potential and incident flux. Thus both the potentials indicated by the ion spectra, and the spectra themselves, are only approximate, average impressions of activity over a 20 second period. With this in mind we nevertheless attempted to simulate the dynamic charging behavior of the satellite.

The NASCAP calculation was carried out assuming that all potentials were close to zero upon entry into eclipse. The simulation was begun using the environment observed at 59813 UT, with zero sun intensity. Only after the elapsed time exceeded 40 seconds were the parameters updated to the next environment, measured at 59853 UT. The simulation continued in this way, always looking backwards to the most "recent" environment data measured. The code does this automatically. A comparison of the resulting NASCAP prediction for the spacecraft ground potential and that implied by the ion spectra is shown in Figure 2.3. The numerical results of this "quick look" reproduce the two major charging pulses detected by SC9 but fail to resolve two smaller pulses due to the coarse-grained timesteps taken. NASCAP predicts a more negative initial pulse than indicated by the ion spectra, but there is closer agreement for the second pulse.

The Day 87 simulation shows that given an active substorm environment, both the observed satellite ground potential and the NASCAP predicted response show similar bursts of negative charging and discharging in eclipse. Furthermore there is a definite correlation between the plasma spectrum in the 0-50 keV range and the degree of charging. Figure 2.4 shows a comparison of the SC9 ion spectra potentials and the results of a simulation carried out by Purvis, et al.[15] using standard single Maxwellian fits to the same Day 87 period, and very short computational timesteps. The electron temperatures of these fits correlate quite closely with both the observed and calculated spacecraft potential.

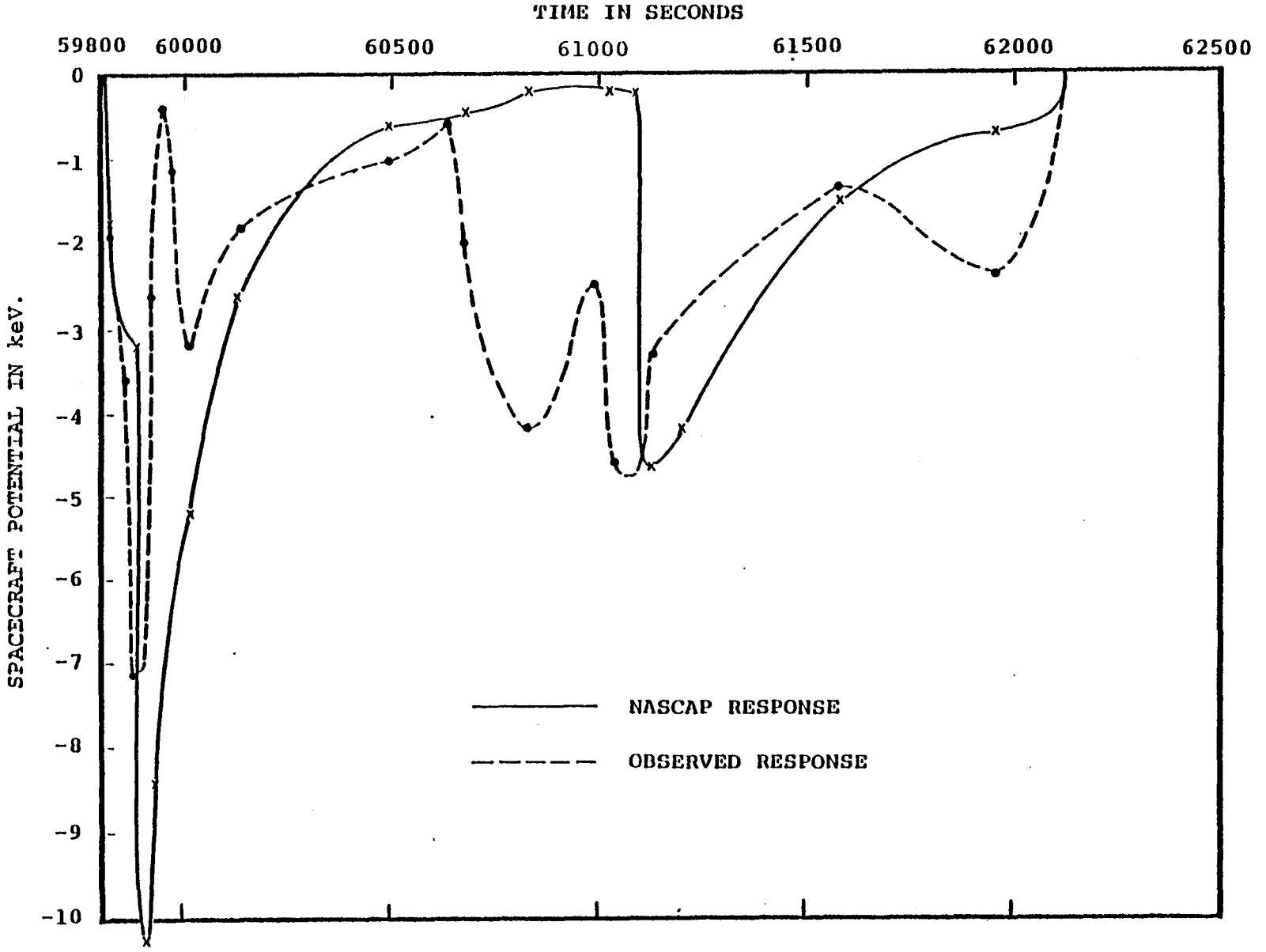

Figure 2.3. NASCAP simulated SCATHA charging response for Day 87 eclipse.

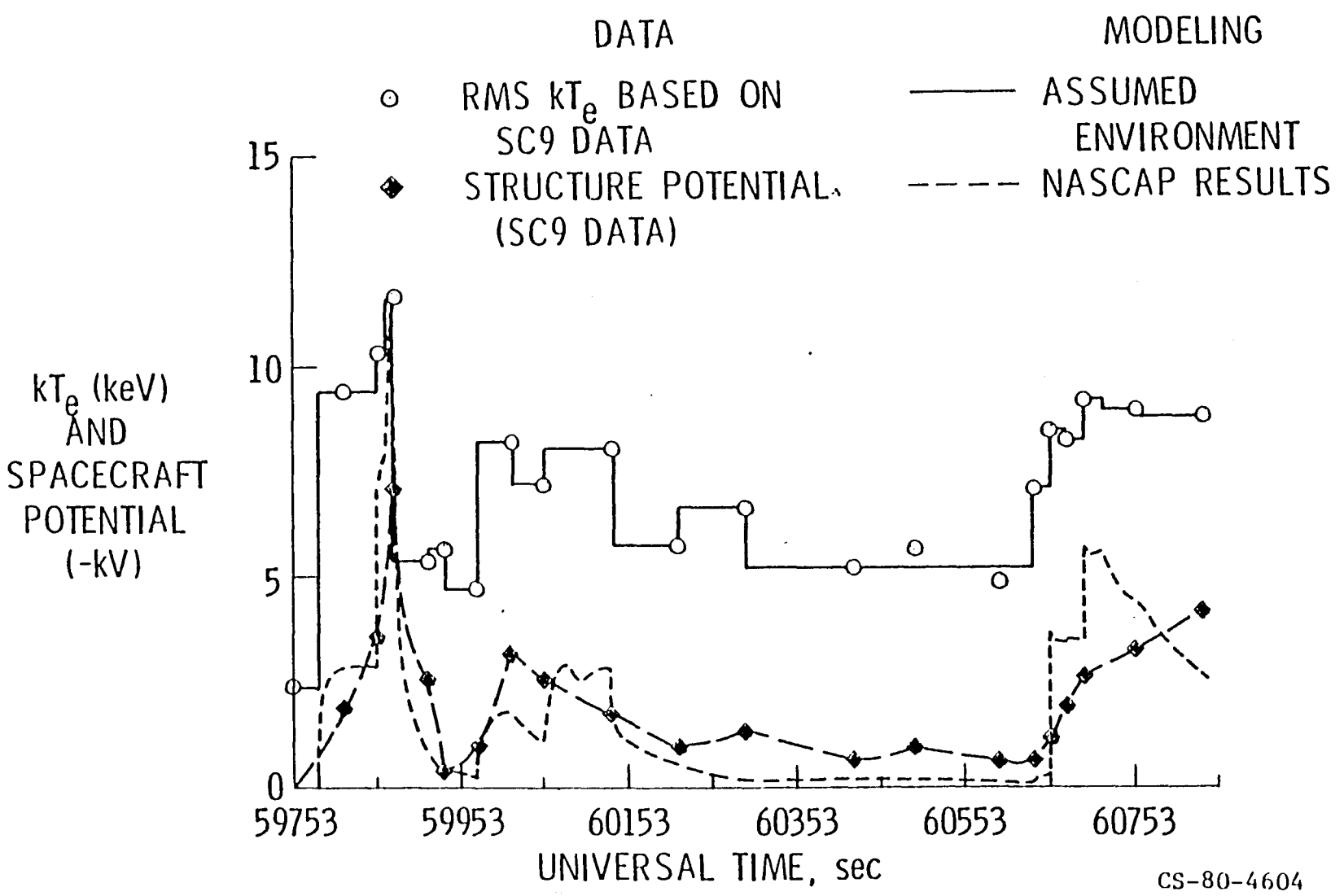

Figure 2.4. Simulation of Purvis, et al. (Reference 15) with single Maxwellian environments.

These results are clear evidence supporting the notion that charging is a surface phenomenon, dominated by the collection of non-penetrating plasma particles with energies below ~50 keV. Quantitative accuracy is again acceptable given the limitation in both the measured spectrum and potentials discussed earlier.

2.7 DAY 114 (1979)

The simulation for the period 25944-26104 UT in eclipse on Day 114, 1979 was carried out in the same way as for Day 87. A comparison of NASCAP predicted potentials and SC9 structure potentials is shown in Table 2.3 and Figure 2.5. Full umbra eclipse begins at ~25950, as shown by the steep climb in structure potential as the surface photoemission current is cut off. After the steep rise the structure potentials settle down in the -4 to -6 kV range. The NASCAP predictions show close agreement: A rapid rise is followed by oscillation. The oscillation is a result of the unnaturally sudden changes made in the plasma spectrum description every 20 seconds. (Nature has the advantage of being able to change the plasma spectrum smoothly.)

Charging on both Day 87 and Day 114 shows similar qualitative behavior. Potentials reached are high, typically in the -5 to -10 kV range. There are rapid fluctuations: The potential changes by many kV in just a few seconds. We characterize this type of behavior as severe charging. NASCAP successfully models this type of charging.

The remaining two periods simulated using NASCAP show a qualitatively different type of charging. This is characterized by negative potentials less than 2 kV and much longer charging timescales, with fluctuations occurring over hundreds of seconds. NASCAP is also able to model this moderate charging behavior. Furthermore, it is able to offer an explanation as to the difference in charging mechanism responsible for the qualitative and quantitative differences between the two cases.

TABLE 2.3. COMPARISON OF STRUCTURE POTENTIALS AND THOSE SIMULATED BY NASCAP FOR DAY 114, 1979

Time (sec)	SC9 Structure Potential (kV)	NASCAP Potential (kV)	Time (sec)
25944	-0.5	0	25950
25960	-2.7	-1.8	25951
25976	-5.4	-3.0	25953
29992	-6.2	-4.2	25994
26008	-5.4	-5.2	26009
26024	-5.4	-3.7	26024
26040	-5.4	-6.8	26041
26056	-5.4	-4.3	26056
26072	-5.4	-7.5	26072
26088	-4.1	-4.8	26088
26104	-3.6	-4.3	26097

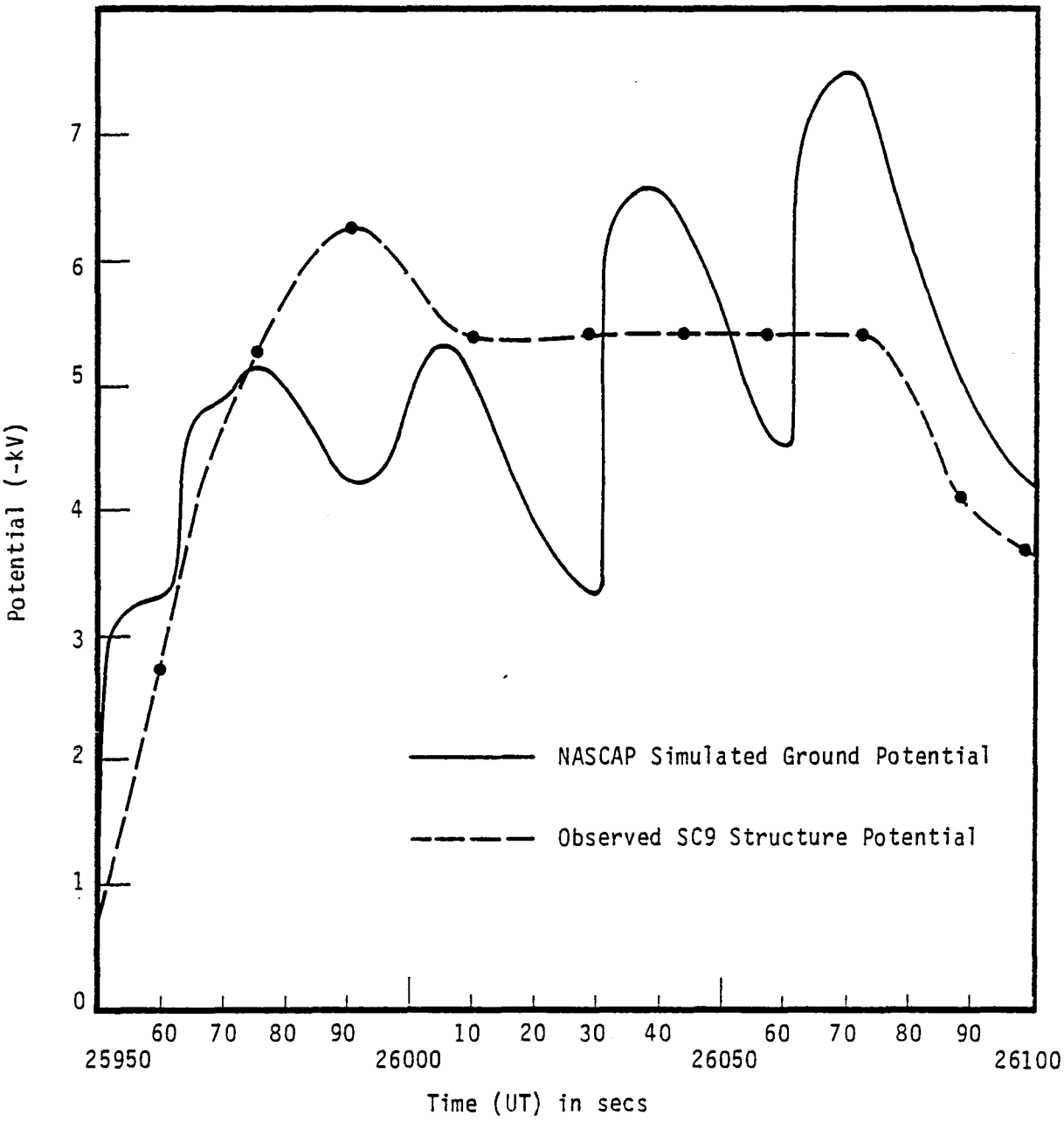

Figure 2.5. Comparison of simulated and observed SCATHA ground potentials during eclipse on Day 114, 1979.

2.8 DAYS 98 AND 272 (1979): MODERATE CHARGING DAYS

Like the period in sunlight on Day 146, the potentials during eclipse on Days 98 and 272 showed considerable stability. Hence, just as for Day 146, no attempt was made to follow the time dependent behavior of the potentials and only equilibrium potentials at fixed times were simulated. Double Maxwellian fits to plasma spectra measured at 44998 sec on Day 98 and 15603 sec on Day 272 were chosen as typical of their respective periods (see Appendix). The NASCAP predicted equilibrium ground potentials are compared with experiment in Table 2.4. The column labeled "one-grid" refers to calculations based on the standard one-grid NASCAP model of SCATHA. Both experiment and calculations agree in indicating moderate charging; however, numerical agreement for the one-grid model is poor. The reason for this, and the reason for the different charging timescales in moderate charging days lies in the mechanism responsible for charging the satellite.

Unlike the two severe charging days (87 and 114) the plasma spectra on moderate days 98 and 272 were not "hot" enough to give an initially negative net current to the solar cell coverglass ("SOLAR"), which covers most of the spacecraft. This means that if all of the spacecraft surface was composed of "SOLAR" the spacecraft would not charge negatively at all. The only reason negative ground potentials are obtained is because the small amount of kapton and white paint on the spacecraft do charge in these environments. The NASCAP calculations show clearly that, as the kapton charges negatively, potential barriers form in front of surrounding "SOLAR" material preventing the escape of the low energy secondary electrons. Hence, the effective secondary yield for "SOLAR" is reduced below unity, so that the net current collected becomes negative, causing the "SOLAR" (and the whole spacecraft) to begin charging. This charging mechanism has been described elsewhere.[16] It is a direct result of the differential charging between surfaces and so occurs on a long (differential charging) timescale. This is because differential

TABLE 2.4. COMPARISON OF NASCAP EQUILIBRIUM POTENTIALS AND OBSERVED VALUES FOR 44998 ON DAY 98 AND 15603 ON DAY 272 (kV)

		One-Grid		Three-Grid	
Day	Observed	Ground	Kapton	Ground	Kapton
98	-1.4	-0.3	-3.2	-1.5	-3.2
272	-1.8	-0.5	-5.9	-2.7	-5.9

charging involves the charging of the large inter-surface capacitances, rather than the smaller capacitance of the whole spacecraft with infinity.[16]

The one-grid model of SCATHA omits realistic representations of the four booms perpendicular to each other in the satellite rotation plane.[6] These booms are composed of alternating bands of platinum and kapton. Such regular arrays tend to charge in a way similar to their most charging component (i.e., kapton).[16] Figure 2.6 shows how important the charging booms are to the electric field structure around the body of the satellite, and hence near the "SOLAR" material. Since the potential reached by "SOLAR" (and the whole spacecraft) depends strongly on the electric field in front of its surfaces, omission of the booms will have a serious effect on the numerical accuracy of any attempt to model charging that depends strongly on 3-D electric field effects ("bootstrap" charging). Conversely omission of the booms is much less important in the "severe" charging case when "SOLAR" (and the whole spacecraft) charge due to an initially negative net incident current, rather than field suppression of low energy emission. To demonstrate this, realistic representations of the booms were added to the standard one-grid model, extending it into three grids. The booms are assumed covered with kapton. The results for this so-called three-grid model is also shown in Table 2.4. As expected, the NASCAP predicted potentials are increased compared to the less field-limiting one-grid model. Agreement with experiment is better though not perfect. As discussed in Reference 16, unless the computational mesh is very fine compared to the object dimensions, exact quantitative agreement cannot be expected for situations involving bootstrap charging. Qualitatively, however, NASCAP is successful in predicting only moderate charging on a long timescale for both Days 272 and 98, and severe charging on a short timescale for Days 87 and 114.

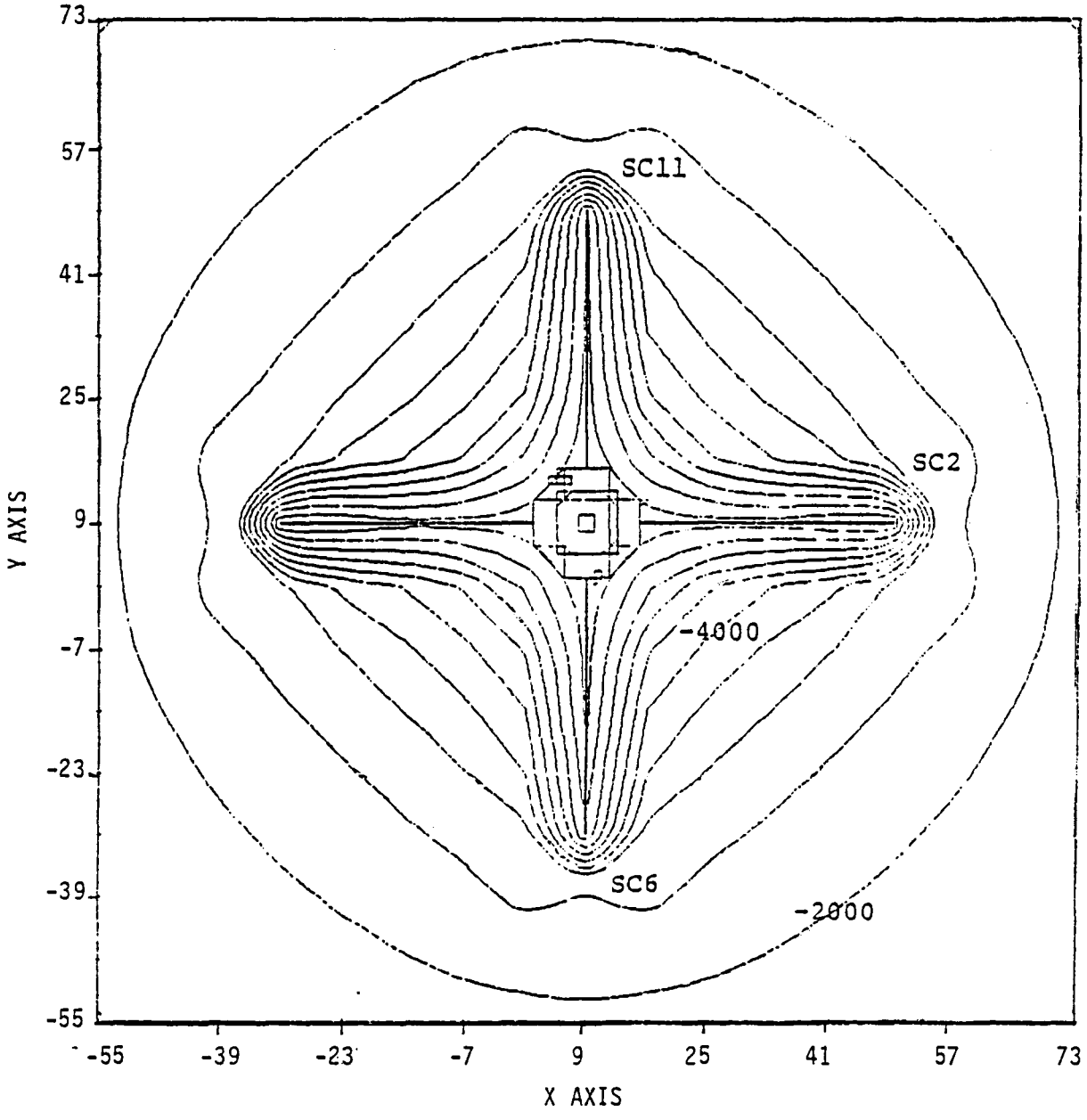

SCATHA charging in eclipse; spacecraft ground = -6200 V;
contour steps = 500 V.

Figure 2.6. SCATHA potential contours.

2.9 DIFFERENTIAL CHARGING OF INSULATING SURFACES

The SCATHA satellite has on board three Satellite Surface Potential Monitors (SSPM's)[17] designed to measure the differential charging of kapton, teflon and quartz cloth. Two of the SSPM's (SC1-1, SC1-2) are on the sides of the spacecraft 180 degrees apart and the third (SC1-3) is on the top. While most of each sample is backed with aluminum, providing strong capacitive coupling to the ground potential, the spot where the insulated potential is actually measured has no backing, and is much more weakly coupled to spacecraft ground. This allows the differential potential monitored to fluctuate on a much shorter timescale than the rest of the sample, and hence to show much wider variations.

The NASCAP simulation of Days 146, 87, 114, 98 and 272 were all carried out using the correct value of the thickness of the kapton and teflon films and assuming a metalized backing. Thus the numerical predictions of the differential potentials refer to the major portion of the sample rather than the small test spot, and show a much slower variation. In the Day 87 case the kapton sample in SC1-1 is predicted to charge gradually to a potential of -1500 volts with respect to spacecraft ground after 900 seconds of charging. The measured differential potential for kapton (SC1-1) on the other hand shows a more rapid climb to ~-2000 V[17] after ~200 seconds.

To simulate properly the SSPM results the value for the thickness of the sample must be increased to reflect the lower capacitance controlling the charging rate of the spot. We have carried out a simulation of the kapton SC1-2 response during the Day 87 eclipse using a model of SC1-2, surrounded by solar cells. A set of material properties for kapton, including effective thickness and dielectric constant, that reproduce laboratory charging experiments were used, along with the same single Maxwellian environments used for the calculation of the ground potential shown in Figure 2.4. The material properties are given in Table 2.5. The results for a

TABLE 2.5. MATERIAL PROPERTIES USED FOR KAPTON SSPM STUDY[15]

	Dielectric Constant	3.0
	Thickness of Patch (m)	0.000127[a]
	Conductivity (mho m^{-1})	3×10^{-15}
	Atomic Number	5
Secondary Emission Properties Ref. 1	Delta max	2.1[b]
	E. max (keV)	0.15[b]
	Range 1. (Å)	71.5[b]
	Exponent 1.	0.60[b]
	Range 2. (Å)	312.1[b]
	Exponent 2	1.77[b]
	Yield for 1 keV Protons	0.455[b]
	Max dE/dx for Protons (keV)	140.0[b]
	Photocurrent (A m^{-2})	2.0×10^{-5}[b]
	Surface Resistivity (ohms)	7.5×10^{12}

Effective Thickness of the Spot[c] = 12.5 x Patch Thickness

NOTES: a. nominal value

b. standard NASCAP value

c. non-NASCAP quantity

simulation of SC1-2 are shown in Figure 2.7. The dynamic charging behavior of the spot is followed very well by the predictions.

Both the electron densities, temperatures, and observed spacecraft potentials were "flared" through the existing data points to give a more smoothly varying environment. (These flared electron environments are shown in Figure 2.8a, b, and c.) The NASCAP predictions for the SSPM currents shown in Figure 2.7 indicate an interesting anomaly. NASCAP predicts a positive leakage current at 180 seconds. This is absent in the data for SC1-2 but does occur (as predicted) for SC1-1. The absence of this feature for SC1-2 is presently unexplained.

These results indicate that given a model of the experiment, material properties and descriptions of the environment, NASCAP can predict differential charging very well, the dynamics as well as the equilibrium values. The behavior of the SSPMs indicated by full SCATHA model simulations is not comparable to the dynamic behavior observed experimentally, but should give accurate estimates of equilibrium potentials. So far NASCAP has been unable to reproduce the anomalous behavior of SC1-3, but its predictions of the remaining SSPM equilibrium potentials have been in reasonable agreement with experiment.

The occurrence of high levels of differential charging in both Day 146 and Day 87 also lends weight to the argument that incident fluxes of high energy particles play only a small part in charge collection. Data from SC3[18] for fluxes of particles with a range of energies measured on Day 87 and Day 146 is compared in Table 2.6. While the currents incident on both days due to particles with energies below 50 keV are of similar magnitude ($\sim 10^{-7}$ A m^{-2}) the higher energy penetrating fluxes observed on Day 146 are lower by almost an order of magnitude than those observed on Day 87. This difference in high energy currents is not reflected in a similar difference in observed potentials, suggesting that the lower energy fluxes do indeed dominate the charging behavior.

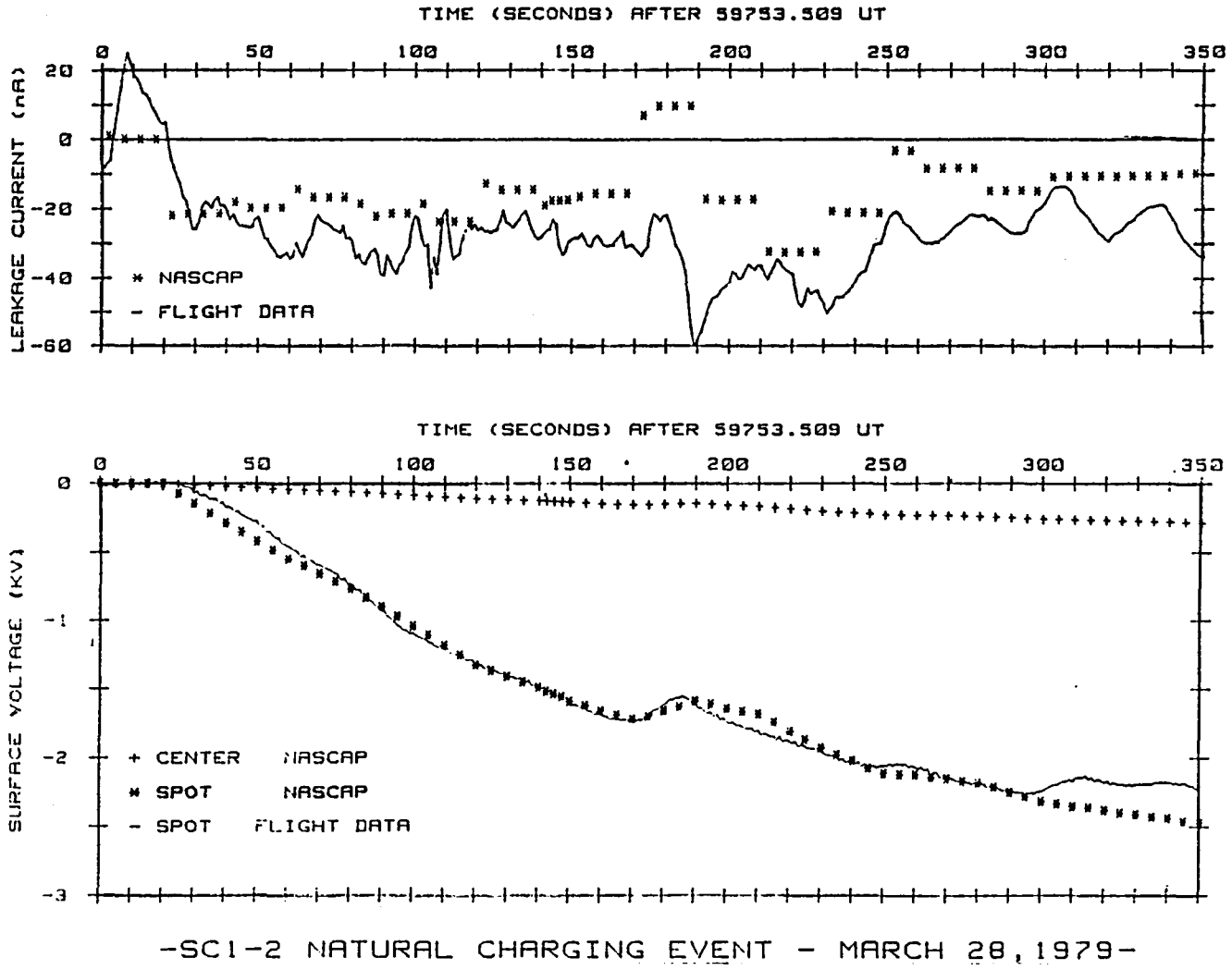

-SC1-2 NATURAL CHARGING EVENT - MARCH 28, 1979-

Figure 2.7. SC1-2 charging on Day 87.

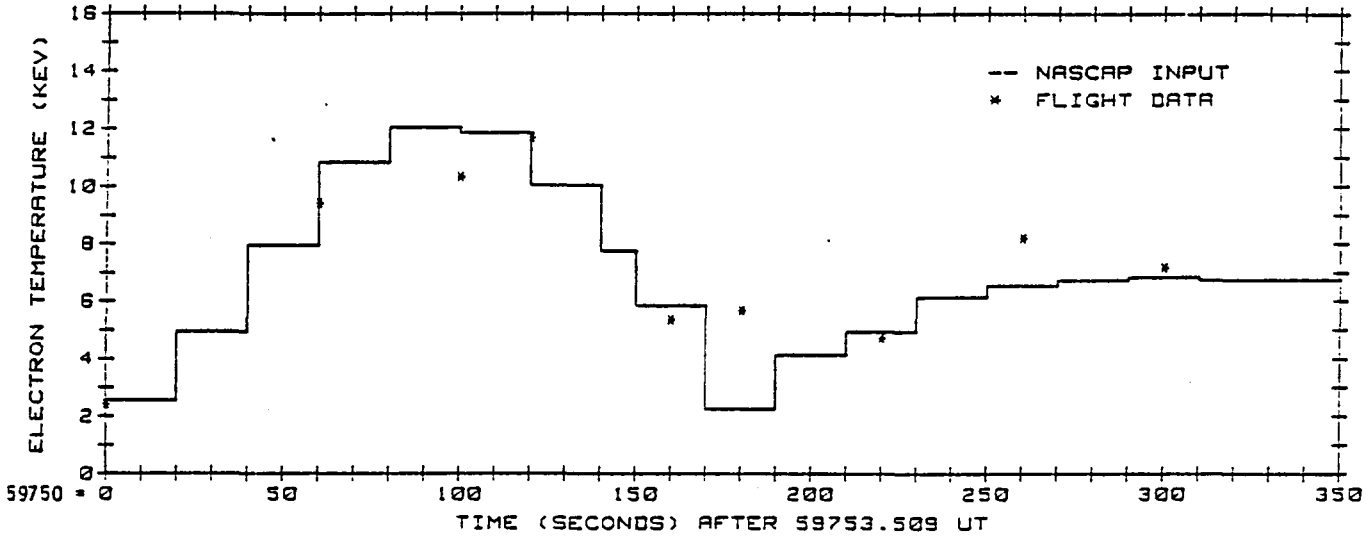

(a)

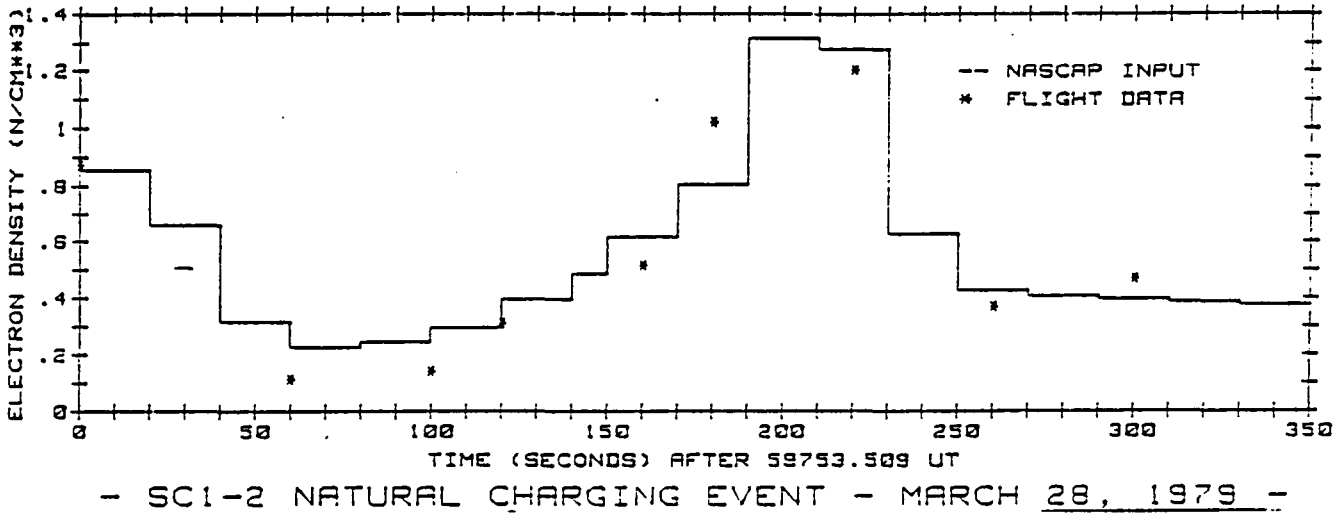

(b)

Figure 2.8. Flared input data for electron environments and spacecraft potential used in SSPM simulation.

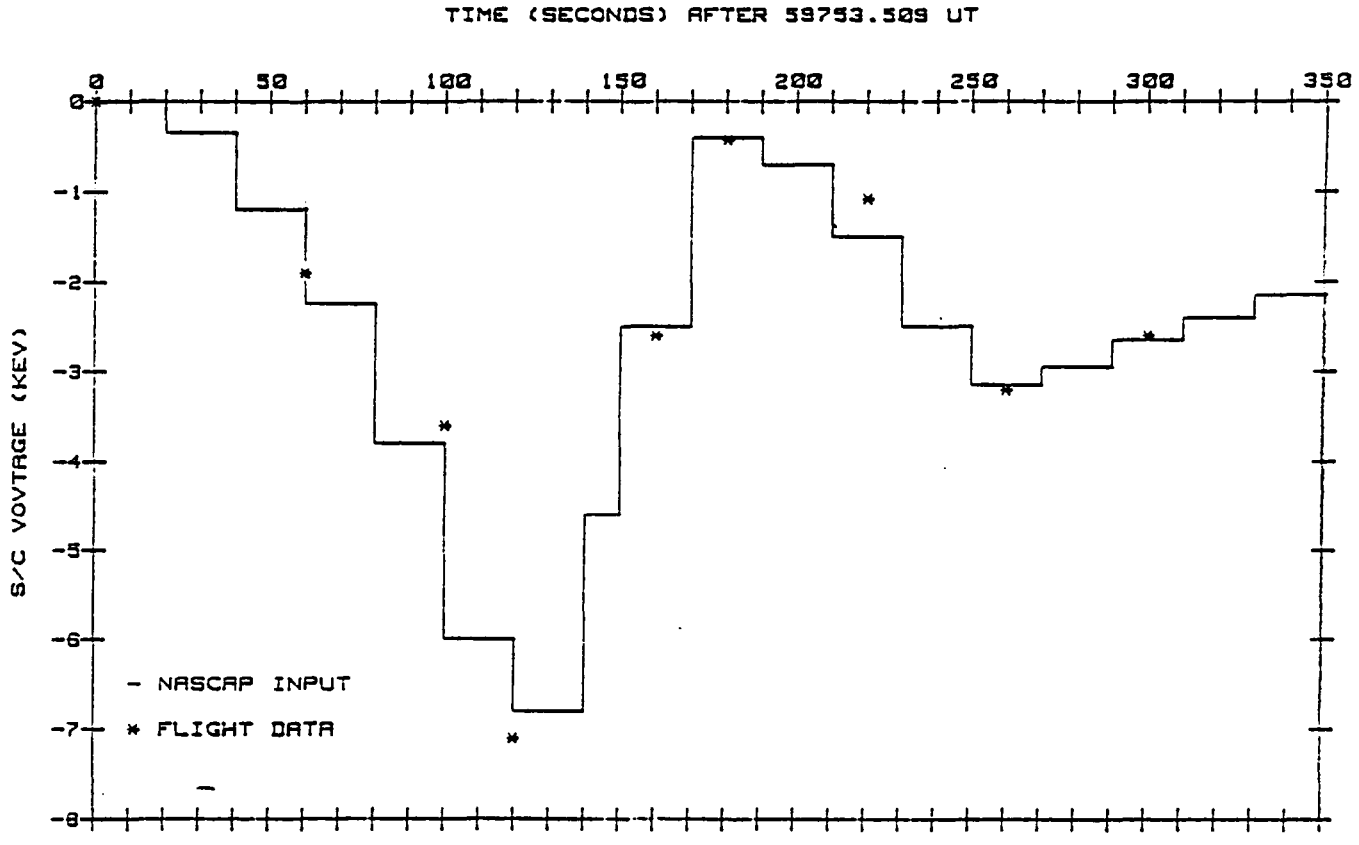

-SC1-2 NATURAL CHARGING EVENT - MARCH 28, 1979-

(c)

Figure 2.8. Flared input data for electron environments and spacecraft potential used in SSPM simulation (concluded).

TABLE 2.6. ELECTRON FLUXES MEASURED BY SC3 (REFERENCE 18) ON DAY 87 AND DAY 146, 1979 OF THE SCATHA MISSION IN ELECTRONS $cm^{-2}\ s^{-1}\ keV^{-1}\ steradian^{-1}$

Energy (keV)	Flux At 60000 UT, Day 87	Flux At 2400 UT, Day 146
47 - 88	1×10^5	5×10^4
66 - 87	5×10^4	5×10^3
87 - 129	2×10^4	3×10^3
129 - 299	2×10^3	7×10^2
269 - 834	2×10^2	7×10^1

2.10 ACTIVE CONTROL SIMULATIONS

During the operation of the SC4-2 electron gun on Day 89, 1979 of the SCATHA mission the sides of the spacecraft were sunlit. As expected on the basis of the ratio of thermal plasma electron current and emitted electron current the satellite ground potential remained close to +1500 V when a 1.5 kV, 1.0 mA electron beam was emitted. During this experiment the differential potential of the kapton SC2-2 SSPM oscillated from -10 V to -80 V respectively as it rotated in and out of the sunlight.[19]

This result can be understood in terms of the onset of field reversal in front of the kapton sample. If the insulating kapton surface is originally at a potential of +1500 V the low energy secondary and photoelectrons are unable to escape and its potential begins to drop towards zero. As the kapton becomes increasingly negative with respect to surrounding surfaces fixed at +1500 V the field in front of it reverses, allowing the low energy electrons to escape to spacecraft ground and halting the decrease in the kapton potential. In darkness, an 80 V differential is required to cause this. In sunlight, photoemission increases the low energy electron yield, and a differential of only 10 V is sufficient to allow enough electrons to escape to balance the incoming current.

When the beam current and voltage were increased to 6 mA and 3 kV, the ground again went to the beam potential (i.e., +3 kV). The kapton surface however now charged to between 1200 and 1400 volts negative with respect to ground (i.e., between +1600 and +1800 volts with respect to the plasma). This much higher differential potential arises because even with all of its photo and secondary electrons escaping to ground the maximum positive potential kapton can achieve lies in this range. This conclusion is supported by a calculation showing that for a neutral plasma with densities and temperatures of 1 cm^{-3} and 1 keV respectively kapton can charge to only ~+2000 V when all of its low energy emitted electrons escape.

2.11 PHOTOSHEATH EFFECTS

To investigate the importance of space charge in the photosheath when the spacecraft is charged to small positive potentials in sunlight, self-consistent space charge calculations were made for the SCATHA satellite fixed at +0.5 volts. Sunlit surfaces were assumed to emit 2×10^{-5} A m^{-2} of photoelectrons. The results are shown for the rotation plane of the satellite in Figure 2.9. A barrier of ~0.75 volts forms ~0.75 m from the emitting surface. Fields due to the space charge of photoelectrons are less than one volt per meter. These predictions are similar to those observed experimentally when the SC10 boom was unfurled for the first time. Aggson[13] observed a dipole moment indicating a barrier of ~1 volt, 4 m from the spacecraft.

These observations and the sample calculations both confirm the validity of NASCAP's assumption that the effect of the photosheath is negligible compared to the 10^4 V m^{-1} fields produced by surface charging.

2.12 HELIOS 1

Finally we look at an example of NASCAP simulation of a satellite other than SCATHA in a plasma environment other than geosynchronous earth orbit. Helios 1 is a solar orbiting satellite whose primary ambient plasma source is the solar wind.[20] The potential of its long antenna has been measured by Kellogg as a function of angle as the satellite rotates in and out the sunlight. The results reproduced from Kellogg's paper[20] are shown in Figure 2.10. They show the familiar pattern of oscillation between positive and negative potentials as the photocurrent is turned on and off as the antenna moves in and out of shadow.

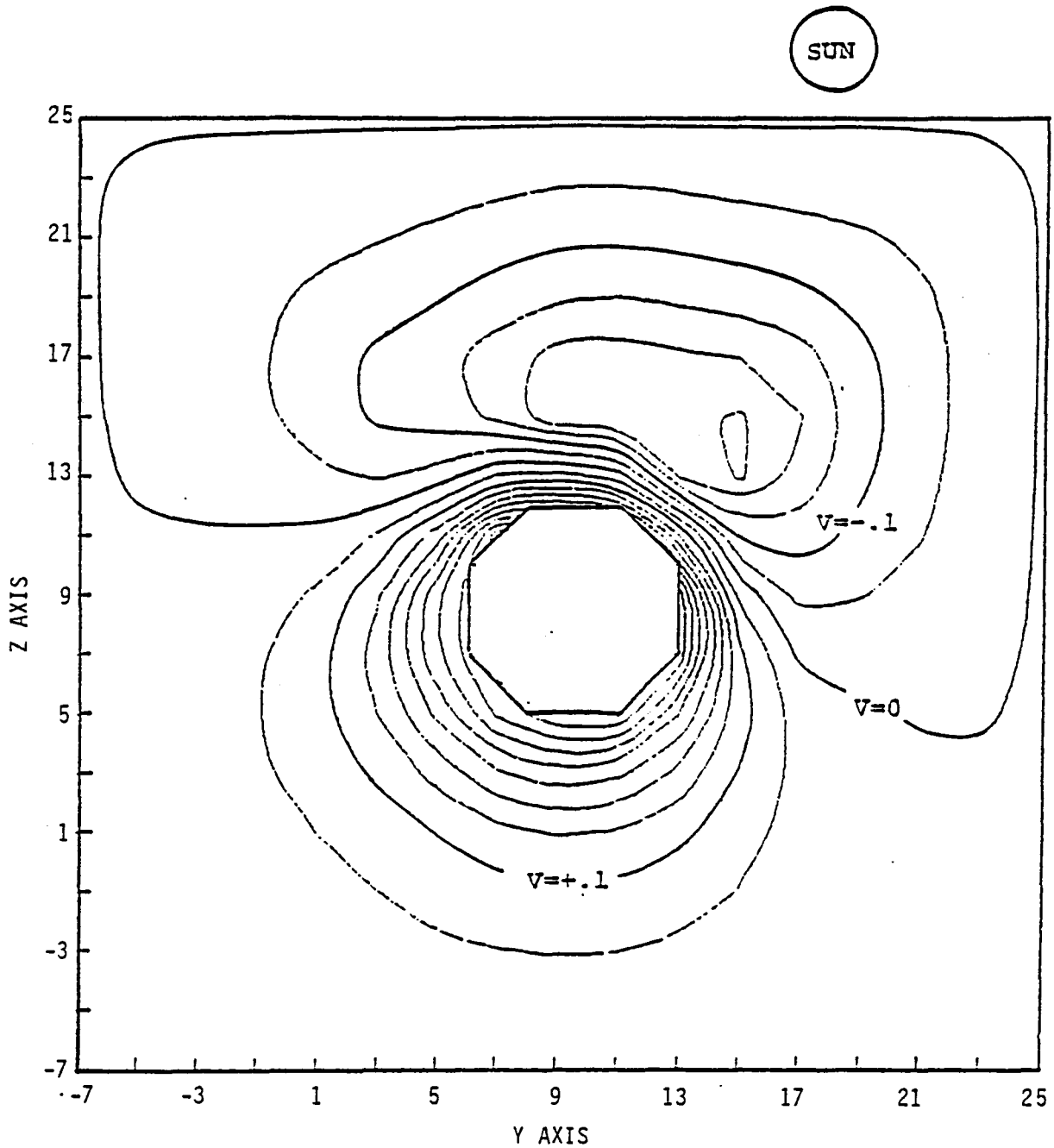

Figure 2.9. Self-consistent potential contours around a simplified SCATHA model, vehicle potential = +0.5 volts, top view. Contour spacing = 0.05 volts.

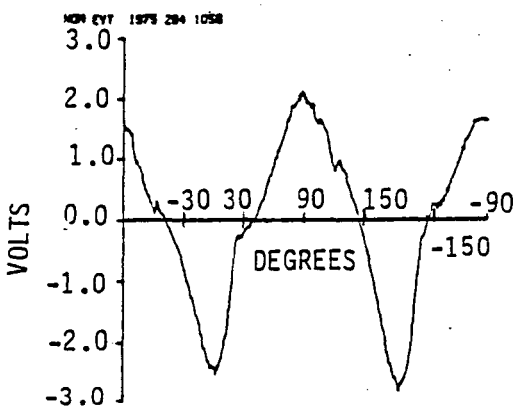

Figure 2.10. Relative antenna potential during one revolution at 0.31 AU. (The DC component of potential is not measured.) (From Reference 20.) Note the same oscillations shown in the simulated response (Figure 2.12).

To demonstrate that NASCAP predicts the same qualitative behavior even in the solar wind environment a crude model of the spacecraft, shown in Figure 2.11, was constructed. The spacecraft was assumed to be a simple 2 m cube with a 16 m antenna extending from one side. The surface material was chosen to be kapton. Since this problem is dominated by the incident electron current and the photoemission, the results should be rather insensitive to the material properties. The material properties of the actual spacecraft are not well known. The electron spectrum estimated by Kellogg, a 20 keV Maxwellian plasma with a density of 5 cm^{-3}, was assumed for both species in the NASCAP calculation (ion collection is also of limited importance in this case). With these input parameters the potential of the boom as a function of angle was calculated using NASCAP in the "ROTATE" mode[6] with a timestep for each 7.5° of rotation. The results are shown in Figure 2.12 for both ends of the boom.

They show excellent qualitative agreement with experiment. No serious attempt at quantitative accuracy has been made in this simulation, but nevertheless the predicted amplitude of the potential oscillations is of the same order as those observed. This calculation shows that even when knowledge of materials, environments and structural details of the satellite is limited, a qualitative picture of behavior can still be obtained using NASCAP. Hence the physical model and algorithms underpinning the code are not crucially sensitive to exact knowledge of input parameters.

2.13 CONCLUSIONS

NASCAP has been validated for charging in a space environment. As in any scientific investigation, confidence in a theoretical model grows with the number and diversity of successful tests. The tests carried out so far do consistently support the crucial assumptions in the NASCAP model. We enumerate these as follows:

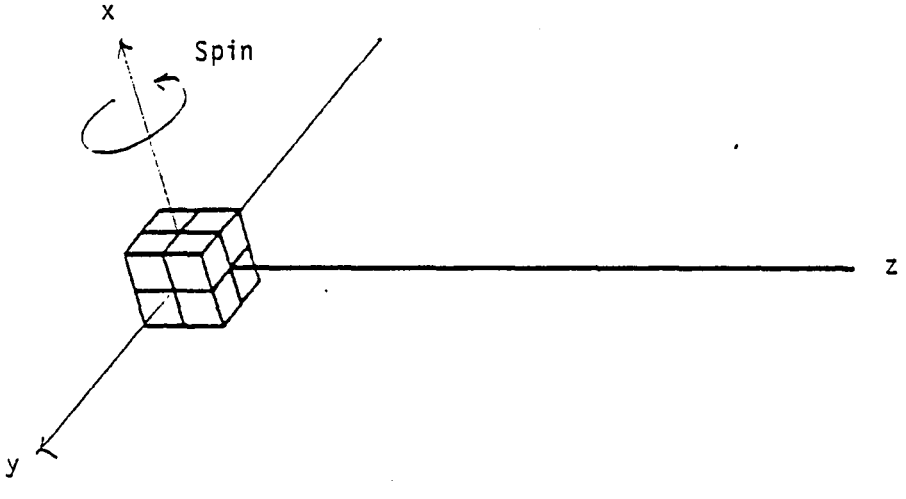

Figure 2.11. NASCAP model of HELIOS 1 spacecraft. (Sun direction lies in the y-z plane.)

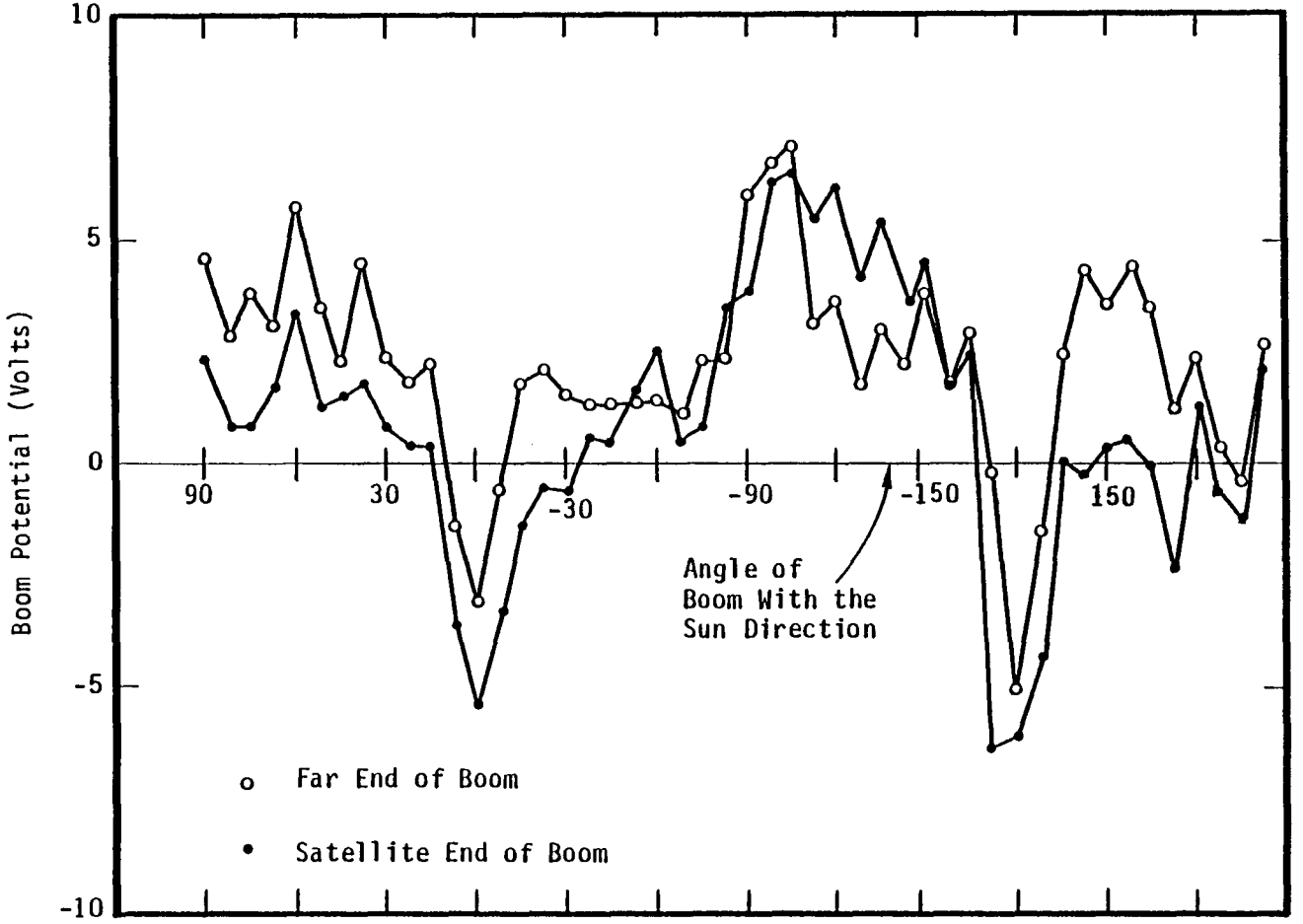

Figure 2.12. NASCAP simulated HELIOS 1 boom potential as a function of sun angle. (See Figure 2.10.)

1. The comparisons show that there is a strong correlation between the collection of particles with energies below 50 keV and the degree of charging. Spectral data for Days 87 and 146 show that this is not true of the higher energy flux. This supports the NASCAP view that charging in space is indeed due to the surface collection of non-penetrating particles.

2. The successful simulation of the charging of spacecraft ground on Day 146 in sunlight, Days 98 and 272 in eclipse, and the explanations of the qualitative behavior of the SSPM's during electron beam emission, support the validity of the description of 3-D electric field effects included in the NASCAP model.

3. The SC10 measurements and NASCAP photosheath calculations conclusively show that the neglect of space charge by the code is a valid approximation.

In addition, on the basis of these tests we arrive at the following conclusions regarding the predictive ability of the code:

1. NASCAP is successfully able to distinguish between <u>severe</u> charging environments, characterized by the following observations:
   - High satellite potentials in the -4 to -10 kV range
   - Rapid fluctuations in potential on a timescale of a few seconds

   and <u>moderate</u> charging environments characterized by
   - Satellite potentials below about -2 kV
   - Very stable potentials changing on a timescale of hundreds of seconds.

   These differences are illustrated dramatically for Days 98 and 114 in Figure 2.13. NASCAP predicts overall charging on SCATHA, via a conventional mechanism in a severe charging environment, when the "SOLAR" material has an initially negative net current. In a moderate environment, charging is predicted via a

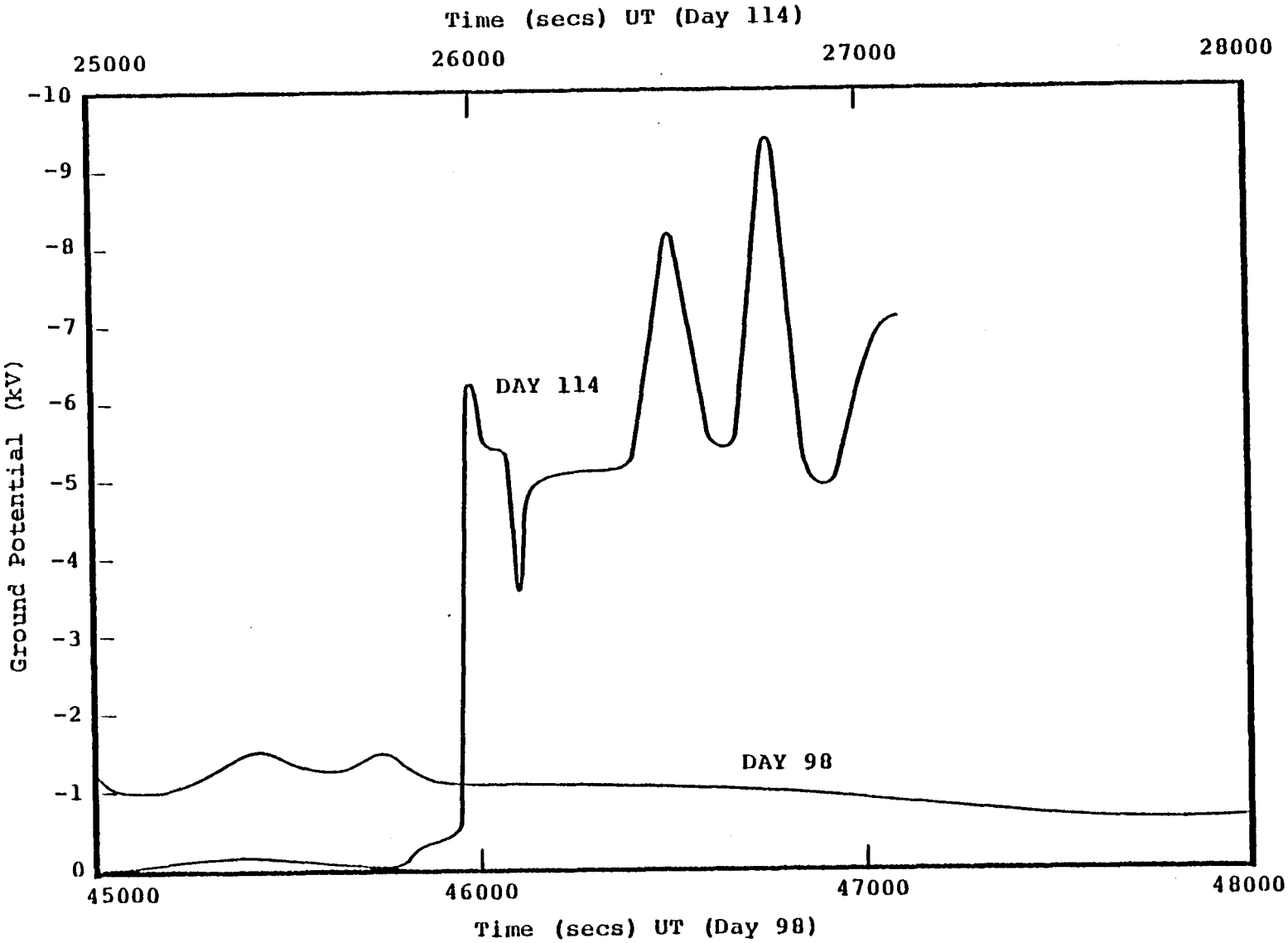

Figure 2.13. Comparison of charging activity in eclipse on Days 114 and 98. (From SC9 data.)

"bootstrap" mechanism when "SOLAR" has an initially positive net current, while other parts of the spacecraft like kapton have negative currents.

Quantitative accuracy is good for severe days. For moderate days, the sensitivity of the bootstrap mechanism to the electric field structure, makes quantitative accuracy dependent upon the representation of the spacecraft. Exact quantitative accuracy cannot always be expected for simple models. Simulations of severe days are much less sensitive to the detail of the spacecraft model.

2. NASCAP successfully predicts negative ground potentials in sunlight (Day 146). The mechanism involved is exactly analogous to "bootstrap" charging in eclipse with low energy photoelectrons playing the role of the secondary emission. The same considerations regarding quantitative accuracy apply.

3. Under conditions that produce considerable differential charging between insulating surfaces in space, the code also predicts the buildup of large differential potentials. In the case of the careful NASCAP simulation of the Day 87 kapton SSPM results, agreement with dynamic behavior was quantitative.

4. Many of the more detailed observations from SCATHA and other spacecraft are successfully reproduced by NASCAP. (These include anisotropy effects, beam emission, and photosheath effects.)

The body of evidence compiled here all lends weight to the conclusion that NASCAP does indeed contain adequate representations of all of the physical processes essential to the understanding of spacecraft charging at geosynchronous altitudes. Furthermore, knowledge of the parameters that characterize these processes is sufficient to allow meaningful predictive calculations of charging effects on real satellites.

One feature the code does not model is the space charge dynamics of emitted particle beams. This is due mainly to the three-dimensional character of the beam spreading and the inordinate computational effort required to follow the beam dynamics by conventional particle tracking methods.

In summary we can say that NASCAP has been able to reproduce, with reasonable accuracy, most of the observations it has been used to analyze so far. It has been able to do this using input parameters obtained using standard procedures, without regard to the outcome of any one simulation, and without any "creative" adjustment to insure agreement with experiment. Furthermore the tests successfully carried out have consistently pointed to the validity of the major assumptions included in the model.

3. NASCAP APPLICATIONS GUIDE

The NASA Charging Analyzer Program (NASCAP) is a large computer code that can be used to provide design information to spacecraft engineers and behavioral information to space scientists involved in space environment studies. NASCAP was developed under the joint AF/NASA spacecraft charging technology investigation to be able to predict the surface charging of complex, three-dimensional objects covered with dielectrics or conductors in geosynchronous, geomagnetic substorm environments. NASCAP can treat surface charging of dielectrics and dielectric/conductor systems in both space environments and ground simulation facilities. For ground simulations, electron and/or ion beams can be used. In ground tests transient data on surface voltages and leakage currents can be obtained for detailed comparisons. In order that optimum use be made of NASCAP, it is necessary that its range of applicability be clearly identified. In this report we shall focus on the cases where best use of NASCAP can be made. This report is not intended as a "how to" guide or as program documentation. Rather, the following descriptions of the general approach and the range of validity of the various formulations employed in NASCAP are intended to assist the user to decide for himself whether it is suitable to his application.

3.1 THE NASA CHARGING ANALYZER PROGRAM

NASCAP is designed to simulate numerically the electrostatic charging of three-dimensional objects exposed to charged particle environments. Negative potentials of several thousands of volts have been observed on satellites in geosynchronous earth orbit (GEO), and have been reproduced in ground based experiments. The sources of this charging are the high temperature plasma near GEO, and low current density electron flood guns in the laboratory. NASCAP is designed for environments which generate substantial charging, i.e., where the mean electron kinetic energy is between several hundred and fifty thousand volts. Ambient magnetospheric densities are of the order of a single

particle per cubic centimeter when the mean energy is thousands of electron volts. The laboratory electron beams have comparable particle densities and generate incident surface currents of about one nanoampere per square centimeter. For both of these environments there is very little screening of object potentials by the ambient plasma.

The geometrical object which NASCAP uses to represent a spacecraft must fit within a 16 x 16 x 32 mesh composed of cubic cells. Thus the maximum possible resolution is 1/32 of the object length. The only exceptions are cylindrical cross-section booms, which may be arbitrarily thin and arbitrarily long. Examples of NASCAP models are shown in Figure 3.1. The surface of the object may be composed of up to 1250 "cells", each of which may be an exposed conductor or a thin dielectric layer over a metallic conductor. Up to fifteen different dielectric materials and fifteen distinct electrical conductors are allowed, connected either with a fixed bias or by capacitive coupling.

The results of a NASCAP calculation are the surface and conductor potentials, currents, and electric fields as a function of time, together with the identification of maximum electrical stresses where discharges are likely to occur. Along with numerical output, NASCAP can optionally generate a large selection of graphical output including various views of the spacecraft model, potential contour plots, and particle trajectories. In order to make optimum use of the computational results, there is an interactive post-processor which enables detailed examination of the final state and charging history of the object.

The conceptual framework of spacecraft charging around which NASCAP is built is extremely simple. Charging is treated as an initial value problem. The surfaces of an object are subject to fluxes of charged particles. These fluxes, after allowing for backscattered particles, secondary electrons, photoelectrons and conduction processes, form net electrical currents to surfaces.

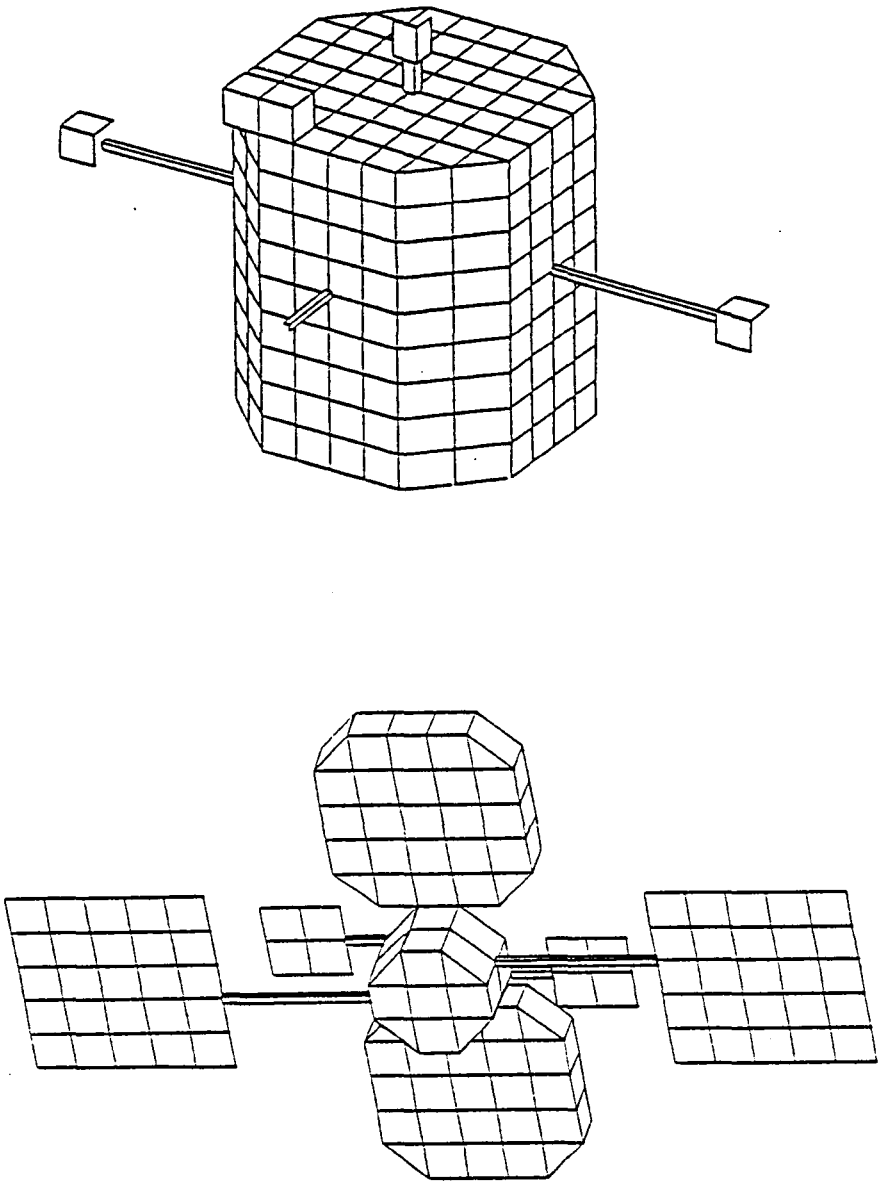

Figure 3.1. Representative NASCAP objects.
(Lower figure courtesy of N. J. Stevens.)

During an interval of time, these currents cause the accumulation of charge. The resultant surface charge distribution is then used to determine the electric potentials and fields on and near the object. This in turn modifies the fluxes and net currents during the next time interval.

Before going on to examine each part of the NASCAP code in detail, we present a survey of the wide range of experimental and engineering examples to which NASCAP has successfully been applied. This should provide a useful "yardstick" for many of the standard applications of the code.

3.2 A SURVEY OF REPORTED NASCAP APPLICATIONS

One way in which the validity of the NASCAP code has been established is by the comparison of the results of laboratory experiments with code predictions. Figure 3.2a shows the excellent agreement between NASCAP predictions for the potential of a simple plate subjected to a moderate energy (~10 keV) monoenergetic electron beam in a test tank with experiment.[8] Figure 3.2b shows similarly good agreement using Satellite Surface Potential Monitors[46] from the SCATHA (P78-2) satellite in a similar environment.[21] Perhaps the most ambitious of these laboratory tests are those involving SCATSAT: a two-thirds scale model of the full SCATHA satellite. Figure 3.3 shows how NASCAP successfully predicts the angular variations in potential around the body of the model, due to divergence of the four spatially separated beams illuminating it.[22] Predictions of such effects could come only from a fully three-dimensional model like NASCAP.[23] Another important feature peculiar to NASCAP is the ability to include potential barrier effects in its calculations and the associated suppression of low energy surface emission.[16] NASCAP predictions involving this phenomenon have been successfully compared with laboratory data for the charging of solar arrays by electron beams.[24]

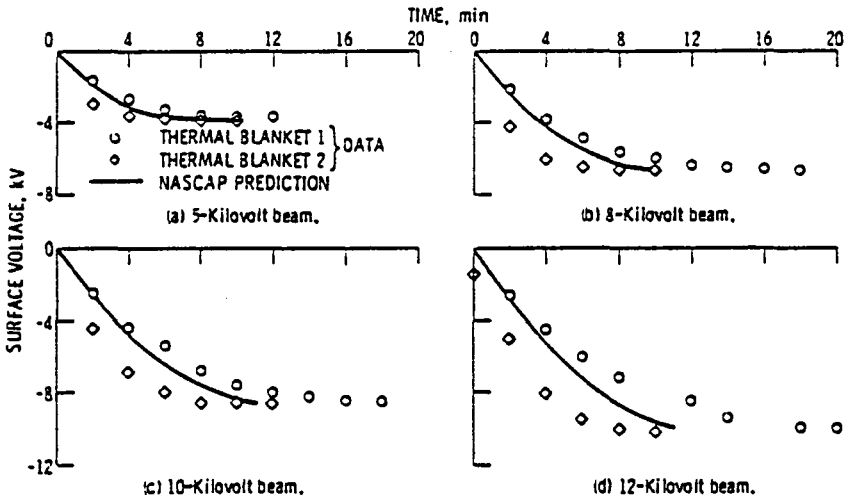

Figure 3.2a. Surface voltage profiles for aluminized kapton (Roche and Purvis, Reference 8).

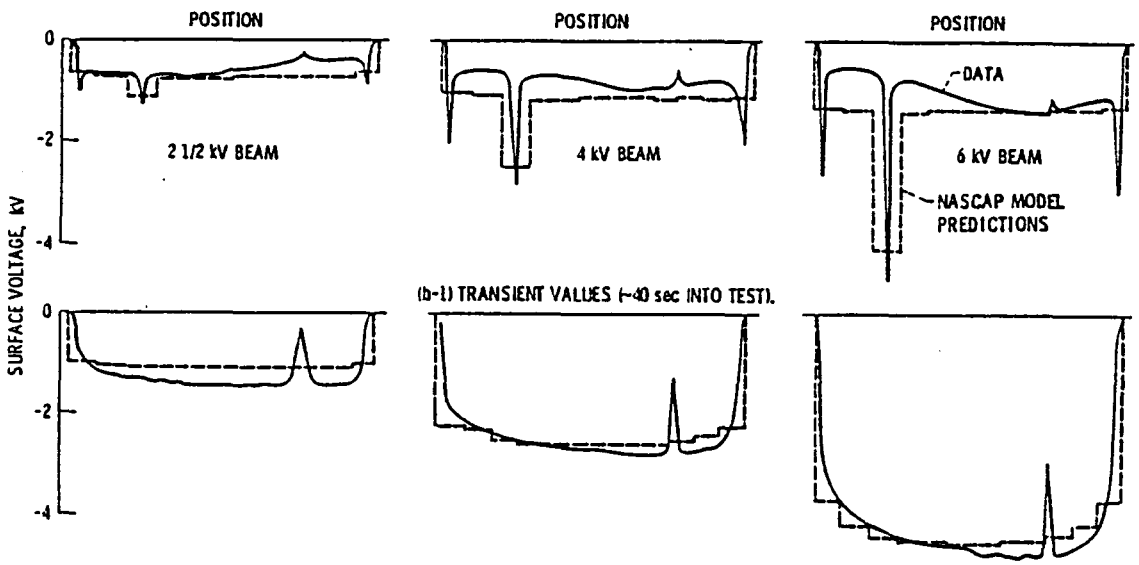

Figure 3.2b. Comparison of SSPM surface voltage data to NASCAP predictions SC1-2 monitor (kapton). 1 nA/cm^2 beam current density (Stevens, et al., Reference 21).

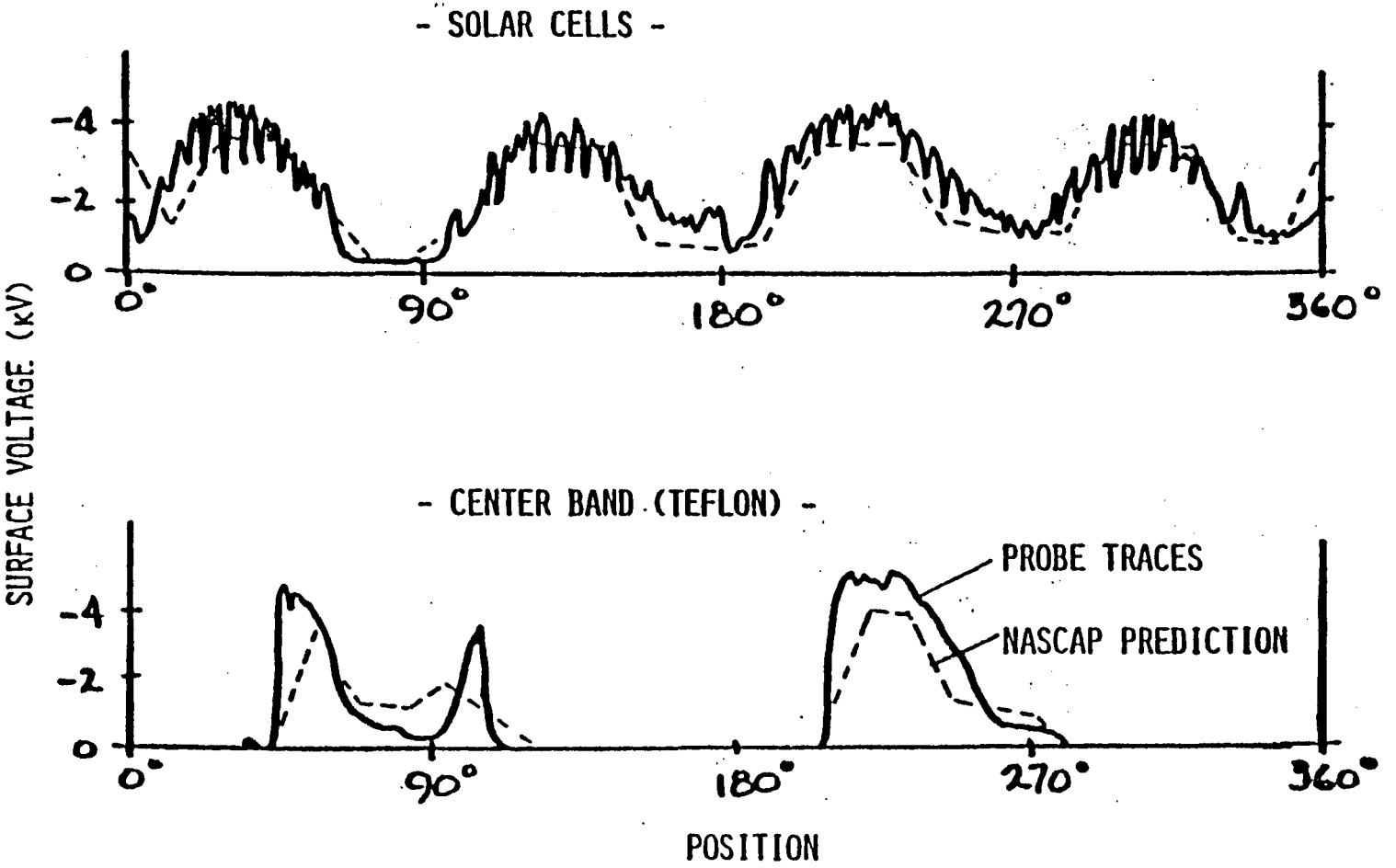

Figure 3.3. Comparison of NASCAP predictions to SCATSAT data (Staskus and Roche, Reference 22).

The other major contribution to the validation of the code has come from direct comparison of NASCAP predictions for the SCATHA satellite and actual flight data. Important analyses of flight data have also been made for the ATS-5 and ATS-6 satellites using the code.[8,25] The spacecraft ground potential has been reproduced for SCATHA in eclipse in both severe and moderate substorms, and in sunlight.[15,26,27,28,29] Both equilibrium and transient potentials predicted agree well with experiment. One example is shown in Figure 3.4 for the day 87, 1979 eclipse event.[15] The dynamic behavior and equilibrium potential values for differential potentials between insulating surfaces have also been accurately modeled (Figure 3.5) using NASCAP.[21,26,15] In these cases descriptions of the plasma spectrum and angular distribution measured by the satellite were used by the code. Other studies including those examining the effect of incident particle anisotropy[29] have been made.

These and many other examples have demonstrated that NASCAP is able to predict, with confidence, the charging behavior of complex objects in both a tank and a realistic space environment. This capability has led to its use as a design tool, in order to predict potential sources of voltage stress, and hence damaging discharge sites on satellites.

While NASCAP can be very useful to the space science community it should not be used indiscriminately. For a scientist or engineer to make the best use of NASCAP he should understand how NASCAP describes objects, determines incident particle fluxes and other currents, calculates electric potentials, and, most importantly, integrates currents forward in time. Below we will deal with each of these aspects of the code with the emphasis on their range of applicability.

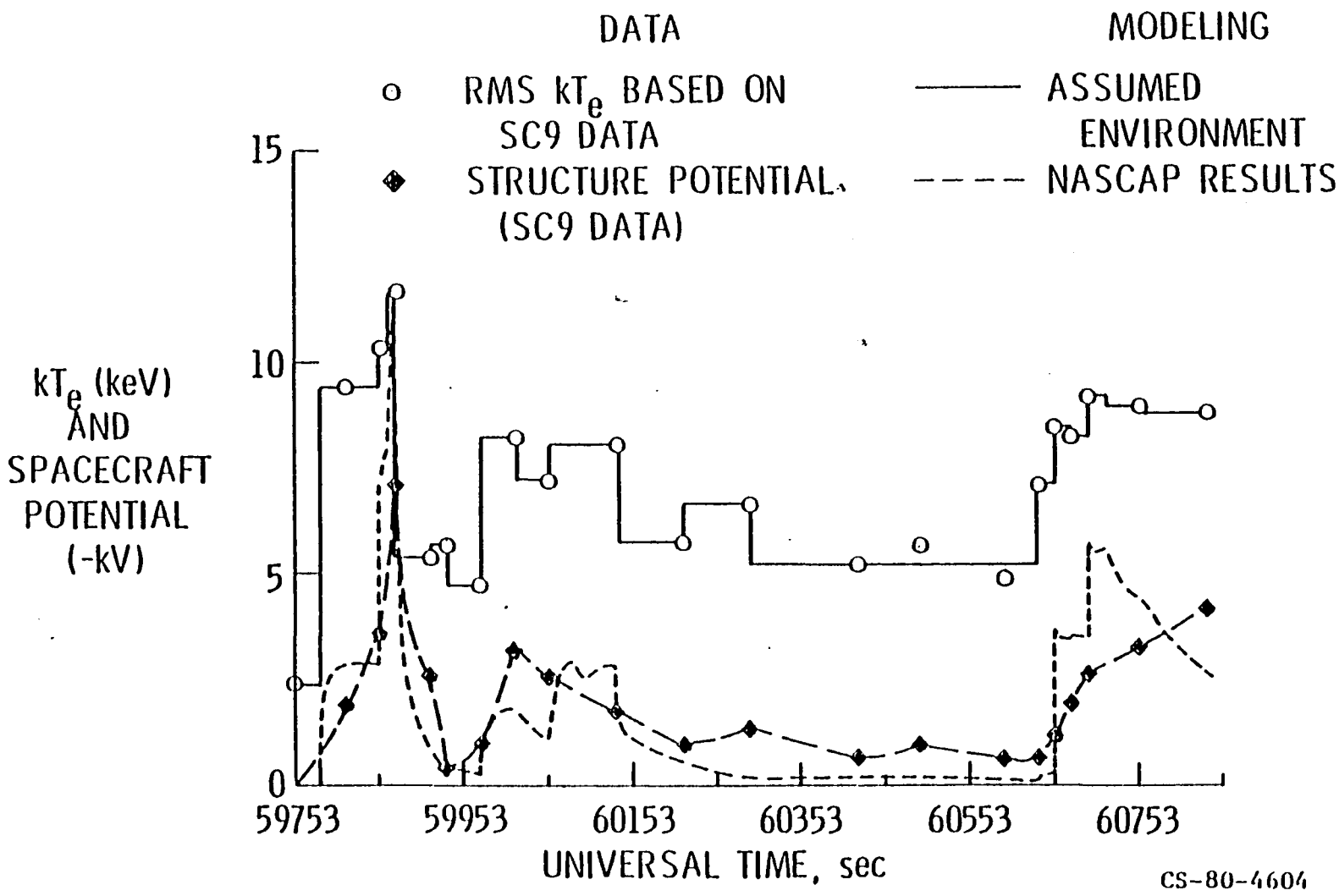

Figure 3.4. Simulation of SCATHA potentials using single Maxwellian environments (Purvis and Staskus, Reference 15).

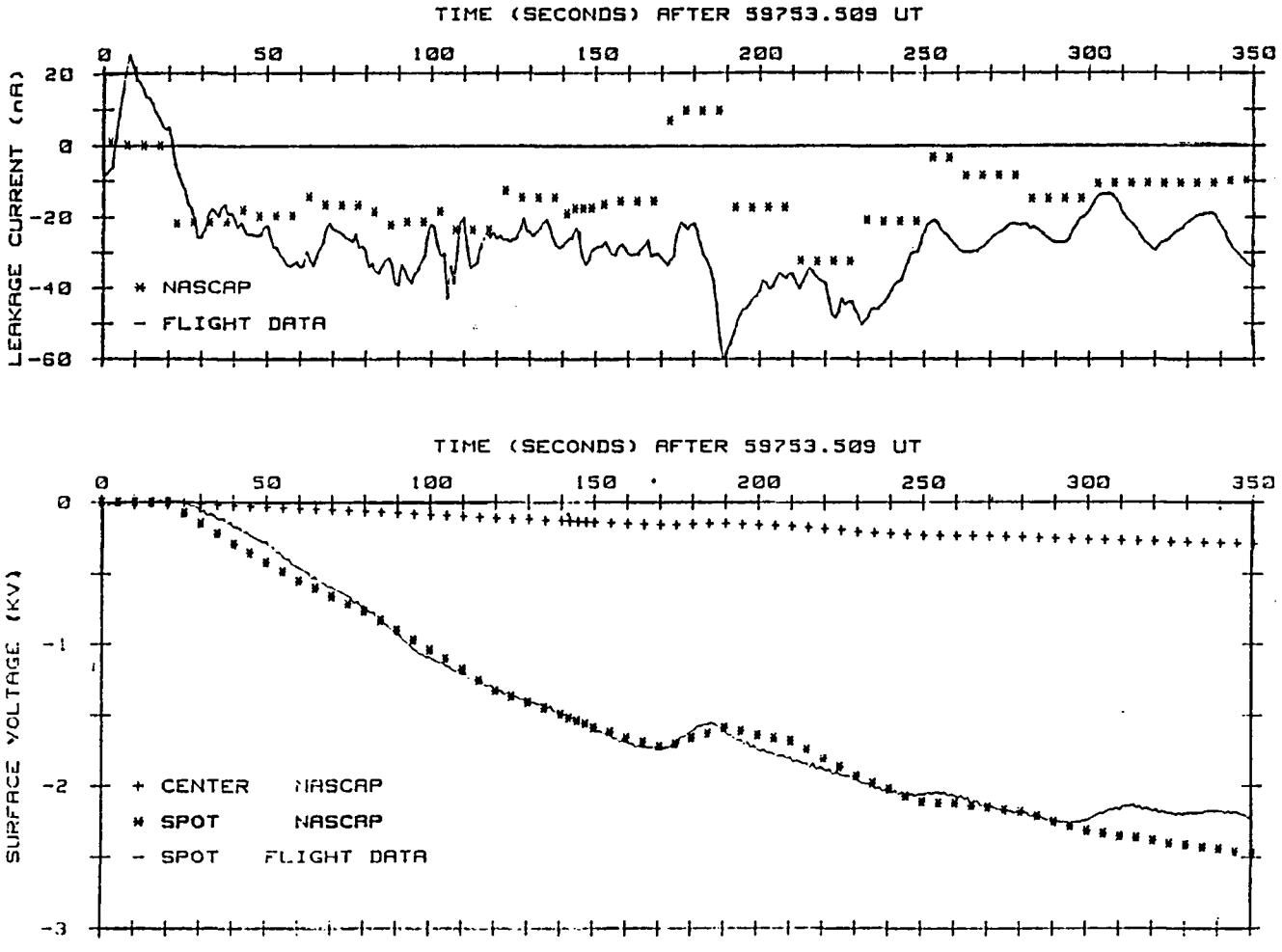

-SC1-2 NATURAL CHARGING EVENT - MARCH 28, 1979-

Figure 3.5. Simulation of SC1-2 charging on Day 87 (Gedeon, Reference 29).

3.3 OBJECTS

The NASCAP computational space consists of a number of nested three-dimensional meshes (Figure 3.6). Each mesh has dimensions 16 units in X, 16 units in Y and up to 32 units in Z. All the meshes for a given problem have the same number of cubic zones, but the edge length of each zone doubles as one goes out from the innermost mesh. The innermost mesh is the most important region of the computational space because the entire object (except for long booms) must be contained within the innermost mesh. Geometrical objects are constructed of building blocks commensurate with the cubic mesh spacing. Note that the spatial resolution along any surface is restricted to the mesh spacing. For example the maximum resolution of a 1.4 meter cube would be 10 centimeters (since objects cannot share surfaces with the edge of the inner mesh). Thus, surface features, such as seams, gaps, or paint spots which are less than 10 cm in extent could not be easily incorporated into a NASCAP object. A user can create an object which incorporates estimated responses of small features through careful consideration of how these responses will manifest themselves on a larger scale. The only high resolution capability built into NASCAP is that cylindrical cross-section booms may have radii less than the mesh spacing.

Surfaces of an object can be either an exposed conductor or a dielectric over a conductor. The thickness of dielectric coverings must be much less than the mesh spacing. NASCAP neglects all components of the electric field internal to the dielectric except that component normal to the surface. The conducting portions of a NASCAP object may be grouped into as many as fifteen electrically separate conductors whose potentials can be allowed to float, be fixed at an arbitrary voltage, or maintain given biases with respect to each other. Electrical coupling between conductors takes the form of user-specified capacitances. Coupling between a dielectric surface and its underlying conductor is both resistive and capacitive, and surface conduction between neighboring surface cells is accounted for.

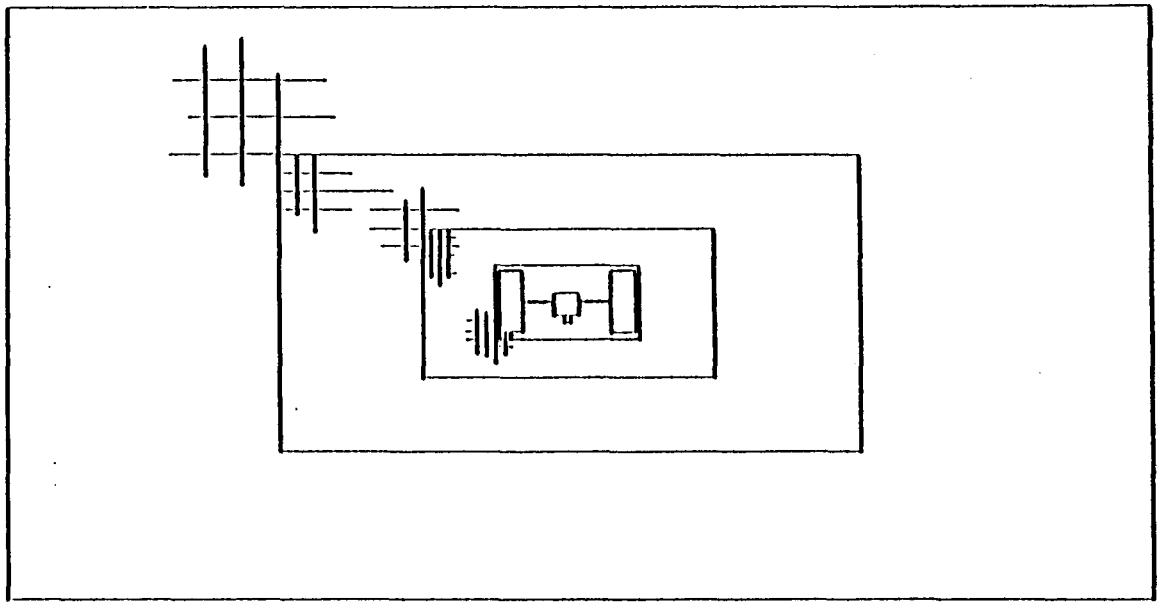

Figure 3.6. Cross-section (y-z plane) of grid, showing first four embedded meshes.

3.4 ENVIRONMENTS

Descriptions of the incident plasma spectrum acceptable to NASCAP allow a great deal of flexibility. For the magnetospheric environment, isotropic single and double Maxwellian descriptions of particle distribution functions are the most easily used; NASCAP also allows the user a wider choice of either looking up tabulated satellite data or inserting his own data in a prescribed format. Approximate descriptions of anisotropic environments are optionally available as well. For the simulation of experiments performed on the ground in vacuum facilities, the code can simulate up to ten ion or electron sources.

While the description of the environment far from the object can be quite flexible and accurate, the techniques used to relate the surface fluxes to the distant environment are very simple and are applied best to convex objects. For Maxwellian environments, orbit-limited spherical probe formulations are used. These are valid for convex objects immersed in an isotropic environment when the object's largest radius of curvature is much less than the ambient Debye length. As these conditions are violated, the errors grow faster for fluxes of attracted species than repelled species. The Debye length conditions can also be described as a requirement that ambient charge be negligible in determining fields and potentials in the vicinity of the spacecraft. This will be true for objects and environments where the Debye length (λ_D) is much greater than the object size. For example NASCAP will work well for a one meter radius satellite in a one particle per cm^{-3}, (n_e) 10,000 eV (θ) plasma because

$$\lambda_D \simeq 700 \sqrt{\frac{\theta}{n_e}} \text{ cm} \sim 700 \text{ meters} >> L_{sat} = 1 \text{ m} .$$

However, NASCAP should not be used for a large object, $L \sim 10^2$ m, in Low Earth Orbit (LEO), $n_e \sim 10^5$, $\theta \sim 0.1$ eV where

$$\lambda_D \simeq 0.007 \text{ m} << L_{sat} = 10^2 \text{ m}$$

Along with high temperature low density plasmas, other possible NASCAP environments are low density ion and electron beams simulating ground based experiments.

NASCAP has a forward particle tracking capability to model the simplest type of laboratory flood gun experiments. Multiple guns with distributed energies can be simulated using analytical descriptions of beam dynamics. Beam divergence due to object charging (as opposed to beam self forces) is reproduced well by the model along with object shadowing for fairly simple, mostly convex objects. The analytical description assumes that monopole fields dominate the beam dynamics, and thus is most applicable to large source-object distances and relatively uniformly charged surfaces. Electron gun calculations have been compared extensively with experiment and the agreement has been quite good, generally within 25 percent on surface potentials. Three-dimensional effects caused by the angular spread of the beam have been well reproduced (see Figure 3.3).

3.5 BACKSCATTERED AND SECONDARY FLUXES

The way in which NASCAP describes the backscatter of electrons and the generation of secondary electrons by incident electrons, ions, and solar photons sets the absolute scale of energies where NASCAP is applicable. The electron impact secondary emission formulas have been designed to fit experimental data for normally incident electrons. NASCAP predictions of electron charge deposition on materials are valid for primary energies ranging from a few hundred eV to several tens of keV, above which the electron range becomes comparable to the typical thickness of insulating films. No particular effort has been made to fit the low energy portions of secondary emission curves, so

that estimates of net charge deposition by electrons in the 20-200 eV energy range should be viewed skeptically. Ground test comparisons have indicated that these are not important to charging.

Secondary electron production by incident ions (protons) is modeled as proportional to the stopping power for primary energies above 1 keV, dropping to very low values below 1 keV. Only for a few materials is there reliable data to which the curves can be normalized.

The energy and angle dependence of secondary and backscatter yields have been studied carefully and compared with the NASCAP models for several typical spacecraft materials.[8,21] In general, for the energy range mentioned, the results are in extremely good agreement. NASCAP is state of the art. It has been used together with the companion single surface MATerial CHarGing code, MATCHG, by experimenters to analyze pure sample response to charged particle fluxes.

The kinetic energies of secondary and backscattered particles are important parameters for spacecraft charging. These spectra are modeled in NASCAP as 2 eV Maxwellians for secondary and photoelectrons, and as a triangular shaped spectrum averaging two-thirds the incident energy for backscatter. Nearly all backscattered electrons escape to distances far from the object, except for cases of substantial positive potential. For the low energy electrons, the choice of energy spectrum has substantial ramifications because it has been shown that in many cases spacecraft charging is dominated by small electric fields that prevent low energy electrons from escaping a surface. Since many surfaces emit large quantities of secondary and photoelectrons, small potential barriers, the order of 10 volts in height, control the current balances. The height chosen for these barriers is directly related to the choice of the secondary spectrum. Thus precise values of potential differences

or absolute potentials of the order of 10 volts depend on the details of this spectrum. NASCAP's values for potentials this small are only qualitatively correct.

Laboratory experiments have shown that secondary electron yields of some materials are sensitive to surface preparation, temperature, age, and mechanical treatment. It is impossible for NASCAP to take any of these things into account. NASCAP results should be evaluated taking into consideration the reliability of the secondary emission coefficients.

3.6 CONDUCTION CURRENTS

Conduction currents through dielectrics to underlying conductors are calculated assuming that only the intrinsic bulk resistivity is important. NASCAP neglects dose and field dependences. If these features are important for a specific calculation it is possible to simulate them by varying material properties. NASCAP includes surface conduction caused by finite surface resistivity and has similar restrictions to those of the bulk resistivity. These surface currents are calculated using Ohm's law and are only limited by the resolution of the potential and the accuracy of the conductivity data.

A suggestion on when to define a surface as an exposed conductor and when to define it as a dielectric with finite resistivity: If to draw the maximum currents available (typically a nanoampere per square centimeter) through the dielectric, requires a potential between the exposed surface and the underlying conductor of less than around 1 volt, the surface should be defined as an exposed conductor. The use of very low resistivities may introduce round-off errors in the numerical treatment. For example, a material 10^{-4} m thick should be defined as a dielectric only if its conductivity is no higher than 10^{-9} mhos/m.

3.7 ELECTRIC POTENTIALS

Potentials are found in NASCAP using the integral variational principle equivalent to Poisson's equation. By using the variational principle along with the finite element interpolation scheme, there is a self-consistent procedure for defining potentials and fields everywhere and for incorporating surface charge boundary conditions.

Resolution of steep potential gradients over a distance less than the grid spacing is not generally possible to achieve in NASCAP. However, most spacecraft have structural booms and struts whose radii are small compared to spacecraft dimensions. The potential variation near such objects cannot be well represented by linear interpolation and the grid size typically is too large to resolve these booms. In order to represent these objects, special cells are allowed which contain the correct logarithmic variation of potential near the boom. Thus the electrical behavior of conducting booms, that is, booms whose potential varies little circumferentially but can vary along their length, are well represented even though they have radial dimensions much smaller than the grid spacing.

Ambient space charge is typically ignored in NASCAP calculations, although there is an option which calculates and uses approximate space charge density. The reason for neglecting space charge is that for kilovolt levels of charging in the magnetosphere the surface charge accumulated is several orders of magnitude larger than the possible space charge. Under such conditions, the Laplacian field strengths, which are typically the order of kilovolts per meter, completely swamp space charge effects of even photoelectrons, which can produce fields like one volt per meter. So for the high temperature, low density spacecraft charging environments that NASCAP was designed to handle, the neglect of ambient space charge density is an excellent approximation.

The optional space charge density treatment in NASCAP is linear Debye shielding. This is the simplest approximation to the screening of potentials by a plasma and is valid only for potentials less than the plasma temperature. While the Debye shielding is easy to use it has limited applicability. Also, the particle fluxes do not reflect the modified space potentials.

Surface cell potentials are defined to be uniform over each surface cell. The surface potentials are obtained from conductor values by using the thin film approximation and assuming the charge density on a surface cell is uniformly distributed. The determination of conductor potentials is addressed in the next section.

3.8 INTEGRATION OF CHARGING CURRENTS

The time integration of currents is the most difficult part of the simulation of the spacecraft charging. The effect of saddle point potential barriers in limiting photoelectron emission was an early NASCAP result. Since potential barrier heights need only be around 2 volts to do this, the shortest timescale of importance is the time to change the entire vehicle potential by that magnitude. This is typically $\sim 10^{-6}$ seconds. A one meter radius sphere, for example, in a nanoampere per square centimeter environment will charge 2 volts in about 2 microseconds. But spacecraft charging is of engineering interest when large potentials develop across a few mil thick dielectric film. For the same environment this takes around 20 seconds. The set of equations governing this charging have about 7 orders of magnitude separating the eigenvalues characterizing the fastest response of the system from those of principle interest. Along with this, the flux equations are nonlinear and nonlocal in the potentials; for example, effective photoemission has almost a step function dependence on the surface electric field. The algorithms which perform the current integration are known to the NASCAP users as the LONGTIMESTEP option.

There are three major conceptual elements to the LONGTIMESTEP algorithm we have developed which allows the stable integration over large enough time intervals, Δt, to make NASCAP simulations of minutes of satellite time take only minutes of computer time: (1) A rapid estimation method for surface potential changes; (2) a partially implicit current integration algorithm; and (3) anticipation of cutoff of low energy electron emission.

NASCAP uses the full three-dimensional potential calculations every timestep, but in order to determine how fluxes change during a time interval, the code needs a quick way of estimating how the surface potentials will change. For that purpose NASCAP constructs a capacitor model with a circuit node for each dielectric surface and each conductor.

Even to use the circuit model to get an estimate, an explicit timestep procedure would still be prohibitive. The second major element of the LONGTIMESTEP is a partially implicit current algorithm. The trade-off in implicit versus explicit is stability versus simplicity. The implicit algorithm gives the correct asymptotic results, but effectively stretches out rapid responses to at least the order of the timestep. Table 3.1 shows the exact decaying exponent solution of the equation $df/dt = -f$ with the results obtained using explicit and implicit algorithms. The comparisons are for timesteps longer and shorter than the characteristic timescale, which for this equation is unity. Notice that the implicit algorithm always gives reasonable answers, but that for long timesteps the timescale of decay is set by the length of the timestep. In NASCAP this means that to determine accurately rapid transient responses, short timesteps must be taken. However, NASCAP used with a long timestep will eventually reach the physically correct solution.

Most spacecraft charging problems are dominated by the electric field suppression of low energy secondary and photoelectrons. The sensitivity of the electron emission to the electric fields and the

TABLE 3.1. COMPARISON OF EXPLICIT AND IMPLICIT ALGORITHM SOLUTION OF df/dt = -f FOR TIMESTEPS SHORT AND LONG COMPARED TO THE CHARACTERISTIC TIME SCALE

SHORT TIMESTEPS

t	0.1	0.2	0.3	0.4	0.5	0.6	0.7	0.8	0.9	1.0
f_{exact}	.905	.819	.741	.670	.607	.549	.497	.449	.407	.368
$f_{explicit}$	.900	.810	.729	.656	.590	.531	.478	.430	.387	.349
$f_{implicit}$	.909	.826	.751	.683	.621	.564	.513	.467	.424	.386

LONG TIMESTEPS

t	10	20	30	40	50	60	70	80	90	100
f_{exact}	4.54-005	2.06-009	9.36-014	4.25-018	1.93-022	8.76-027	3.98-031	1.80-035	8.19-040	3.72-044
$f_{explicit}$	-9.00+000	8.10+001	-7.29+002	6.56+003	-5.90+004	5.31+005	-4.78+006	4.30+007	-3.87+008	3.49+009
$f_{implicit}$	9.09-002	8.26-003	7.51-004	6.83-005	6.21-006	5.64-007	5.13-008	4.67-009	4.24-010	3.86-011

$$\text{EXPLICIT} \qquad f(t) = f(t - \Delta t) + \Delta t \left.\frac{df(t')}{dt'}\right|_{t' = t - \Delta t}$$

$$\text{IMPLICIT} \qquad f(t) = f(t - \Delta t) + \Delta t \left.\frac{df(t')}{dt'}\right|_{t' = t}$$

large magnitude of photocurrents mean that implicit algorithm inaccuracies can cause the entire calculations to become unstable. The third major concept underlying LONGTIMESTEP is to identify all surfaces which are dominated by low energy emission and to impose the physical constraint that the 2 eV photoemissions can only generate a potential barrier between the surface and the region of space above it of above 2 eV. For these surfaces the dependent and independent variables are interchanged. While for ordinary surfaces we solve for potentials given charges, for these surfaces we fix the height of the potential barrier exterior to the surface (and hence the surface potential) and solve for the change in net charge. This procedure is a good approximation to the actual physics where the barrier height stays in the range of a few volts, since a much higher barrier would stop all emission and a lower barrier would let too many photoelectrons out, driving the entire object to unphysically high positive potentials.

The LONGTIMESTEP algorithm is a considerable refinement beyond the procedure discussed above. It includes multiple passes and iterative selections of surfaces where low energy particles are emitted but is basically an application of a large capacitor model using a combination of first order implicit fluxes and self-consistent barrier heights in order to evaluate the time integrals of the charging currents. NASCAP, during the current integration, estimates that the potential one mesh unit in front of a surface cell changes just under half as fast as the cell potential itself. The difference between this estimate of the barrier and the full 3-D potential calculation at the end of the timestep has proved to be a good compromise between exact accuracy of transient response and stability.

The one user entered parameter for LONGTIMESTEP is the maximum charging per timestep, DVLIM. The length of the timestep is automatically cut back to limit the maximum change in potential of any conductor to DVLIM. The magnitude of DVLIM sets the accuracy of the

results for each timestep. In problems where nonlinear or nonlocal effects are particularly manifest, oscillations of order DVLIM may persist. The use of smaller timesteps and smaller DVLIMs will reduce these fluctuations.

We should point out that the LONGTIMESTEP option is introduced as a convenience to the user who is interested in the charging behavior on timescales much greater than the very rapid transient responses. The transient responses themselves can still be modeled accurately by taking very short timesteps, if desired. (For example, see Figure 3.4.)

3.9 CHARGED PARTICLE EMITTERS

NASCAP has options for simulating the emission of charged particles from a satellite. These were designed to model electron and ion guns such as the SC-4 experiments on the SCATHA vehicle. NASCAP predicts well the dependence of spacecraft potentials and incident ambient particle fluxes given an escaping beam current. The primary results are I-V characteristics as a function of environment and relative surface potentials. The limitations on these calculations are similar to those of other calculations and are primarily due to spatial resolution.

The gun algorithms are designed for low density beams. Low density means that two conditions are satisfied. First, the Child-Langmuir limiting distance ℓ_{CL} must be much greater than the beam radius. For example the SC4-2 electron beam when operated at 3000 keV 0.1 ma clearly satisfies this condition.

$$\ell_{CL} = \sqrt{\frac{2.3 \text{ v } 10^{-6} \text{ V}^{3/2}}{\sqrt{m/m_e}} \frac{(\pi r^2)}{I}} = 54 \text{ cm} >> r_{beam} = 0.5$$

However, the same device at 1500 volts and 12 milliamperes is less obviously in compliance.

$$\ell_{CL} = 3 \text{ cm} > 0.5 \text{ cm} = r_{beam}.$$

Ion guns are far more susceptible to near-satellite space charge effects than electron guns. For example, a Xenon device when operated aboard SCATHA at 1100 volts and 2 ma was very space charge limited.

$$\ell_{CL} \simeq 0.3 \text{ cm} < 0.5 \text{ cm} = r_{beam}$$

The NASCAP particle tracking algorithms lack the necessary resolution of beam space charge effects, and are therefore not directly applicable to the high current modes of ion beams.

The second condition on the applicability of NASCAP for beam simulations relates to the total beam current compared to the ambient current. When the beam current is larger than the current that the satellite could ordinarily draw from space while at the beam voltage, then a portion of the beam must return to the vehicle. For example, a 1 meter radius sphere in a 1 keV, 1 cm^{-3} plasma will attract 0.04 ma of electron current if the sphere potential is 3000 volts. If the sphere has an onboard particle emitter of 3000 volts and 6 ma then less than 1 percent of the beam current can escape to infinity. The dynamics of the returning current are quite difficult to predict since it is entirely a self space charge effect. The excursion length turns out to be very large (44 meters), and there is not necessarily a steady state solution. NASCAP is not suited for such calculations.

3.10 DETECTORS

NASCAP has DETECTOR routines which accurately determine the energy and angular variation of the particle fluxes incident upon particular satellite surfaces. These routines employ particle tracking algorithms and are quite accurate. However, they calculate

the particle fluxes, not the readings of a particular scientific instrument. Therefore when comparing with experiment, the response function of the actual physical detector must be taken into consideration.

3.11 SUMMARY

NASCAP has proven to be a reliable and accurate tool for predicting the electrostatic charging of objects exposed to space and laboratory environments. The code has been shown to be most successful when applied to problems that fit within the following set of constraints:

- The object is constructed of conductors all or partially covered with thin dielectric surfaces. The resolution required to model the object is no finer than 1/32 of the object length.

- The environment is dominated by electron and/or ion fluxes with energies between several hundred electron volts to about fifty thousand electron volts.

- The ease of running NASCAP is greatly enhanced if the environment is well represented by an analytical form such as a multiple Maxwellian.

- The ambient Debye length is larger than the length of the object.

- The materials which comprise the surface of the object are stable with well-characterized secondary emission and backscatter yields.

- Low resistance surface dielectrics are modeled as exposed conductors.

- The calculations are run using short enough timesteps such that the voltage change allowed per timestep is of the same order as the accuracy required.

- Any onboard particle emitters are of low enough current that their self space charge does not dominate the ambient natural environment.

- The DETECTOR routines are used to accurately determine incident particle fluxes.

For the conditions which prevail at geosynchronous altitude, these constraints are not severe and NASCAP will correctly predict surface charging.

4. DIFFERENTIAL CHARGING OF HIGH-VOLTAGE SPACECRAFT: THE EQUILIBRIUM POTENTIAL OF INSULATED SURFACES

4.1 INTRODUCTION

The design of high-voltage spacecraft is a subject of increasing technological importance. In particular, operation of solar arrays at high voltage will eliminate the need for heavy bus bars and power converters on such future projects as a solar electric power stage[30] or a solar power satellite.[31,32] Parker[33,34] has done extensive analysis of the plasma interactions of such systems. Some laboratory data is available on the behavior of high voltage spacecraft surfaces in plasmas.[35,36,37] Additionally, a great deal of information may be obtained from experiments in which spacecraft were artificially maintained at high voltge by emission of charged particle beams.[38,39,40,25] Other authors[41,42,43] have previously addressed the issue of potentials during beam emissions. Here we focus on the differential potentials developed by electrically insulated surfaces, either dielectric surfaces or electrically isolated metallic surfaces, in the presence of high voltages.

Recently, measurements of the voltages of electrically insulated surfaces during active control operations have been reported. On the SCATHA[44,45] satellite voltage differences have been measured between the spacecraft structure and a variety of material samples,[46] boom-mounted probes,[39] and a 100 meter antenna.[39] The vehicle potential was controlled by the emission of energetic electrons or ions.[39] A xenon ion gun of the same type that is on board SCATHA has also been used to vary the potential of a sounding rocket.[38] The potential difference between the main rocket body and an electrically insulated end section was monitored. In laboratory experiments, the surface potentials of solar array segments immersed in simulated space environments have been measured as functions of array voltages.[36]

This chapter presents computations which predict the voltages of electrically insulated surfaces during such experiments. The theory sets upper and lower bounds for the surface potential at which there is net current balance, and shows how external electric fields determine the true equilibrium potential. The NASA Charging Analyzer Program (NASCAP) is used to predict potentials of insulated surfaces in the presence of exposed high voltage surfaces for a model space vehicle. Examination of the calculated potentials around the model shows clearly that the electric field component along the normal to insulated surfaces can either accelerate or suppress the emission of low energy secondary or photo electrons. For many cases this electric field control of the low energy electron currents plays a dominant role in determining the equilibrium surface potentials. The application of the theory to several charging problems is discussed. An important result is an explanation of the voltage "snapover"[36] phenomenon of coverslips on positively biased solar cells.

The computations herein deal with a generic spacecraft material exposed to plasmas near thermal equilibrium. They are not claimed to represent precisely any particular experiment. Our "typical material" has emissive properties similar to such insulators as kapton or teflon, and (to simplify the analysis) a conductivity so high as to be effectively metallic. It might be regarded as a conducting paint. However, the conclusions drawn are quite general, and should hold for all but the most extremely non-equilibrium environments and the most anomalous materials. Also, in performing calculations for low earth orbit conditions we have knowingly used NASCAP for a physical regime where it is not truly applicable. Here we have drawn only those conclusions which would be even more strongly supported by a more accurate model.

4.2 THEORY

In the presence of a fixed external voltage configuration, the voltage on a given surface varies according to the amount of charge accumulated on that surface. For highly resistive materials and for isolated conductors, the mechanism for changing the amount of charge accumulated is the collection and emission of charged particles by the surface. This is well known in spacecraft charging.[47,48] An insulated surface is at equilibrium when it achieves current balance, i.e., when the algebraic sum of the incident and emitted particle fluxes is zero. We restrict ourselves in this discussion to incident electrons and ions with kinetic energies in the 1 keV to 50 keV range. Such electrons have stopping distances short compared to material thickness, but they have sufficient energy to penetrate any surface effect barriers.

In a plasma, both electrons and ions are incident upon exposed surfaces. For a surface at plasma ground potential the electron current will be greater than the ion current by approximately the square root of the mass ratio unless the plasma is highly non-Maxwellian or non-neutral. By "plasma ground potential" we mean the potential measured by a Langmuir probe distant from the spacecraft. The particles emitted by the surface are almost exclusively electrons. These emitted electrons fall into two categories: The first consists of originally incident particles which have undergone large-angle scattering inside the material such that they re-emerge from the top surface. These backscattered, or redirected, primaries have, on average, about two-thirds of the incident electron energy.[1] The second consists of secondary electrons. These electrons are generated via ionization of the material by primary ions and electrons. The secondary electrons have only a few electron volts of kinetic energy. While the fraction of primary electrons undergoing backscatter is a fairly weak function of the incident spectrum, the secondary electron yield is a strong

function of energy, and can be well in excess of unity. Figure 4.1 shows the secondary yield curve, as calculated by NASCAP, for our typical spacecraft material. It is the relatively low kinetic energy of the secondary electrons that complicates the response of isolated surfaces, as even a small potential barrier can substantially reduce the effective emitted current.

If one assumes an orbit limited formulation for the incident current densities, it is easy to generate a current-voltage characteristic for a surface material in a given plasma environment. As an example, the I-V characteristic for a spherical probe covered with our typical spacecraft material in an isotropic θ = 1 keV, n_e = n_i = 1 cm^{-3} Maxwellian plasma is shown in Figure 4.2. (We assume the probe to be small compared with the 235 m plasma Debye length, so that space charge effects are totally negligible.) The lower current-voltage characteristic has been generated assuming that all low energy secondary electrons escape from the surface. For this case, the I-V characteristic is non-monotonic. The backscattered, electron-produced-secondary and proton-produced-secondary electron currents were calculated using analytical models from NASCAP. These models have been shown to compare well with experiment. Table 4.1 shows the components of the current as a function of voltage. Notice how the secondary electron current is always comparable to the incident current.

When incident upon an uncharged surface, this spectrum of electrons produces more backscattered and secondary electrons than there are captured primary electrons. This leads to a net positive current. It is a property of orbit-limited-collection of a Maxwellian plasma that the spectrum of the incident repelled species is independent of the surface voltage.[49] As a result the net current remains positive for all negative voltages, but the amplitude of the electron contribution drops off with increasing negative voltages. The rise in net current at high negative voltages is due to the increased ion current. For positive surface voltages the electron

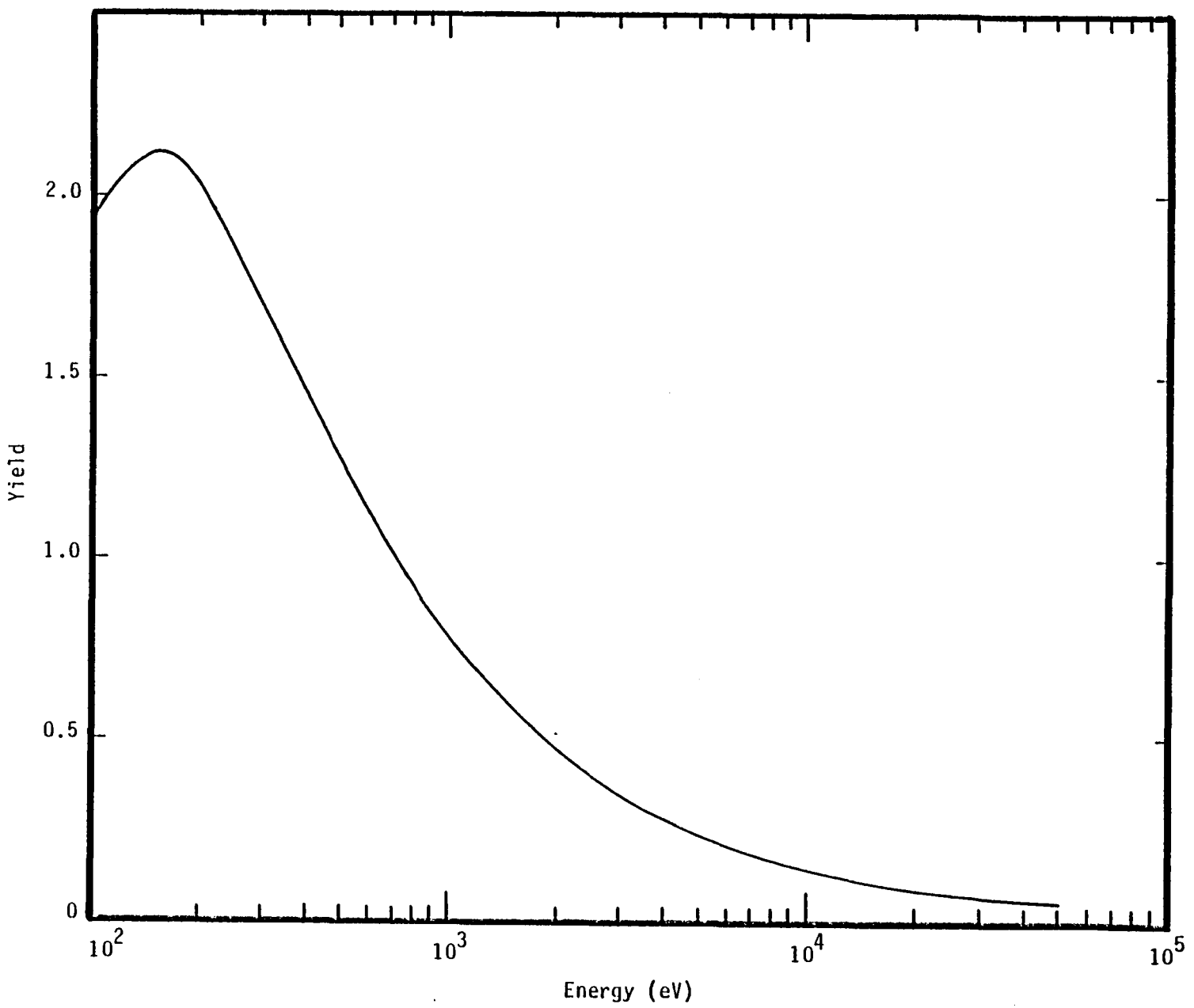

Figure 4.1. Secondary electron yield for normally incident primaries as a function of primary electron energy for the material used in the calculations below.

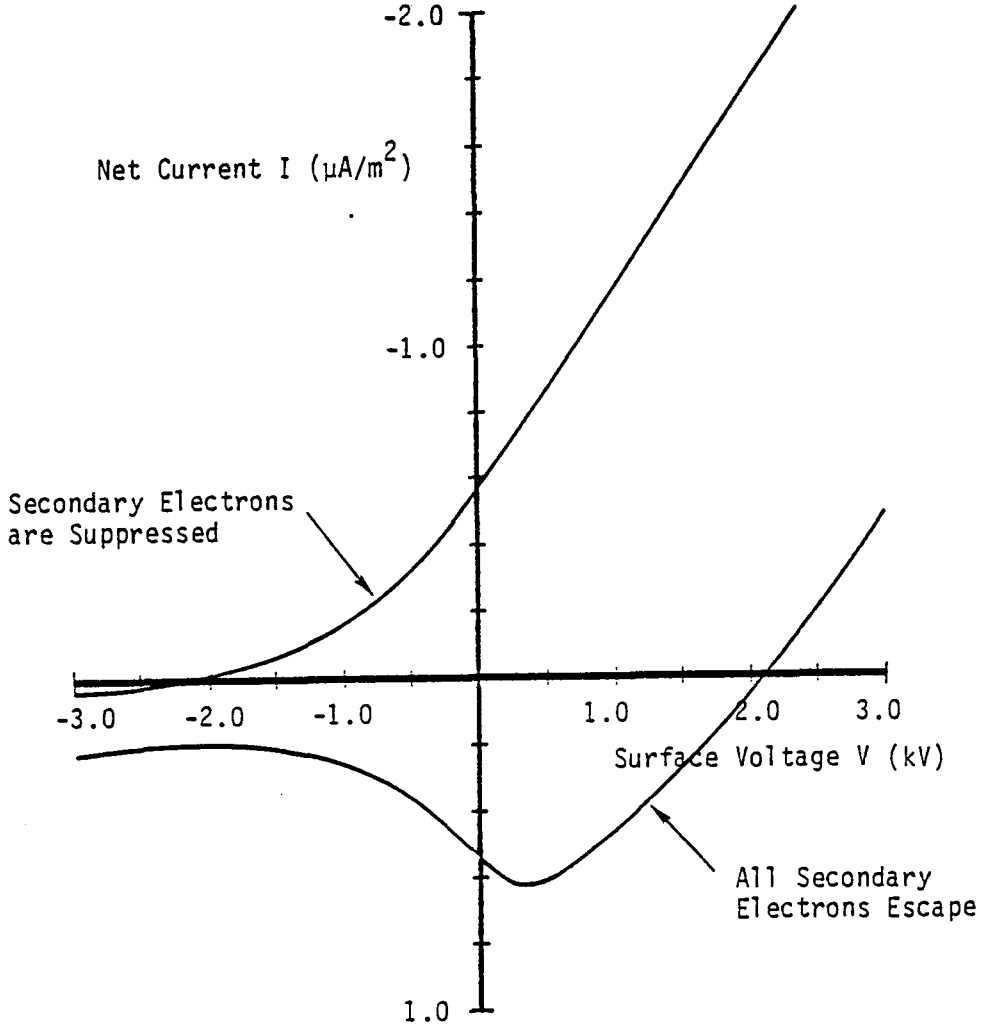

Figure 4.2. The current-voltage relation for a typical spacecraft material, with and without secondary electron emission, in a hydrogen plasma of temperature 1 keV and density 10^6 m^{-3}. The lower curve is the second column of Table 4.1, and the upper curve is the sum of the third, fifth and sixth columns.

TABLE 4.1. PARTICLE FLUXES FOR TYPICAL SPACECRAFT MATERIAL EXPOSED TO A 1 keV, 10^6 m^{-3} MAXWELLIAN. All currents are in amps/meter^2.

Surface Voltage V (keV)	J_{tot}	$J_{incident\ electrons}$	$J_{secondary\ electrons}$	$J_{backscattered\ electrons}$	$J_{incident\ ions}$	$J_{secondary\ electrons\ (from\ ions)}$
3.00+000	-4.78-007	-3.39-006	1.93-006	9.77-007	9.87-010	7.66-010
2.70+000	-3.25-007	-3.13-006	1.89-006	9.14-007	1.33-009	1.03-009
2.40+000	-1.75-007	-2.88-006	1.85-006	8.49-007	1.80-009	1.40-009
2.10+000	-3.03-008	-2.63-006	1.81-006	7.83-007	2.43-009	1.88-009
1.80+000	1.09-007	-2.37-006	1.76-006	7.15-007	3.28-009	2.54-009
1.50+000	2.42-007	-2.12-006	1.71-006	6.46-007	4.42-009	3.43-009
1.20+000	3.67-007	-1.86-006	1.65-006	5.75-007	5.97-009	4.63-009
9.00-001	4.79-007	-1.61-006	1.57-006	5.02-007	8.06-009	6.25-009
6.00-001	5.68-007	-1.36-006	1.48-006	4.24-007	1.09-008	8.44-009
3.00-001	6.15-007	-1.10-006	1.35-006	3.43-007	1.47-008	1.14-008
.00	5.38-007	-8.50-007	1.09-006	2.61-007	1.98-008	1.54-008
-3.00-001	4.19-007	-6.29-007	8.08-007	1.93-007	2.58-008	2.07-008
-6.00-001	3.35-007	-4.66-007	5.99-007	1.43-007	3.17-008	2.77-008
-9.00-001	2.78-007	-3.45-007	4.44-007	1.06-007	3.76-008	3.62-008
-1.20+000	2.41-007	-2.56-007	3.29-007	7.85-008	4.35-008	4.60-008
-1.50+000	2.18-007	-1.90-007	2.44-007	5.82-008	4.94-008	5.69-008
-1.80+000	2.07-007	-1.40-007	1.80-007	4.31-008	5.54-008	6.88-008
-2.10+000	2.04-007	-1.04-007	1.34-007	3.19-008	6.13-008	8.15-008
-2.40+000	2.08-007	-7.71-008	9.90-008	2.37-008	6.72-008	9.51-008
-2.70+000	2.16-007	-5.71-008	7.33-008	1.75-008	7.31-008	1.09-007
-3.00+000	2.29-007	-4.23-008	5.43-008	1.30-008	7.91-008	1.25-007

spectrum drifts toward higher energies, with the minimum incident electron energy equal to the surface voltage. Since higher energy electrons produce fewer secondaries, the net current decreases with increasing voltage. The single point of zero net current corresponds to an equilibrium surface voltage of +2100 volts. This can be achieved only if there are sufficient higher voltage surfaces in the vicinity to create a surface electric field that allows the secondary electrons to escape. Note that space charge has a negligible effect under these conditions. The largest component of space charge, that due to emitted photoelectrons, has a current of $\sim 10^{-4}$ A/m^2, an energy of ~2 eV, and thus a density of $\sim 10^{-10}$ coul/m^3. Thus, space charge creates field gradients ($\nabla \cdot \vec{E}$) of ~10 V/m^2. Since we are dealing with kilovolt potentials and meter lengths, the maximum effect of space charge is about 1 percent.

In Figure 4.2 the upper curve shows the current-voltage characteristic of the same material if secondary electrons were neglected. Physically this would occur in the presence of strong electric fields which suppress secondary electron emission. Again the surface has only one equilibrium potential, but now it occurs at -1950 volts. The change in equilibrium is over 4000 volts, and is brought about by the confinement or escape of the secondary electrons. The behavior of the secondaries can be controlled by the direction of the component electric field normal to the surface.

The direction of the surface normal electric field is a function of the local potentials and geometry. Near two coplanar conducting surfaces of different voltage, the field lines are semicircular as shown in Figure 4.3. This means that near their mutual boundary two conducting surfaces with differing potentials have surface normal electric fields of opposing directions. In this region the more negative surface will emit secondary electrons, while secondary emission will be suppressed on the more positive surface.

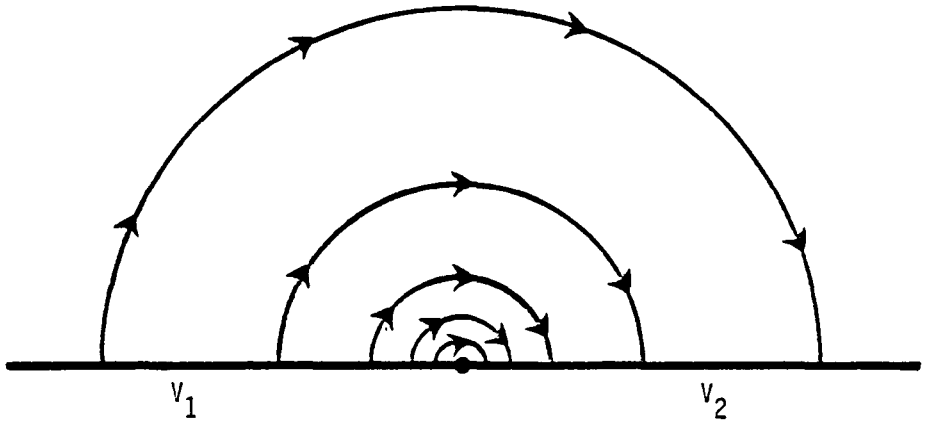

Figure 4.3. Electric field structure near the boundary of two conductors. The potential ϕ, is given by

$$\phi = V_2 + \frac{(V_1 - V_2)}{\pi} \theta$$

where θ is the angle measured counterclockwise from the boundary line.

Since the normal electric field magnitude and direction are not uniform over a complicated object, specific multidimensional calculations are necessary to determine the current-voltage relationship of a given surface in the presence of other high voltage surfaces. Under these circumstances we commonly encounter surfaces in a state of "field reversal", i.e., positive surfaces which repel electrons ($V > 0$ but $\vec{E} \cdot \hat{n} < 0$) and negative surfaces which attract electrons ($V < 0$ but $\vec{E} \cdot \hat{n} > 0$). Here V is the potential of the surface relative to plasma ground potential, $\vec{E}$ is the electric field external to the surface, and $\hat{n}$ is the unit outward surface normal. The equilibrium achieved by such surfaces is often between the extremes of all secondary electrons escaping and all secondaries being trapped. For conducting surfaces, equilibrium means

$$I = \int j \, ds = 0$$

where the current density j is a function of the potential and the local electric field. From the data in Table 4.1 we may calculate an entire family of floating potentials for a conducting surface in a 1 keV plasma. When at potential V the surface, due to the presence of other high voltage surfaces, will have a positive (electron attracting) field over a fraction $\alpha(V)$ of its area, and negative (electron repelling) fields over a fraction $(1 - \alpha(V))$. The mean current density (the total current I(V) divided by the area A) is given by

$$I(V)/A = [1 - \alpha(V)] \, J_{TOT}(V) + \alpha(V)[J_{TOT}(V) - J_{SEC}(V)]$$

where $J_{TOT}(V)$ is given by the second column of Table 4.1, and $J_{SEC}(V)$ is the sum of the fourth and seventh columns. Setting the mean current density to zero allows solution for

$$\alpha_o(V) = J_{TOT}(V)/J_{SEC}(V).$$

Figure 4.4 shows (solid line) the function $\alpha_o(V)$ calculated from Table 4.1. The condition $0 \leq \alpha_o(V) \leq 1$ leads to a family of solutions $-1950 \leq V \leq 2100$ volts. To find the solution to a given problem, one must calculate $\alpha_E(V)$, the fraction of surface area

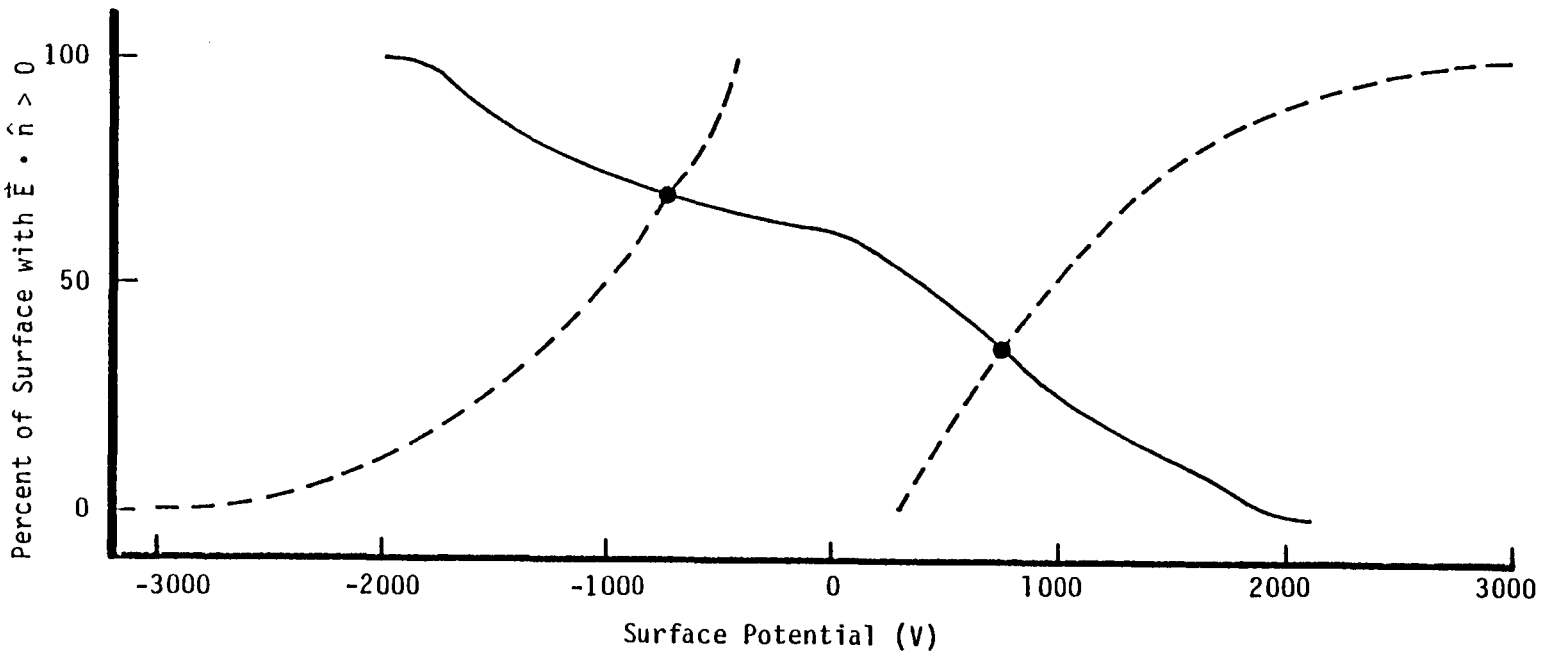

Figure 4.4. Locus of floating potentials, $\alpha_0(V)$, for the material of Table 4.1 (solid curve). The dashed curves (schematic) are $\alpha_E(V)$ for the two problems discussed below.

having positive electric field as obtained by solving the electrostatic problem with the surface in question at potential V. The dashed curves in Figure 4.4 indicate (schematically) such solutions for two problems described below. The intersection point $\alpha_o(V) = \alpha_E(V)$ gives the floating potential for the conducting surface.

Similar considerations obtain for dielectric surfaces, the difference being that a dielectric surface need not be an equipotential. Neglecting conductivity effects, the net current to each surface point varies from J_{TOT} to $J_{TOT} - J_{SEC}$ as the local surface normal electric field varies from zero to a small positive (electron-attracting) value. Thus the potential of an insulating surface may be found by solving an electrostatic problem where each insulating surface point satisfies either:

a. $V = V_1$ and $E \leq 0$,
   where V_1 is defined by $J_{TOT}(V_1) = 0$

or

b. $V = V_2$ and $E > 0$,
   where V_2 is defined by $J_{TOT}(V_2) - J_{SEC}(V_2) = 0$

or

c. $V_2 < V < V_1$ and $\vec{E} \cdot \hat{n} = 0^+$

where 0^+ indicates a small, positive value. For good insulators, the equilibrium voltage is frequently just that voltage where the electric field starts to suppress the secondaries. Indeed, if secondaries are copious, many different materials will respond alike, charging to within a few volts of where the electric field changes sign.

For photoemission this effect, previously suggested by several other authors[50,51,52] was shown computationally by Mandell et al.[12] and Stannard et al.[16] Recent calculations by Chaky et al.[53] have shown the importance of secondary emission in determining voltage profiles for low temperature plasma collection.

To summarize, this section presents a theory for materials, environments, and potentials lying within a "regime of uncertainty", defined as the set of conditions for which the surface in question has a net positive current if all secondary electrons escape, but a net negative current if secondary emission is suppressed. Such a surface achieves equilibrium either by (a) leaving the "regime of uncertainty", or (b) achieving a condition in which an appropriate fraction of secondary emission is suppressed. Normally a surface at positive potential relative to plasma ground has full suppression of secondaries, and will discharge toward plasma ground in search of equilibrium. However, if still more positive surfaces are present, secondary emission may not be suppressed. In such a case the surface will search for equilibrium at higher potential. Similarly, a surface negative with respect to plasma ground may have suppression of secondary emission in the presence of still more negative surfaces. The main determinant of secondary electron suppression is the sign of the electric field component normal to the surface. Thus, a conducting surface will achieve condition (b) at a potential such that an appropriate fraction of its area is electron attracting. A dielectric surface must achieve condition (b) point by point, and thus have near zero normal component of electric field over its entire area

4.3 NUMERICAL CALCULATIONS

As an illustration of the physics that controls surface response we have performed a series of calculations using NASCAP. The test object, shown in Figure 4.5, is a right octagonal cylinder with an electrically distinct end section covered by our typical spacecraft material. The dimensions were chosen to represent the Aerobee F sounding rocket whose flight was reported by H. Cohen et al.[38] During the flight, positive ions were ejected from a gun mounted on the main rocket body. Measurements were made of the potential difference between the main rocket body and the electrically isolated end section. The NASCAP calculations presented here predict the equilibrium end section voltages for both positive and negative main

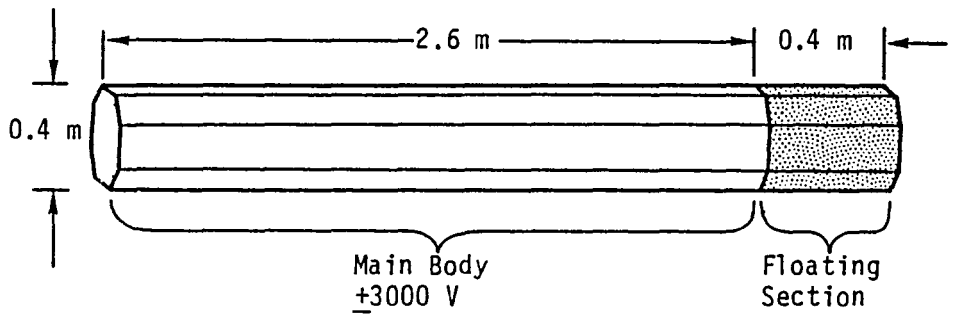

Figure 4.5. The object used for the NASCAP calculations.

body potentials. The environments were selected to represent a non-charging Geosynchronous Earth Orbit (GEO) (1 cm^{-3}, 1 keV) plasma and a Low Earth Orbit (LEO) (10^2 cm^{-3}, 0.1 eV) plasma. (The LEO particle density is set artificially low by a factor of a thousand in order to give the same thermal currents as the GEO environment.) In both cases a hydrogen plasma was assumed. Since NASCAP does not predict the space charge limited collection actually occurring in LEO (Debye length equal to .23 m), these calculations were intended to show some features that can be predicted and, particularly for the LEO positive ground calculations, the problem areas which remain unsolved. (As this problem has cylindrical symmetry, it is feasible to perform a more elaborate calculation taking space charge into account. Such a calculation is beyond the scope of this chapter.)

4.3.1 NEGATIVE GROUND

The first two calculations were carried out with the rocket body arbitrarily fixed at -3 kV. This is a situation similar to the ejection of unneutralized high energy positive ion beams whose current is controlled to maintain the rocket body potential. The NASCAP calculated end section potentials are shown in Table 4.2. For low altitude (Calculation I) we find this end section to be near plasma ground. This agrees with the experimental measurement[38] of the potential difference between the end section and the main body. For this the normal component of the electric field on the floating section is electron attracting everywhere, and the secondary electrons do not escape. Whether or not the secondary electrons escape makes little difference in the potentials for a 0.1 eV Maxwellian. Since the secondary electron yield is less than 1 percent of the incident current, its existence or absence makes less than a 1 percent change in the negative equilibrium potential (see Table 4.3). This is demonstrated in Figure 4.6 which shows the bounding I-V curves for a cool plasma environment. Notice how for negative potentials the boundary curves are extremely similar and that the negative equilibrium potentials are almost identical.

TABLE 4.2. RESULTS OF THE NASCAP CALCULATIONS ON THE OBJECT SHOWN IN FIGURE 4.1.

Calculation	I	II	III	IV
Main Body Potential	-3000 V	-3000 V	+3000 V	+3000 V
Plasma Density	100 cm^{-3}	1 cm^{-3}	100 cm^{-3}	1 cm^{-3}
Temperature	0.1 eV	1000 eV	0.1 eV	1000 eV
Floating End Potential	∿-1 V	-731 V	650 V	725 V
Required Beam Current*	4.5 mA*	23 μA	78 mA*	10 μA

*For cases I and III, screening effects would cause these values to be substantially reduced.

TABLE 4.3. EQUILIBRIUM SURFACE POTENTIALS FOR TYPICAL SPACECRAFT MATERIAL EXPOSED TO TWO PLASMAS. Note the existence of two stable equilibria in the cold plasma when all secondaries escape.

Plasma Environment	0.1 eV, 100 cm^{-3}	1000 eV, 1 cm^{-3}
Equilibrium Surface Voltage		
All Secondaries Escape	-0.2 V	+2040 V*
(Second Root)	+3100 V*	
Equilibrium Surface Voltage		
All Secondaries are Trapped	-0.2 V	-1950 V

*This equilibrium voltage is only achievable when neighboring surfaces are fixed at very high positive potentials.

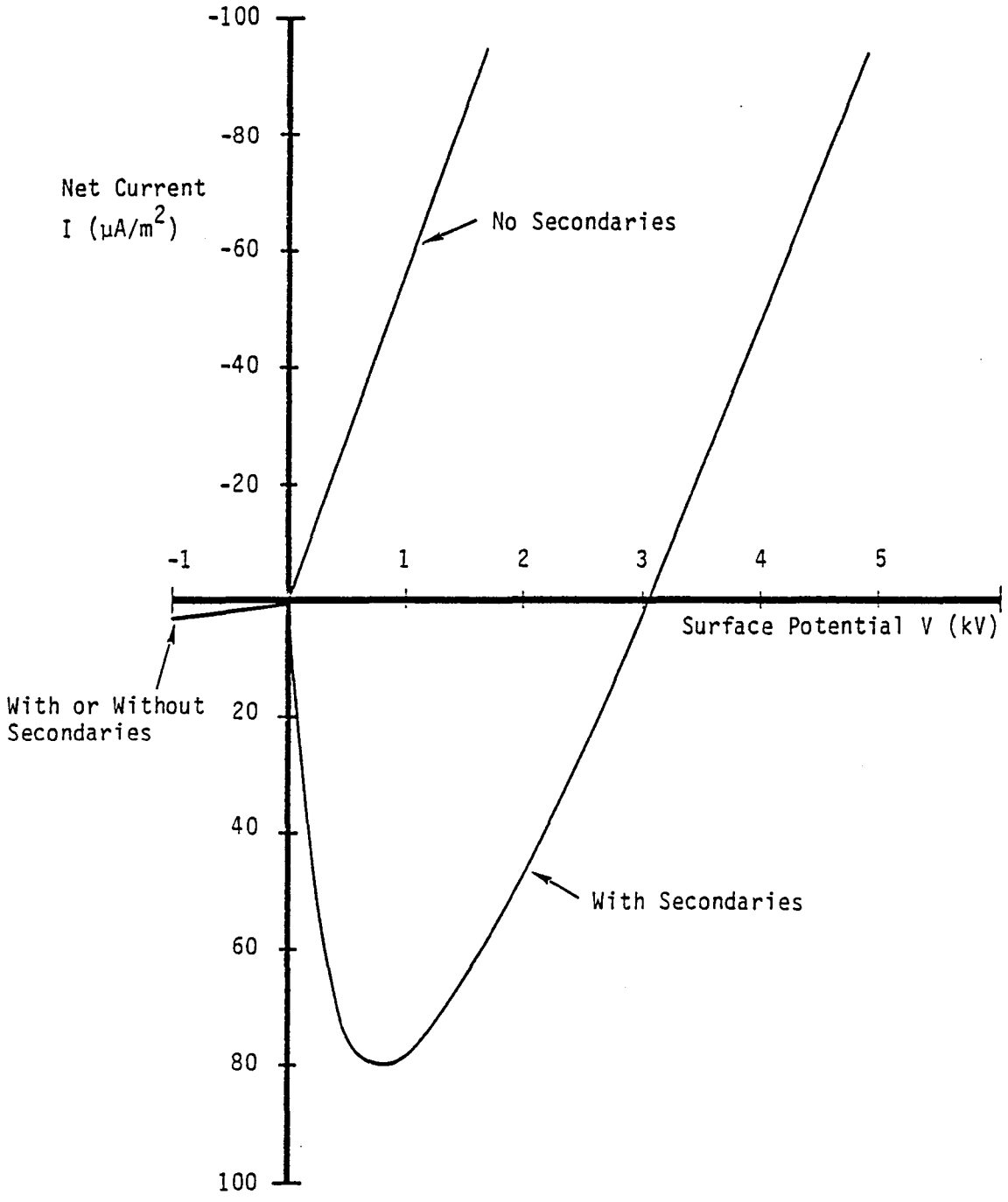

Figure 4.6. Net current-voltage relations for spacecraft material in a θ = 10 eV, n_e = 10 cm^{-3} Maxwellian plasma.

In the GEO-like environment (Calculation II) the end section voltage is much more negative with respect to plasma ground. The physical response is governed by the same phenomenon, that is, the normal component of the surface electric field stops low energy secondary electrons from escaping to the plasma. In Table 4.3, we see that for the GEO environment the escape of secondary electrons has a dramatic effect, causing up to a 4000 volt difference in the surface equilibrium potential. An examination of the zero volt fluxes (Table 4.1) shows that the secondary electron current is greater than the incident electron current, in contrast to the response for the 0.1 eV plasma. This is expected since the secondary yield starts out at zero for cold incident electrons and peaks at a yield of greater than one for several hundred volt incident electrons.

The floating voltage is not trivial to calculate because the sign of the electric field is not constant over the entire end section. While no secondary electrons escape from parts of the surface adjacent to the main rocket, the electric field at the end panel farthest from the rocket allows all secondaries generated there to escape. No single region of the end section is in local current balance, but at the calculated -731 volts the surface integral of the current is zero. This solution is indicated by the intersection of the left dashed curve and the solid curve in Figure 4.4. This type of calculation is inherently multidimensional in character. The more negative the main body, the further to the left on Figure 4.4 will be the solution, approaching the limiting case of full suppression of secondary electrons. For the 1 keV, 1 cm^{-3} environment we ran another NASCAP calculation with -10 keV on the rocket body. The result was that the end section went to -1750 volts, close to the -1950 volt limit from Table 4.3.

4.3.2 POSITIVE GROUND

Calculations with the spacecraft frame potential fixed at +3 kV were designed to simulate low current electron beam emission (such as that carried out on board the SCATHA spacecraft) when the beam current is just able to balance the incident plasma electrons. The geometry and environments used are the same as those for the negative ground cases. Again, the current levels for the 0.1 eV, 100 cm^{-3} plasma are overestimated because an orbit-limited (rather than a space-charged limited or a turbulent sheath) formulation is used for the current collection. However, the qualitative trends are clearly shown, and the results are general in their implications.

Table 4.2 shows the equilibrium potentials of the end section. The first point to notice is that for both environments the order of magnitude of the potential results is the same. This is in sharp contrast to the negative ground case. For the case of positive ground in the low temperature plasma the potential reached was 650 volts, while for the higher temperature plasma the potential was 725 volts. The solution for the higher temperature case is the intersection of the right dashed curve with the solid curve in Figure 4.4.

The electric field configuration (Figure 4.7) shows that in both cases the underlying physical processes are the same. Indeed, the particle flux description is much the same as that for negative ground; that is, for all surfaces the net flux would be positive (that is, more electrons out than in) if the secondaries were able to escape.

Examination of the field structure (Figure 4.7) in the region dividing the rocket body shows that while the electric field is electron attracting almost everywhere, there is field reversal very close to the boundary of the end section (as in Figure 4.3). Here, secondary electrons are accelerated off the surface and onto the main rocket body. If the electric fields were in this direction over the

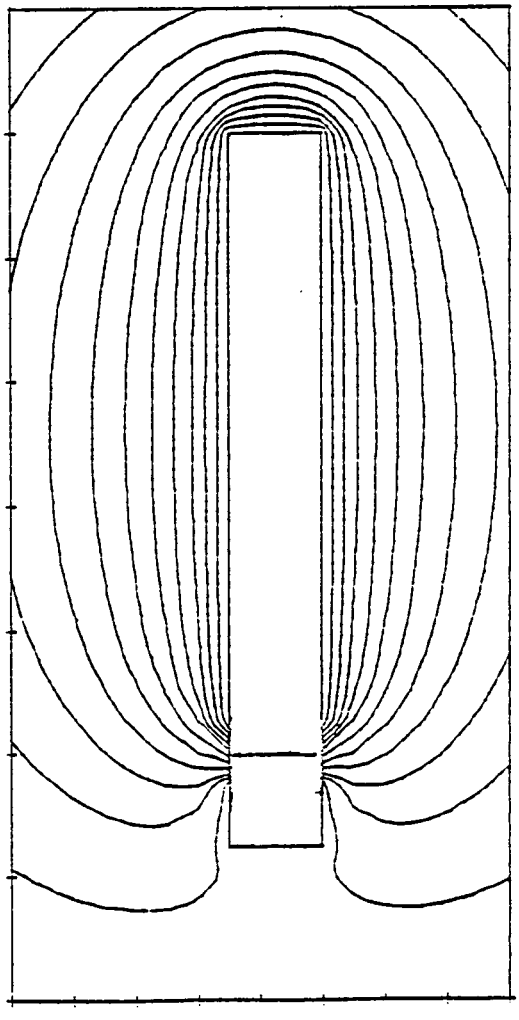

Figure 4.7. Potential contours (unscreened) around the object of Figure 4.5. The main body is at +3000 V and the end section at +725 V. The contour interval is 200 V. Secondary electrons emitted from the sides of the end section escape to the main body, while secondaries from the circular end cap are partially suppressed.

entire end section, the end potential would be 3100 V and 2040 V for the two low and high temperature environments respectively (Table 4.3). Over much of the end section, as on the entire main body, retarding electric fields suppress secondary electron emission. The equilibrium voltage is such that the secondary electrons leaving the field reversal region are exactly balanced by the total incident electrons collected by the end section. In the GEO environment the smaller secondary yield requires a smaller field reversal region to achieve current balance. This results in a smaller potential difference. In general, the higher the ratio of secondary electron currents to incident electron currents, the smaller the voltage difference between spacecraft sections. The region of positive field in case IV is about one-third of the end section area while it is about one-fourth the area in case III.

4.4 DISCUSSION

The phenomenon of equilibrium surface voltage being determined by the surface electric field structure is of general importance to studies of spacecraft high voltage interactions. In this section we will discuss how the previously described NASCAP calculations relate to experimentally observed phenomena. We will then show how this same theory provides an insight into the solar cell voltage snapover effect.

4.4.1 ROCKET EXPERIMENTS

The calculation which correlates most closely with rocket experiment[38] is case I. The calculation showed that when the main rocket body is charged to a negative potential of several kilovolts with respect to a plasma that has a temperature of a fraction of an electron volt. The rear section remains within a volt of plasma ground, i.e., almost the same voltage it would have achieved if the main body had not been charged. During the flight experiments reported by Cohen, Sherman and Mullen[38] the main rocket body potential was controlled by the emission of a one or two

kilo-electron-volt beam. Two sets of potentials were recorded: One from a thermal emissive probe mounted on a 152 cm boom extending into the sheath surrounding the rocket, and the other the voltage difference between the end section and the main body. Table 4.4 shows data taken at a plasma of ~1 x 10^3 cm^{-3}. At low currents the end section potential difference exceeds the probe potential difference by about two-thirds. A possible interpretation is that the end section was truly at plasma ground and the emissive probe was within the "plasma sheath" and measured 40 percent of the vehicle potential. Such an interpretation is supported by accompanying evidence that the full return current was collected from the ambient plasma. As the thermal ion current is ~5 x 10^{-8} A/m^2, the implied sheath radius is ~4 m. At a current of 400 μA of 2 keV ions the potential difference between the probe and the main body was saturated at just over a kilovolt. At such a high current level the effects of space charge are probably important. Nonetheless, the data are consistent with the interpretation that the main body is nearly 2 kV negative relative to plasma ground, the end section near plasma ground, and the sheath extends beyond the thermal probe.

Table 4.4. Experimental Data for Positive Ion Emission[38]

Current	Energy	$V_{probe} - V_{main}$	$V_{end} - V_{main}$
9 μA	1 keV	250 V	420 V
12 μA	2 keV	340 V	550 V
400 μA	2 keV	1000 V	(not given)

4.4.2 SCATHA MEASUREMENTS

While the positive ground calculations are not simulations of actual experiments, they do offer a great deal of qualitative insight into the electron gun experiments on board SCATHA. Analysis of the NASCAP calculations shows that the isolated surface achieves a potential such that the integral of the incident electron current is

balanced by the emission of low energy secondary electrons on that part of the surface which had field reversal; that is, where the low energy electrons could escape. The potential is determined by the ratio of low energy electron emission current to incident electron currrent. In the calculations presented in the previous section the low density, high energy plasma, drives the end section to +725 volts, which is 2275 volts negative with respect to the main body. The identical calculation but including solar photon generated secondary electrons (photoemission) produced an end section equilibrium of -1550 volts relative to the main body. The SCATHA measurements in general indicate smaller voltage differences between the spacecraft frame and various monitored surfaces when the surfaces are exposed to sunlight. This is in contrast to when they are shadowed, with the magnitude of this effect diminishing as the return current density becomes substantially greater than the photocurrents.

When the electron gun aboard the SCATHA spacecraft is operated at 1.5 keV at currents of 0.1 ma or higher the SCATHA structure potential reaches about +1500 volts, as expected. Potential measurements were made of electrically isolated surfaces.[46] Potential versus time for an isolated kapton surface is shown in Figure 4.8. The measurement was made on a spot where the metallization had been removed, so that the response time was a few seconds. Each spin period the potential varies between -10 and -80 volts with respect to the spacecraft structure, i.e., the surface voltage ranges between +1420 and +1490 volts with respect to plasma ground. From Figure 4.4 it is seen that in order to reach current balance at these voltages the external electric field must be limiting most, but not all, of the secondary electrons. Figure 4.8 shows that for the specific SCATHA geometry field reversal, which allows the escape of low energy electrons, occurs on this surface with less than a 100 volt difference between the surface and the positive satellite ground.

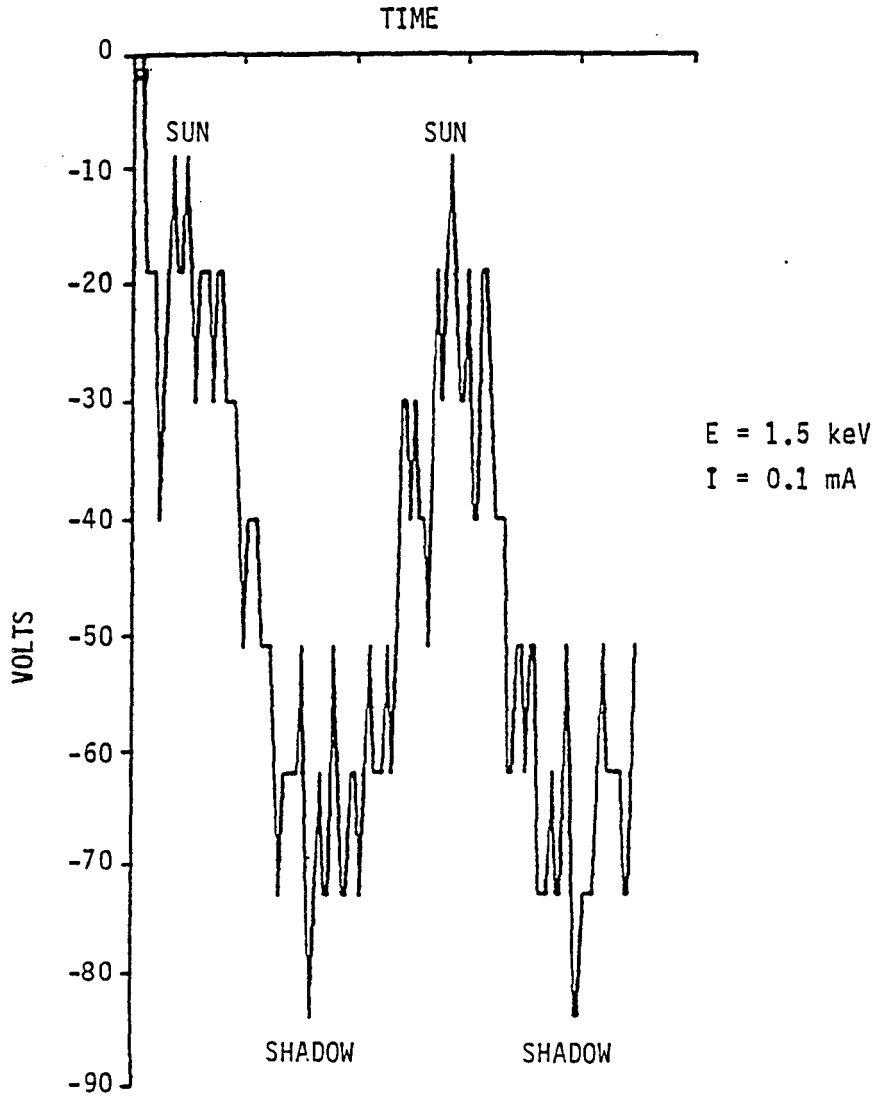

Figure 4.8. Voltage (relative to spacecraft structure) versus time for a kapton patch on the SCATHA spacecraft during beam operation (0.1 mA, 1.5 keV) and sunlight exposure. (The abscissa is marked in units of twenty-five seconds.)

As the kapton surface rotates into sunlight, the increased production of low energy photoelectrons requires proportionately fewer of them to escape to maintain current balance. For a positive structure potential this implies less of a voltage difference between the surface and the structure. This effect is also shown in Figure 4.8. Initially, in full sunlight, the potential of SSPM surface is only 10 V negative relative to the spacecraft frame. As the rotation of the satellite moves the surface into full shadow the potential difference rises to -80 volts. Returning to sunlight again the potential difference drops back to -10 volts, and continues to oscillate with the satellite rotation. (The apparent low amplitude modulation superimposed upon this pattern is due to the discreteness of the data collected.) NASCAP modeling of this SCATHA case is hampered by the detailed spatial resolution necesary to calculate field reversal regions, and by difficulties in determining the space charge limited beam dynamics. However, NASCAP does predict that surfaces in sunlight charge to potentials close to the spacecraft frame potential, as opposed to discharging to plasma ground.

When the electron gun on board SCATHA operates at 3 keV and 0.1 ma the satellite frame goes to about +3000 volts. When the surface from the previous example is in the sunlight the observed voltages are again similar to the spacecraft frame potential, since the low energy photoemission is much larger than either the collected ambient electrons or the returning beam electrons. However, as seen in Figure 4.9, in shadow the surface potential drops to about -800 volts with respect to spacecraft structure or +2200 volts with respect to the plasma. From the discussion of the example with the 1500 volt structure potential we saw that a differential as small as 100 volts between the sample and the spacecraft was enough to enable low energy electrons to escape the surface. Thus, for a several hundred volt differential all secondaries will escape and the surface will have a current-voltage response like the lower curve of Figure 4.2. Figure 4.2 shows that in the absence of photoemission the material used in our calculations would charge to only +2100 volts, similar to the

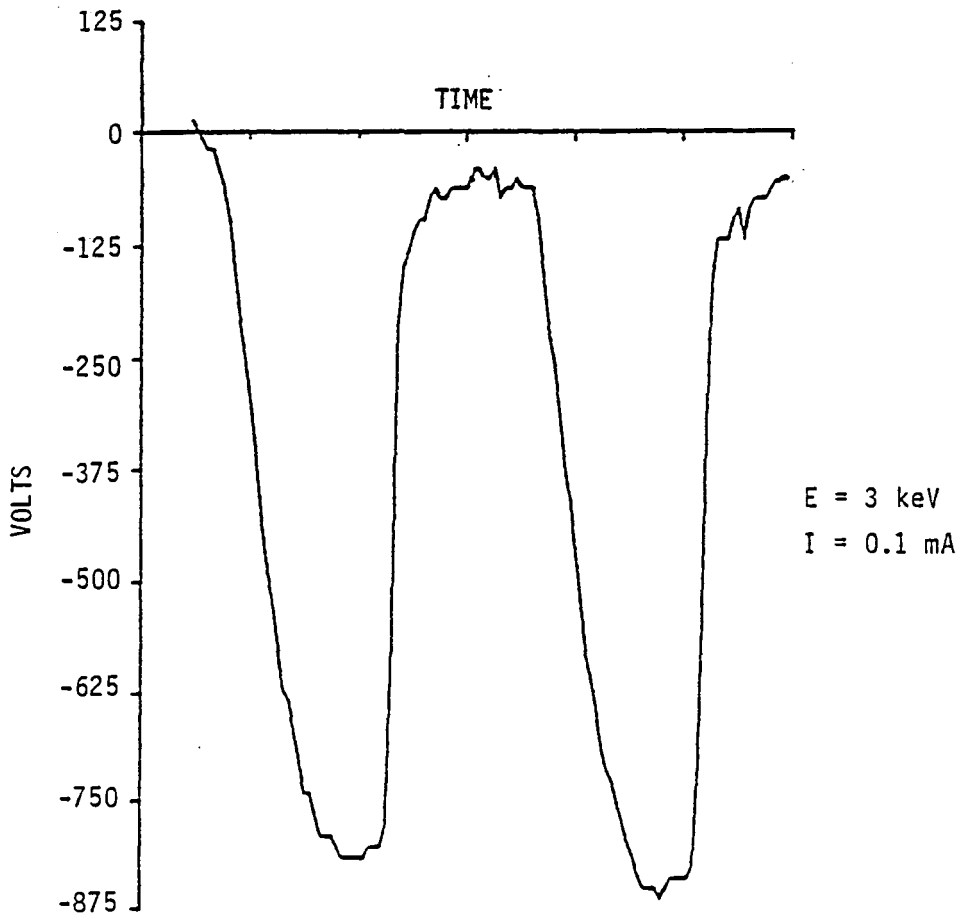

Figure 4.9. Voltage (relative to spacecraft structure) versus time for a kapton patch on the SCATHA spacecraft during electron beam operation (3 keV, 0.1 mA) and sunlight exposure. (The abscissa is marked in units of twenty seconds.)

observation. Note the contrast between the +1500 volt case, where the equilibrium was on an intermediate I-V curve due to field limiting, and the +3000 volt case, where the equilibrium was on a bounding curve; without the extra photoemission, there is not enough secondary emission to reach a potential greater than +2200 V relative to plasma ground.

4.4.3 SOLAR CELL "SNAPOVER"

An interesting product of these calculations is a possible explanation of the "snapover" effect in high volt solar array experiments. As observed by N. J. Stevens[36] when a solar array is biased to less than 100 volts positive with respect to a surrounding plasma, the surface of the quartz coverslide remains near zero potential. However, if the array voltage is over +200 volts, the coverslide surface potentials jump to within about 50 volts of the array potential. This can be explained in terms of the current voltage relations of a surface in a cold plasma. Figure 4.6 shows the current voltage relations with and without secondary electrons for a surface exposed to a 10 eV plasma. The curve without secondary emission is monotonic. The curve with secondary emission is non-monotonic and its three zero current points are shown schematically in Figure 4.10. The zero current points at -18 volts and +3100 volts correspond to stable equilibria. The zero current point at 17 volts is unstable; if secondary electrons can escape, a surface which starts at a voltage below 17 volts will go towards -18 volts; a surface which starts above 17 volts will go towards +3100 volts.* However, as we saw in the positive ground calculations, the highest possible positive voltage equilibrium point is frequently not achieved because as the surface voltage nears that of the underlying ground, the direction of the surface electric field changes sign,

---

*The existence of multiple roots have been discussed previously by several authors[54,55] for multiple Maxwellian spectra and magnetic surface potentials.

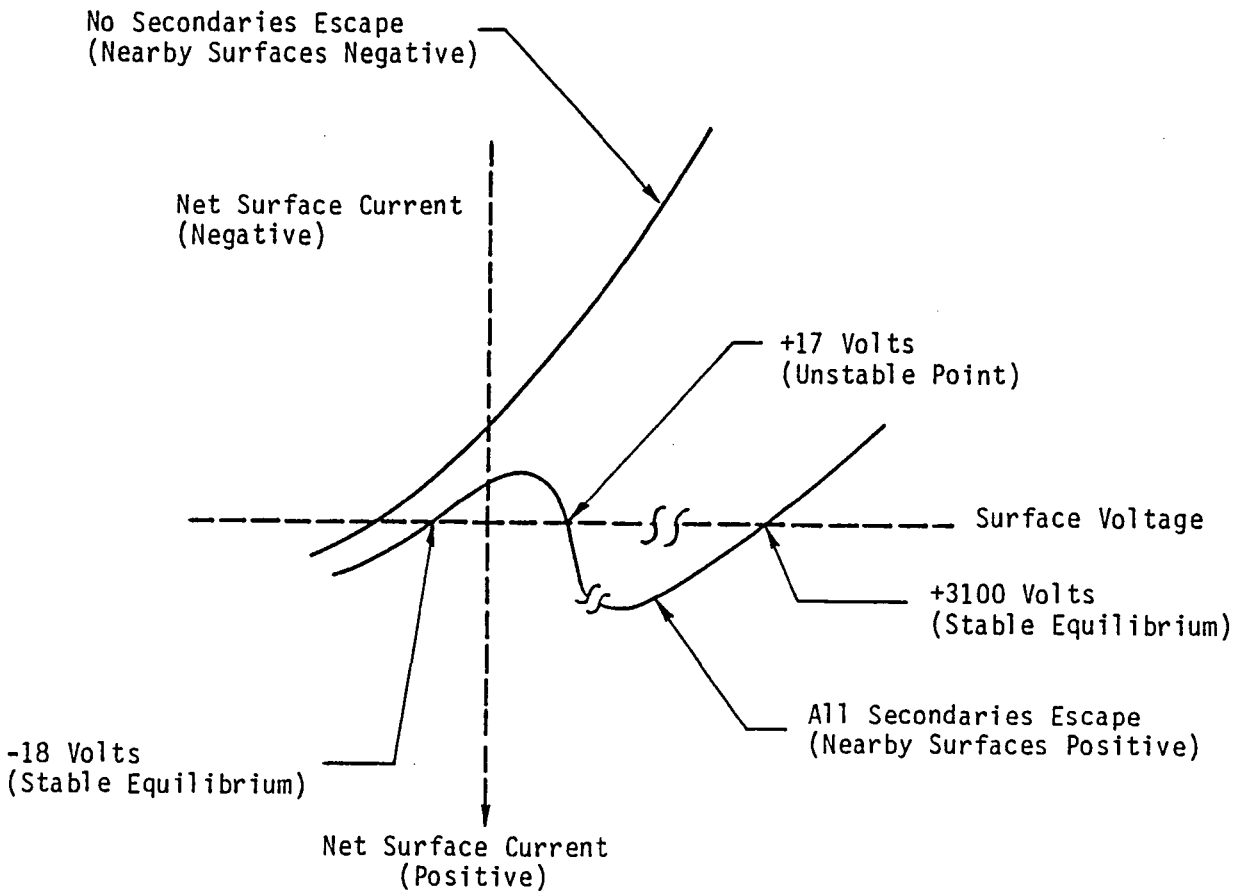

Figure 4.10. Schematic representation of the two bounding I-V curves for spacecraft material in a 10 eV Maxwellian plasma. Notice that in the presence of positive surfaces there are two possible equilibria. Which is achieved depends upon the initial conditions.

suppressing the secondary electron emission. For a cooler plasma, the zero current voltages are modified somewhat; e.g., for the θ = 0.1 eV, n_e = 100 cm^{-3} plasma they occur at -0.2, 25 and 3100 volts. Sheath effects which alter the angular distribution of incident electrons can also change the zero current voltages.

In a typical experiment positive voltage is applied incrementally to the solar array. Since the front surface of the coverslide is coupled capacitively to the array, all changes in the array voltage are transmitted instantly to the surface. The surface current then charges or discharges the coverslide until a zero current point is reached. If the initial voltage increments are small (i.e., no larger than 17 volts) the coverglass will constantly relax towards plasma ground. However, if the voltage increment is larger (~50 volts) the coverglass will go towards a positive stable equilibrium point. As the array potential becomes sufficiently high a similar effect can also be caused by surrounding potentials modifying the incident electron spectrum. When the coverglass potential is sufficiently positive to suppress most of the secondaries, the voltage will stabilize. Experimentally this has been observed to occur at about 50 volts below the array voltage.

4.5 SUMMARY

We have presented a theory of isolated surfaces in the presence of high voltages. We have shown that in given plasma environments there are two bounding current-voltage characteristics: one for the case with all emitted secondary electrons escaping, the other for the case with all the secondaries suppressed. Numerical calculations have indicated that for many cases the steady state surface voltage is not an equilibrium value associated with either of these bounding curves, but lies somewhere in between, occurring where the external electric field suppresses an appropriate fraction of the secondary electrons. The calculations performed here agree qualitatively with flight experiments. They also suggest a possible explanation of the solar array "snapover" phenomenon observed in the laboratory.

5. LARGE SPACE STRUCTURE MODELING

5.1 INTRODUCTION

Since the launch of the space shuttle the interaction of large space structures with the plasma environment in the earth's polar regions has been of increasing interest. In the next section we discuss briefly some of the physics pertinent to this problem. Based upon these considerations we have developed a physical model capable of modeling the interactions of large objects with the Polar Earth Orbit (PEO) environment. This is discussed in Section 5.3. This model will be incorporated into a new computer code (to be called POLAR, Potentials of an Orbiting Large Spacecraft in the Auroral Region). A very preliminary version of this code is discussed in Section 5.4, along with a test case in Section 5.5. Finally, some considerations concerning beam emission in PEO are discussed in Section 5.6.

5.2 BACKGROUND

The plasma environment in the polar regions is strongly affected by the earth's magnetic field. The ambient plasma at altitudes of several hundred km is both dense and cool. Flux distribution functions are characterized by temperatures on the order of 0.1 eV, and by densities of $\sim 10^{11}$ m^{-3}. If this represented all of the charged particles present there would be little concern about spacecraft charging. However, electron fluxes with energy in the 10 keV range regularly penetrate into the auroral region along terrestrial magnetic field lines. Objects encountering these fluxes accumulate charge and acquire a net negative potential. A spacecraft exposed to a steady high energy electron flux will charge to a sufficiently negative potential to draw a balancing ion current from the relatively cold ambient plasma.

In a cold dense plasma, Debye lengths are short ($\lambda_D \sim 0.01$ m) and collection of attracted particles (ions) is space-charge limited. Under these conditions an ion sheath surrounds the spacecraft, so that a much greater negative potential is required to collect a given ion current than under orbit limited conditions. Furthermore, the required (equilibrium) potential shows a more than linear increase with the size of the object. Thus while a small spacecraft like the INJUN 5 satellite was observed to charge to -40 volts in the auroral region, objects many times larger, such as the shuttle orbiter or a space based radar antenna, might charge to kilovolt potentials.

The presence of kilovolt potentials on a spacecraft greatly increases the possibility of perhaps damaging discharges. Parks and Katz[56] showed, on the basis of a simple analytical model, that the currents and potentials possible for a spacecraft having dimensions similar to the shuttle orbiter correspond to those immediately preceding the discharge-induced interruption of telemetry, and failure of instrumentation, that occurred onboard the P78-2 (SCATHA) satellite on day 89-4, 1979. Obviously, this raises serious questions regarding the operation of shuttle and other large space structures in the auroral region. The POLAR CODE will address these questions in the much greater detail that they deserve.

The code is intended to model a spacecraft, large compared to the ambient plasma Debye length, moving at supersonic speed and creating a wake in the plasma behind it. Charge collected from precipitating auroral electrons is balanced by positive charge collected from the ion sheath, mainly as ram ions in front of the spacecraft. (Collection from the wake region is diminished due to depletion of the ion density. This raises the possibility of differential charging between the front and back of the spacecraft.) The operation of onboard electron emitters introduces the possibility of a positive ground and collection of current from an electron sheath. The structure of the electron sheath is complicated by secondary ionization and heating effects as discussed in Section 5.6.

5.3 THE POLAR PHYSICAL MODEL

To calculate the potentials on an object (e.g., the shuttle orbiter) the net charge flowing to the object must be calculated. This requires algorithms for electron and ion current collections. These are discussed below.

5.3.1 ELECTRON CURRENT COLLECTION

The presence of the surrounding ion sheath effectively excludes the cold ambient electrons from the spacecraft surface, and electron collection is derived entirely from the high energy electrons concentrated in the auroral region by the terrestrial magnetic field. The spectrum of this flux corresponds approximately to a Maxwellian accelerated by the terrestrial fields to several kilovolts. The portion of the spectrum with energy comparable to the accelerating potential has an angular distribution that is strongly aligned with the magnetic field lines. The remainder of the spectrum above and below this region is more isotropic and makes a smaller contribution to the total current collected. With this picture in mind a suitable analytical representation of the flux distribution function, $f_e(E,\underset{\sim}{\Omega})$ for the auroral electrons may be devised, for both energy E, and direction $\underset{\sim}{\Omega}$.

The ion sheath has little effect upon the incoming high energy electrons and the incident current will be calculated assuming that it is orbit-limited in three dimensions; i.e., the incident flux is given by

$$FIN = \int dE \int d\Omega \left(\frac{2E}{m}\right)^{1/2} f_e(E,\Omega) \left(1 + \frac{V}{E-V}\right)$$

where V is the electrostatic potential of the spacecraft. The backscatter and secondary electrons (FOUT) resulting from FIN can be calculated analytically for each surface cell in the same way:

$$FOUT = \int dE \int d\underset{\sim}{\Omega} \left(\frac{2E}{m}\right)^{1/2} \delta(E,\underset{\sim}{\Omega})\ f_e(E,\underset{\sim}{\Omega}) \left(1 + \frac{V}{E-V}\right)$$

where δ is the relevant yield. Analytical models for the secondary emission and backscatter yields are available that reproduce the behavior of each surface material as accurately as possible, within the constraints of practical computation time.

5.3.2 ION CURRENT COLLECTION

Ions are collected from the cold dense plasma surrounding the spacecraft. Since the Debye length of the environment is so short (~0.01 m) compared with dimensions of the orbiting vehicles of interest (several meters), the flow of attracted ions to a negatively charged spacecraft is space-charge limited. Under these conditions a sheath of ions forms around the object and screens its potential very effectively. It should be noted that ion collection has been observed to behave classically, that is without sheath heating or ionization.[39]

To calculate the ion current incident at each surface cell of the spacecraft, the outer boundary of the ion sheath, beyond which the spacecraft potential is assumed completely screened, must be identified. The sheath boundary is defined to be the locus of points where the potential energy $e\phi$ is of the same order as the thermal energy of the undisturbed ions.

The total ion current crossing the boundary into the sheath may be calculated by summing over the currents incident at each boundary surface cell. By choosing an analytical representation for the ambient ion flux distribution function, the incoming current for each boundary cell can be found in a way similar to that described for the

electrons in Section 5.2.1 for the case of zero spacecraft potential. (Recall that we assume it to be perfectly screened.)

Not all of the ions entering the sheath will arrive at the surface of the spacecraft. The proportion of the current collected by each surface cell, along with its energy and angle of incidence, can be determined statistically by tracking particles from the sheath boundary to the surface. The ion induced secondary electron emission from the surface materials depends only upon incident angle and energy and can be calculated from the particle tracking information. The particle tracking can be performed using the latest algorithms based upon the well-tested and computationally economical "leapfrog" method.[2] This technique is more reliable than predictor-corrector methods for arbitrary cases.

In order to calculate the sheath boundary, the potential in space around the object, $\phi(\vec{r})$, must be known; i.e., we must solve the Poisson-like equation

$$\varepsilon\nabla^2\phi + \rho(\phi) = 0$$

where $\rho(\phi)$ is the charge density.

If we assume an object moving through the plasma at supersonic speed, the natural frame in which to solve this equation is that moving with the spacecraft velocity $\vec{V}_o$. In this frame one can define a potential ϕ_o such that

$$\phi_o(\vec{r}) \to 0 \text{ as } \vec{r} \to \infty$$

then

$$\phi_o(\vec{r}) \to \phi_{surface} - \phi' \text{ as } \vec{r} \to \vec{r}_s$$

where ϕ' is defined below. At distances far from the spacecraft the potential ϕ_0 is shielded and falls to zero. The potential actually on the spacecraft ($r = 0$) may be divided into a contribution $\phi_{surface}$, that would survive for a stationary object, and a term ϕ' that results directly from the interaction of the spacecraft motion and the terrestrial magnetic field. A conductor moving across a magnetic field $\vec{B}$ experiences an electric field (the Hall effect) resulting in "eddy" currents. The potential ϕ' opposes these currents and is derived from the $\vec{V}_0 \times \vec{B}$ electric field:

$$\phi' = -\vec{V}_0 \times \vec{B} \cdot \vec{r}$$

Before the potential equation can be solved a form for the charge density $\rho(\phi)$ is required. An analytical representation for $\rho(\phi)$ will be chosen that shows the expected limiting behavior for large and small potentials. As an example consider a stationary object. The charge density in the surrounding space is adequately modeled by the form:

$$\frac{\rho(\phi)}{\varepsilon_0} \approx -\frac{\phi}{\lambda_D^2}\left[1 - (4\pi)^{1/2}\left(\frac{e\phi}{k\theta_i}\right)^{3/2}\right]^{-1}$$

When the potential ϕ is much smaller than the ambient ion temperature θ_i this form reduces to a simple Debye shielding formula

$$\frac{\rho(\phi)}{\varepsilon_0} = -\frac{\phi}{\lambda_D^2}$$

where the Debye length, λ_D, is given by

$$\lambda_D^2 = \frac{\varepsilon_0 k\theta_i}{N_0 e^2}$$

In the opposite limit $\rho(\phi)$ corresponds to that for an accelerated Maxwellian, given simply by the ratio of the one-sided thermal current density j and the ion velocity v_i.

$$\rho = -j/v_i$$

Inspection of these relationships show that $\rho(\phi)$ depends on just the ion temperature, number density, N_0, and current density. For a neutral stationary object these are independent of position $\vec{r}$. This is unfortunately not the case for an object moving with supersonic speed.

The moving spacecraft leaves a wake, depleted of ions, behind it. This will naturally affect the density of electrons in the wake region and cause both the number and current density to be dependent on position in general. The analytical form for the density, $\rho(\phi)$ included in the POLAR code will utilize iteratively determined estimates of the local number and charge densities.

In the absence of electric and magnetic fields the local densities can be calculated by assuming that the ions follow straight-line trajectories and behave as a collisionless gas. The number and current densities (N_0,$\underset{\sim}{j}_0$) are given by the zeroth and first moments of the velocity distribution $f_i(v,\underset{\sim}{\Omega})$, respectively.

$$N_0^r = \int d\Omega \int dv\ f_i(v,\Omega) = \int d\Omega\ N(\Omega)$$

$$\underset{\sim}{j}_0^r = \int d\Omega \int dv\ \underset{\sim}{v} \cdot f_i(v,\Omega) = \int d\Omega\ J(\underset{\sim}{\Omega})\ .$$

In the moving frame the velocity distribution function assumed for the ions in free space is displaced by the spacecraft velocity V_0, but $f_i(v,\Omega)$ retains its analytical form in v and can be integrated to give the angular distributions $N(\Omega)$ and $J(\Omega)$. The integration over solid angle, $\underset{\sim}{\Omega}$, is complicated by the shadowing of points $\vec{r}$ by the

spacecraft. This is illustrated in Figure 5.1. The angular integration can be approximated numerically by calculating the fraction S_k^r of each of the set of k solid angle cells on the surface of a sphere centered at r that is shadowed by the spacecraft. The integral may then be replaced by the finite sum:

$$N_o^r = \int d\Omega\, N(\Omega) = \sum_k \left(1 - S_k^r\right) N_k\, \Delta\Omega_k$$

In reality of course N_o^r and j_o^r are modified by both the magnetic and electric fields present.

The earth's magnetic field causes the ions to move in spiraling orbits along the field lines. The radii of the orbits (Larmor radius) r_L depend on the magnitude of the particle velocity perpendicular to the field direction, $v_\perp$, and the magnetic flux density B:

$$r_L = \frac{mv_\perp}{qB}$$

For a Maxwellian plasma of oxygen ions with a temperature of ~0.1 eV r_L is of the order of a few meters. The period, T, taken to complete one revolution is independent of r_L.

$$T = \frac{2\pi m}{eB}$$

and has a value of $\sim 10^{-2}$ s in the auroral region. In the spacecraft frame this periodic thermal motion is superimposed upon the bulk velocity $\vec{V}_o$. At high Mach numbers $\vec{V}_o$ dominates the overall particle velocity and a cyclotron period is not completed until the particles have moved many lengths of the spacecraft along the direction of bulk motion. Thus close (within a spacecraft length) to

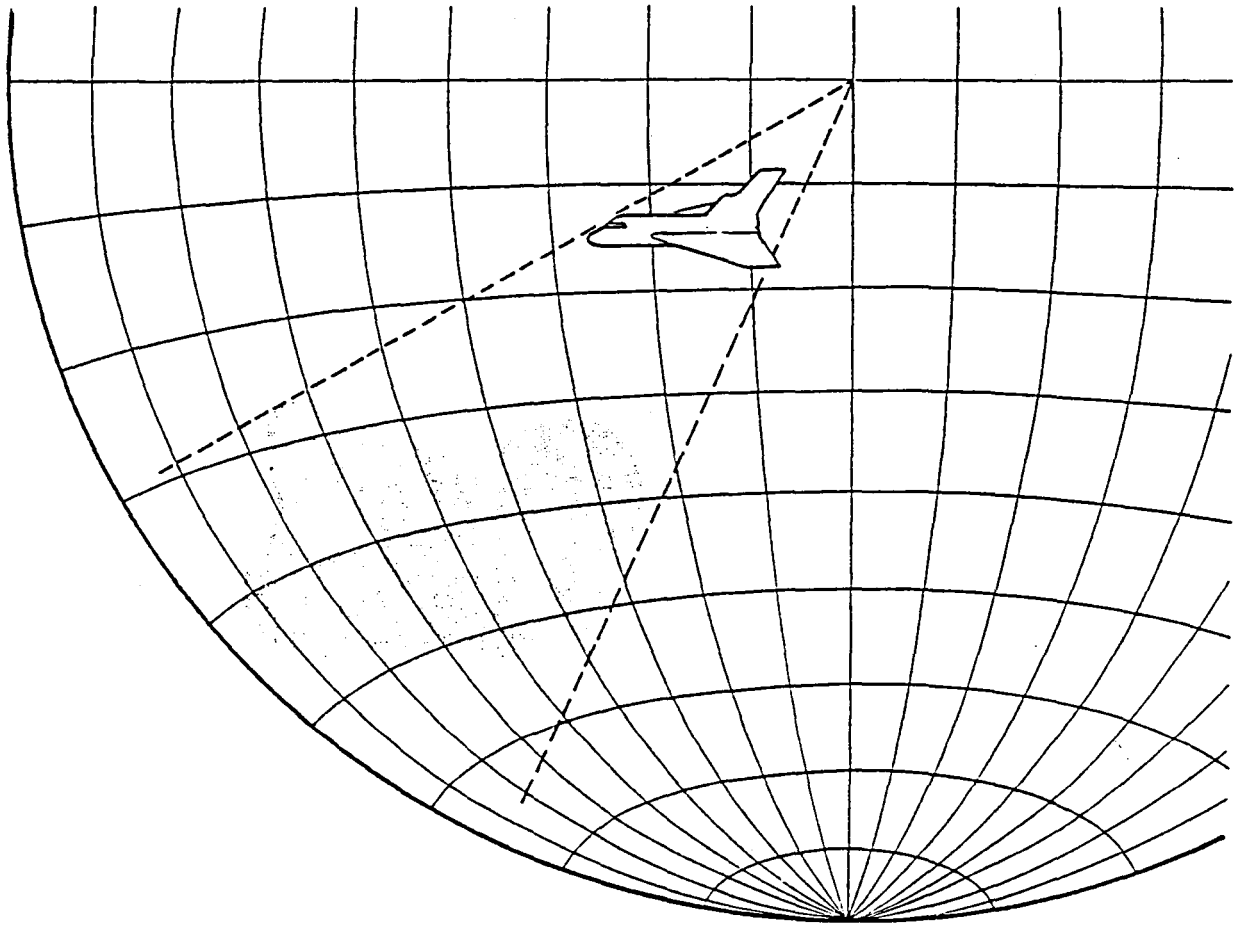

Figure 5.1. Calculation of local densities.

the object the assumption of straight line ion velocities is certainly a good approximation, and further away is probably a suitable starting point for calculating the zero order ion density.

The overall effect of the magnetic field is to enhance the depletion of the wake regions over that calculated on the basis of simple shadowing. If we imagine the spacecraft to leave "ion-holes" as it sweeps out a wake, the holes propagate as "negative particles". Instead of proceeding outwards in a radial fashion, the field turns them around and concentrates them in the wake region, increasing the depletion relative to the plasma far from the spacecraft. We can include this effect as a perturbation to the shadowing calculation outlined above, by modeling the gradually de-phasing of the hole orbits and subsequent re-phasing after a cyclotron period farther down the wake.

The effect of the electric field on the ion density will be treated separately for the regions inside and outside the sheath. Inside the sheath the mean density, given by the ratio of incoming ion flux crossing the boundary to the ion velocity, is modified by the focusing of particle trajectories about regions of the spacecraft that are differentially charged. This effect can be included in the iterative cycle, used to calculate the sheath boundary and potential field, by applying an analytical representation of the focusing behavior implied by the previous particle tracking calculation.

Outside the sheath boundary there may still be large regions with considerable ion depletion. Considering the area outside the sheath to be quasi-neutral implies a parallel depletion of electrons, and hence a potential ϕ_B, with respect to the undisturbed plasma, to force the electrons out. ϕ_B is the so-called "barometric law" potential because of its exponential relationship with the particle density, N_o.

$$\phi_B = \frac{kT}{e} \log \left(\frac{N_o}{\bar{N}_o} \right)$$

where $\bar{N}_o$ is the undisturbed ion density.

The electric field E_B associated with ϕ_B tends to focus ions into the depleted regions increasing the density and reducing the potential. We treat this effect in a fluid dynamical way. Given the value of E_B at each node in the three-dimensional mesh, the mass and momentum equation

$$\vec{\nabla} \cdot (\rho \vec{v}) = 0$$

$$\vec{\nabla} \cdot (v_\alpha \rho \vec{v}) = \rho \frac{eE_\alpha}{m} \quad (\alpha = x,y,z)$$

may be solved for the density ρ and velocity $\vec{v}$ at each node, using a finite element method.[57] The new spatial distribution of velocities and density, given by each solution implies a new ion distribution function $f(v,\Omega)$. Using the shadowing procedure, modifed to include magnetic field effects, this in turn implies a new barometric law electric field E_B and hence a new solution to the fluid equations. By iterating this cycle we will arrive at a self-consistent solution for the ion density (and current density) around the spacecraft including both electric and magnetic field effects. Armed with this information and a formula for translating it into a charge density we may begin the solution of the potential equation.

5.3.3 CALCULATION OF THE POTENTIALS

The calculation of the potential field on and about the spacecraft will be carried out using a finite element variational technique. The variational principle associated with the Poisson-like potential equation is

$$\frac{\delta}{\delta\phi}\left\{\int dv\left[\frac{\varepsilon_0}{2}|\nabla\phi|^2+\rho\phi\right]\right\}+\int\left\{\varepsilon_0\phi\nabla\phi\cdot d\underset{\sim}{S}+\sigma\, dS\right\}$$

The first term leads to the Laplacian operator and volume space charge terms, and the second to surface terms. The computational techniques involved in the solution of these equations is discussed in detail elsewhere.[1]

A self-consistent solution to the potential equation will be sought for a finite timestep. Using the net incoming current calculated from the previous timestep (or for the first timestep the net current in the absence of a space charge limited sheath) the total amount of charge collected on each surface cell is added to that previously collected, and the new potential field calculated. Using the condition $\varepsilon\phi \sim k\theta_i$ to define a new sheath boundary, new values of the incoming electron and current are calculated and used to adjust the previous estimate of net incoming charge during the timestep. At the same time, focusing information derived from ion tracking from the boundary to the surface is included to adjust ρ within the sheath. The value of ρ elsewhere is estimated using the values of ion density calculated in the way described in Section 5.3.2. The potential calculation is then repeated, leading to a new estimate for the boundary region. This cycle is repeated until a self-consistent solution for the potential everywhere is obtained.

The calculation of the ion density outside the sheath region is based upon shadowing of flux by the spacecraft alone. This will be a good approximation while the sheath remains thin. But because the sheath also collects ions, the density calculation may have to be updated to include shadowing by the sheath itself. Whether this will prove necessary will depend on the size of the sheath and hence the particular physical situation being modeled.

5.4 THE POLAR CODE

5.4.1 CONJUGATE GRADIENT METHOD

Consider a charged object isolated in space. The potential ϕ everywhere is given by the solution to Poisson's equation

$$\nabla^2\phi = -\rho/\varepsilon \tag{1}$$

The variational principle[1] associated with this equation is given by:

$$\frac{\delta}{\delta\phi}\left[\left(\int dV\,\frac{1}{2}\,(\nabla\phi)^2 + \frac{\rho\phi}{\varepsilon}\right) + \int_{C_S}\frac{\sigma\phi}{\varepsilon}\,ds + \int_{C_B}\phi\cdot\phi\cdot dS' = 0\right]$$

where we integrate over both the object and boundary surfaces (C_S, C_B).

With fixed potentials on these surfaces and zero charge density this equation simplifies to

$$\frac{\delta}{\delta\phi}\int dV\,\frac{1}{2}\,(\nabla\phi)^2 = 0 \tag{2}$$

Equation (2) involves an integral over the volume of the computational space. One way to treat this integral is to divide the space up into finite cubic volume elements.

$$\int dV\,\frac{1}{2}\,(\nabla\phi)^2 = \sum_e \int_{V_e} dV_e\,\frac{1}{2}\,(\nabla\phi)^2$$

In this finite-element approach the potential ϕ is defined at each grid point, or node, defining the vertices of the elements. The potential inside each element is then trilinearly interpolated from the values at each of its eight vertices.

$$\phi^e (x,y,z) = \sum_{i \in e} N_i^{xyz} \phi_i$$

where "i" are the nodes of element "e"

$$\nabla\phi^e(xyz) = \sum_i \nabla N_i^{xyz} \phi_i$$

and

$$dV \frac{1}{2} (\nabla\phi)^2 = \sum_e \sum_i \int dV_e \quad |\nabla N_i^e(xyz) \phi_i|^2$$

The quantity

$$W_{ij}^e = \int_e dV_e \quad \nabla N_i^{xyz} \cdot \nabla N_j^{xyz} \tag{3}$$

is completely defined just by knowledge of the shape of the element "e" (i.e., whether the cube is empty or partially filled). The variational principle therefore becomes:

$$\frac{\delta}{\delta\phi} \left[\sum_j \sum_i \sum_e W_{ij}^e \phi_i \phi_j = 0 \right] \tag{4}$$

Let $\sum_e W_{ij}^e = M_{ij}$. Equation (4) becomes

$$\frac{\delta}{\delta \phi}\left[\sum_{ij} \phi_i M_{ij} \phi_j\right] = 0 = \underset{\approx}{M}\ \underset{\sim}{\phi}$$

Thus the set of ϕ values at each node ($\underset{\sim}{\phi}$) that satisfy $\underset{\approx}{M}\ \underset{\sim}{\phi}$ is the solution to the Poisson equation (1) under conditions of fixed object and boundary potentials and zero charge density.

We may solve Eq. (4) iteratively. Our initial choice of $\underset{\sim}{\phi}$ will yield a residual $\underset{\sim}{r}$

$$\underset{\approx}{M}\ \underset{\sim}{\phi} = -\underset{\sim}{r}$$

The iterative scheme used is the Conjugate Gradient technique. It is based on the following equations:[2]

$$\underset{\sim}{r}^0 = -\underset{\approx}{M}\ \underset{\sim}{p}^0$$

$$\underset{\sim}{u}^0 = \underset{\sim}{r}^0$$

$$a^i = (r^i, r^i)/(u^i, Mu^i)$$

$$p^{i+1} = p^i + a^i u^i$$

$$r^{i+1} = r^i - a^i Mu^i$$

$$b^i = (r^{i+1}, r^{i+1})/(r^i, r^i)$$

$$u^{i+1} = r^{i+1} + b^i u^i$$

These equations may be iterated upon until $|\underset{\sim}{r}|$ reaches a small value and the resultant $\underset{\sim}{p}$ vector becomes the solution to Poisson's equation.

5.4.2 COMPUTATIONAL CONSIDERATIONS

The major computational operation in the iterative set of equations is the evaluation of the matrix-vector product $\underset{\approx}{M}\underset{\sim}{u}$. The vectors $\underset{\sim}{p}$, $\underset{\sim}{u}$, and $\underset{\sim}{r}$ all have the same number of elements as the number of grid points. $\underset{\approx}{M}$ contains the square of this number. Such a huge array is impractical to store all at once and so $\underset{\approx}{M}\underset{\sim}{u}$ is evaluated using the following implicit algorithm

$$\underset{\sim}{r} = \sum_e \underset{\sim e}{r} = \sum_e \underset{\approx e}{\omega}\underset{\sim}{u}$$

The residual $\underset{\sim}{r}$ is constructed element by element (where the $\underset{\approx e}{\omega}$ matrix is only 8 x 8) and then summed. This procedure is carried out by routine 'COPROD'.

5.4.3 TOP-DOWN VIEW OF PROGRAMMING

ROUTINE CONGRD

Performs conjugate gradient calculations and tests for convergence: Calls

a. INITP (initialize potential arrays)
b. COPROD (Mu product)
c. PUPDAT (p equation)
d. RUPDAT (r equation)
e. UUPDAT (u equation)

Before we go on to describe the details of COPROD, etc., we must describe the grid system in detail.

5.4.4 DISPLACED-SLICE GRID SYSTEM

The displaced-slice grid system is designed to provide the computational space in which to solve Poisson's equation for the shuttle orbiter, including its wake extending perhaps several spacecraft lengths behind. Hence the space must continue for an arbitrary length along the direction of the spacecraft velocity vector.

To faciliate this, the grid is composed of an arbitrary number of thin slices with fixed x and y dimensions, stacked along the z axis, rather like a loaf of sliced bread. Any velocity vector can, via rotation of the object axis system, be made to make an angle of 45 degrees or less with the z axis. To extend the computational space along the direction of the velocity vector and yet still retain cubic volume elements, the slices are stacked with displacements in the x and y direction of $\pm$ 1 mesh unit every m_x and m_y mesh units along the z direction. If θ_x is the projection of the velocity vector direction in the y-z plane

$$m_x = \text{Cot } \theta_x$$

Similarly

$$m_y = \text{Cot } \theta_y$$

An example of such a grid is shown in Figure 5.2. To sum the residuals, element by element, at least two "slices" of grid point information must reside in core at any one time. The rest of the information may be stored on disk. The entire computational volume may then be swept across sequentially, by swapping successive slices in and out of core from the disk, e.g., if the total z dimension is 5 but only three slices are allowed in core at one time, information in slices 1, 2, and 3 would be read in initially and the residuals for the elements bounded by these slices would be evaluated. This

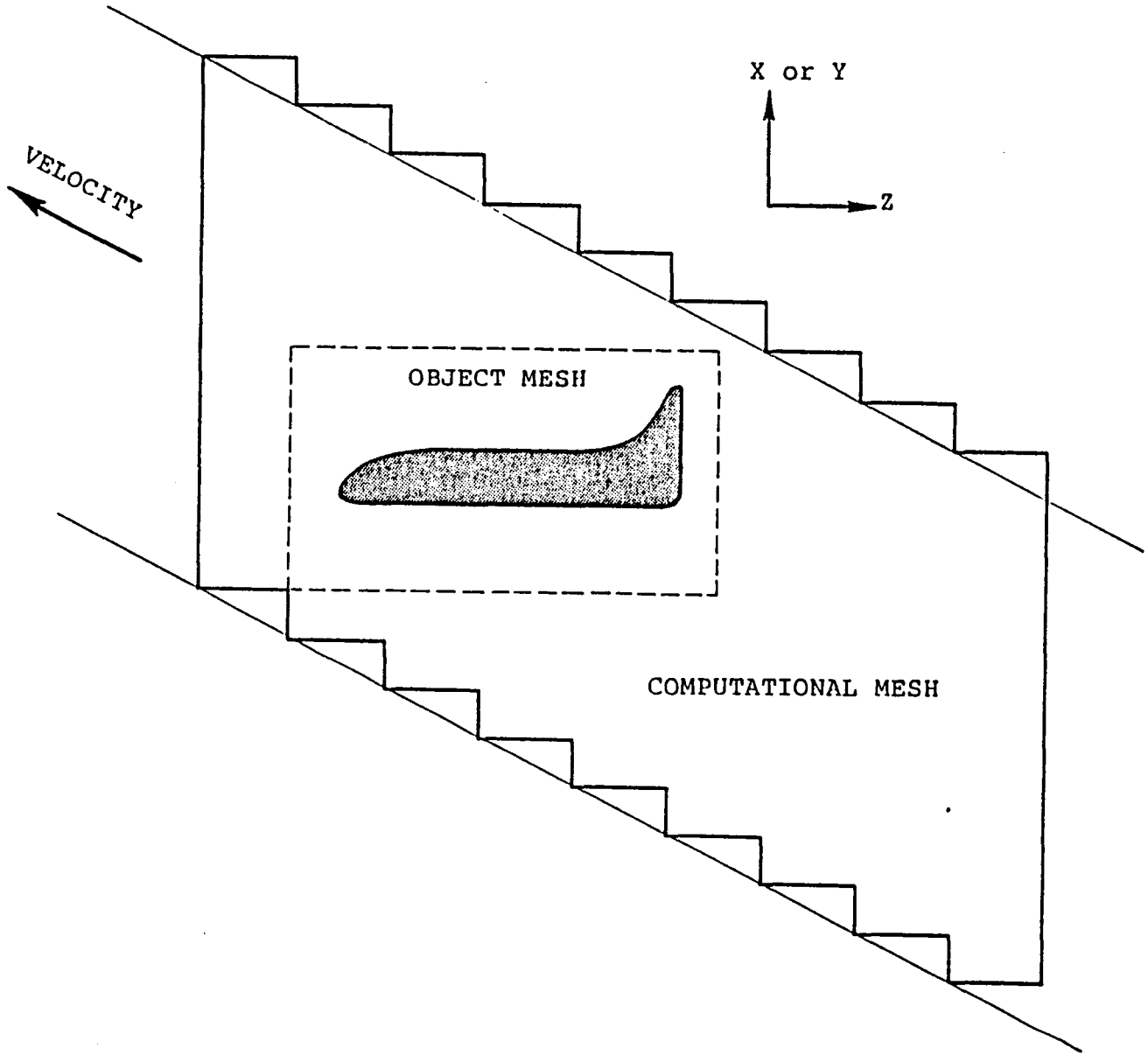

Figure 5.2. 2-D view of displaced slice mesh system.

information is then written out to disk and slices 4 + 5 read in to replace 1 + 2. Now 3, 4, and 5 reside in core and the residuals for the remaining elements can be evaluated.

We describe the machinery that carries out these operations in detail below.

5.4.5 GRID MACHINERY

The grid machinery consists of routines designed to move grid information between disk storage and core. In both media, information for each of the vectors involved in the calculations ("p", "r", "u", etc.) is organized into individual one-dimensional arrays corresponding to each x-y slice. The computational space is characterized by the following parameters:

- NX - The dimension of each slice along the x direction in mesh units.
- NY - The dimension of each slice along the y direction in mesh units.
- NZ - The extent of the space in the z direction (i.e., the total number of slices).
- NG - The number of slices of any one vector allowed in core at one time (depends on NX and NY).

Each of the one-dimensional slice arrays has a length of NY x NX, and is accessed by assuming the convention that the x-coordinate varies faster (e.g., the X = 3, Y = 1 value is found in array element 3, while Y = 3, X = 1 resides in element 2NX + 1).

On disk each vector has associated with it NZ mass storage files, one for each XY slice. Information is moved between disk and core only in units of slices. The information in core at any one time all resides in a single one-dimensional array /CBUF/. Up to three different vectors may be simultaneously referenced in /CBUF/. The

number of slices in core belonging to each of these three vectors is given by NG. This is determined by NX and NY. The greater the length of each slice, the smaller NG. NG has a minimum of 2 and a maximum of NZ.

The beginning address of the Kth slice belonging to the first vector is recorded in array element IA1(K). Similarly for the second vector in IA2(K), etc. K runs from 1 to NG and refers only to the order of slices in core, e.g., if slices 5 → 8 were resident, K = 1 would refer to Z = 5, K = 2 to Z = 6, etc. These relative Z coordinates may be transformed into absolute values simply by recording the lowest Z value in core at any particular time. This value is stored in KSTART. Knowing KSTART, K and IA1(K) allows any member of the first vector to be addressed.

Slices are exchanged from disk to core sequentially. Initially the first NG slices of three chosen vectors are read in. Subsequently the first NG-1 are replaced by the slices from NG+1 to 2NG-1 at the same addresses, e.g., consider a total of eight slices of the vector p, each with ten elements (NX = 2, NY = 5). Let NG = 3. Initially, at the addresses 1, 11, and 21, slices 1-3 are read in:

Address	1	11	21
Slice	1	2	3

After using this information slices 4 and 5 are copied over 1 and 2:

Address	1	11	21
Slice	4	5	3

and so on

Address	1	11	21
Slice	7	5	6

Address	7	11	21
Slice	7	8	6

Note that in the last case slice 6 sitting in addresses 21-30 is not referenced. If there were nine slices, the ninth would have replaced it.

We now describe each subroutine carrying out these tasks in detail.

READMS (LUN, BUFFER, NWDS, KEY)

READMS mimics the CDC mass storage routine of the same name.

LUN - Is the logical unit information is to be read from.

BUFFER - Is the array into which information read from LUN is written. BUFFER may be an element of an array.

NWDS - Is the length of the record to be read.

KEY - Specifies the location of the mass storage file on LUN to be read.

That is, READMS (IFILE, P(NAD), LEN, J) will cause a record J of length LEN to be read from IFILE into array P, beginning at element NAD. Routines WRITMS, OPENMS, and CLOSMS also mimic their CDC counterparts.

GRIDIO (IWORD, NAME, IGRID, NAD)

GRIDIO moves data between disk and core one slice at a time.

IWORD - May be "WRITE" or "READ". The former causes transfer from core to disk and the latter vice-versa.

NAME - Must be one of the key words describing a vector (e.g., "POT", "MU", "LTBL", etc.) or "NULL" in which case the call to GRIDIO results in an immediate "RETURN". If NAME is "ZERO" all elements in the slice are replaced by zeros.

IGRID - Is the absolute Z coordinate.

NAD - Is the beginning address of the slice array in /CBUF/.

GRIDIO calls READMS and WRITMS.

CURSOR (KEND, KSTART, NAME1, W1, NAME2, W2, NAME3, W3)

CURSOR moves information for slices KSTART → KEND (inclusive) between disk and core for the three vectors NAME1, NAME2, and NAME3. The words W1, W2, W3 specify whether information is "read" from a "written" to the disk.

KSTART, KEND - Are updated internally. Only the previous KEND need be supplied by the calling routine. If this is less than two, CURSOR automatically assumes that a new "sweep" of the space if beginning.

KEND = KSTART + NG - 1

NAME1, (2,3) - May be any of the vector key words, "ZERO", or "NULL".

W1, W2, W3 - May be "READ" in order to transfer information from disk to core only, "WONLY" to write information from core to disk only, or "WRITE" to do both. Additionally, W1 may be specified as "ALLR", when all three arrays are to be read-only.

CURSOR operates in two modes. When KEND is 1 or less, it assumes that a new sweep of the computational space is beginning and it sets the beginning addresses for all three vectors in IA1, IA2, and IA3. The first NG slices are read in and nothing is written out. KEND is then updated to NG. When KEND is greater than 1, all but slice KEND is written out over the previous information on the disk (if so specified) and the next NG-1 slices are read in. The address arrays and KEND are then updated. If KEND is equal to KZ (i.e., it is the last slice) all of the slice information is written out (if so specified) and no more slices are read in. If "WONLY" is specified the relevant array is initialized to zero.

CURSOR calls GRIDIO.

5.4.6 VOLUME ELEMENT MACHINERY

Once slice information has been accessed and resides in core, COPROD must calculate residuals, element by element, and return the vector so calculated back to the disk in slices. These operations are complex and require fairly elaborate machinery. We begin by offering a brief overview.

COPROD begins by reading in the relevant slice information, establishing a section of the computational space in core. This volume is swept, element by element. Each element is characterized by the coordinates of its lowest indexed vertex. The potentials, and other vector information, for each of the eight vertices of a particular element are extracted from the main /CBUF/ array by VERTIO. VERTIO also replaces or augments array entries with calculated vertex information.

The potentials at the boundary of the computational space are assumed to be fixed and known (presently set to zero). Hence they are not stored explicitly in CBUF. Instead, COPROD examines each vertex of each volume element and determines if any be an implicit boundary. Those that do are fixed at the boundary potential. VERTIO takes the X-Y displacement of the slices into account in picking out the vertices. Having set the potentials at the vertices of a particular element with VERTIO, COPROD calls ELEMNT to look up its characteristics in the list "LTBL". LTBL is a vector array with an entry for each grid point, and hence each volume element. The entry is bit-coded as follows:

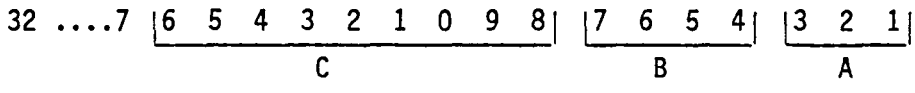

As the code now stands, only the first 16 bits are assigned any significance. These are divided into three fields.

A - The element-type number.

B - The number of surface cells sharing nodes with the element (up to 15) (NCELLS).

C - The orientation of the cell. This is only significant for partially filled cells and is explained in Reference 1.

The following element types are allowed:

Type Number	Bits	Description
0	000	Empty cube
1	001	Half-empty wedge
2	010	Cube with diagonal on one face
3	011	Tetrahedron
4	100	Truncated cube
5	101	Empty special cell (Ref. 1)
6	110	Unused
7	111	Filled cube

The number of surface cells (NCELLS) sharing nodes with the element is used to refer to a second list, LCELLV. If NCELLS is non-zero, DCVCEL is called to look up the next (NCELLS+1) entries in the LCELLV list. The first entry encountered is simply the number of the element as a check. The remaining NCELLS entries are coded in a way similar to LTBL.

ELT# = 4096 x K + 4096 x 64 x J + 4096 x 4096 x I

NCELLS ENTRIES

CODE
CODE
...
...
...
...
ELT#

CODE

32..6	5 4 3 2 1 0 9 8 7 6 5 4 3 2 1	0 9	8 7 6 5 4 3 2 1
	B		A

Only the first 25 bits are presently used. These are divided into two fields.

A - Bits 1-8 are set if the corresponding vertex is shared with the surface cell. The vertices are numbered with X changing faster than Y which changes faster than Z, e.g., for element 1, 1, 1

	Coordinates		
Number	X	Y	Z
1	1	1	1
2	2	1	1
3	1	2	1
4	2	2	1
5	1	1	2
6	2	1	2
7	1	2	2
8	2	2	2

B - Is the cell number. Fifteen bits gives a maximum number of ~16,000 surface cells.

If a vertex is shared by a surface cell, its potential is replaced with the surface potential for that cell, stored in the array SURFV, sequentially by cell number. In the same way the contribution to the residual derived from the shared vertex is returned to the list SURFR rather than the residual vector. Hence the surface potentials play the part of additional grid points, or variables in the matrix conjugate gradient equations. Thus the solution will yield surface and spatial potentials that are self-consistent, eliminating the oscillation that can occur in the present NASCAP implementation. If a vertex is shared by more than one surface cell, the cell potentials

are blended before being assigned to vertex by BLENDR. A surface cell that forms a face of the element takes precedence over all other non-face cells sharing its nodes. Once the final set of potentials are assigned to the vertices, the residuals are calculated using standard sets of "weights".[1] This procedure is repeated for all of the volume elements in the piece of computational space in core. The resulting information is then written out to disk and replaced with the next piece of computational space until the entire volume has been swept.

We now describe each of the volume-element routines in detail.

COPROD (VEC1, VEC2, UDOTMU)

COPROD drives the residual calculation machinery. In general, it calculates the matrix product $\underset{\approx}{M}\,\underset{\sim}{u}$ and the inner product $\underset{\sim}{u}\,\underset{\approx}{M}\,\underset{\sim}{u}$. ($\underset{\approx}{M}$ is derived from the weights looked up by ECUBE.)

VEC1 - contains the vector information $\underset{\sim}{u}$. The $\underset{\sim}{u}$ addresses must reside in IA1.

VEC2 - is the resulting $\underset{\sim}{r}$ vector ($\underset{\approx}{M}\,\underset{\sim}{u}$) which is written out to disk. The $\underset{\sim}{r}$ addresses reside in IA2.

UDOTMU - is the value of the inner product $\underset{\sim}{u}\,\underset{\approx}{M}\,\underset{\sim}{u}$.

COPROD calls CURSOR, VERTIO, ELEMNT, DCVCEL, BLENDR, and ECUBE, etc.

VERTIO (P1, P2, IX, IXD, IY, IYD, MX, X)

VERTIO stuffs the array X with the values of the potentials (or other vector) at the vertices of the element at hand, or alternatively returns X values to the main vector arrys.

P1 - is the array element corresponding to the beginning of the Z slice in the /CBUF/ block.

P2 - is the array element corresponding to the beginning of the next (Z+1) slice in /CBUF/.

IX - is the lowest X coordinate of the element in the Z slice.

IXD - is the corresponding X coordinate in the Z+1 slice and may differ from IX by ±1 due to displacement. (IXD is calculated in COPROD.)

IY,IYD - are similar quantities for the Y coordinate.

MX - is an eight membered array that is initially set to -1 everywhere. Its value for each of the vertices signifies whether they are to be set to zero, returned to the array or taken from the array as follows:

MX = -1: X(N) ← P(ADD)

MX = 0: X(N) = 0

MX > 0: P(ADD) ← P(ADD) + X(N)

X - is the eight membered array containing the vertex information.

The slice displacement is taken into account by a shift in the relative P addresses. Visually a "+" and "-" displacement means up and down as shown below.

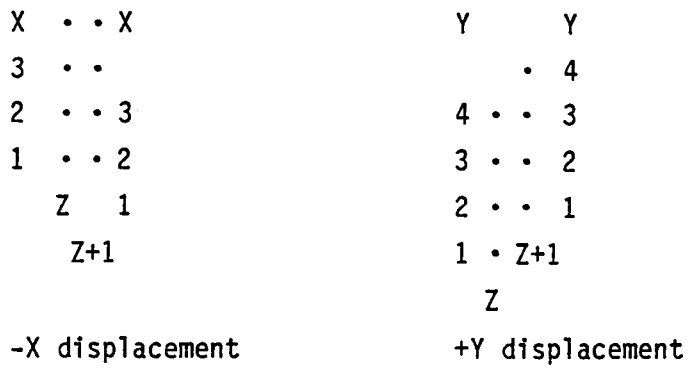

ELEMNT (KSTART, I, J, K)

ELEMNT looks up information for cell I, J, K, in the element table LTBL.

KSTART - is the current absolute Z coordinate of the first slice in core.

I,J,K - are the X, Y, Z coordinates of the lowest vertex of the element in the relative (core) system.

The cell information, decoded by ELEMNT is stored in the /CELINF/ block.

DCVCEL (NELT, NCELLS, NCOUNT, LNODE, ISURF)

DCVCEL looks up and decodes information from the LCELLV list.

NELT - is the volume element sharing nodes with surfaces

$$NELT = 4096 \times K + 4096 \times 64 \times J + 4096 \times 4096 \times I$$

NCELLS - is the number of surface cells sharing nodes with element NELT.

NCOUNT - is the running total pointer for the list LCELLV. NCOUNT is incremented once for every record read by DCVCEL.

LNODE - is a logical array LNODE(8,15). For each surface cell (1-15) elements 1-8 (corresponding to vertices) are set to .TRUE. if they are shared with that cell.

ISURF - is the array of surface cell numbers decoded from the LCELLV entries.

BLENDR (SURFV, LNODE, ISURF, NCELLS, X)

BLENDR uses the DCVCEL information LNODE and ISURF and blends the potentials of nodes shared by more than one surface cell.

SURFV - list of surface cell potentials.

LNODE - see "DCVCEL".

ISURF - see "DCVCEL".

NCELLS - number of surface cells sharing nodes with the volume element.

X - the eight member vertex array for the element.

5.5 A SAMPLE TEST CASE

In order to test this machinery NASCAP was used to define a simple cuboid of 2 x 3 x 4. Using information generated by NASCAP, POLAR-compatable files for the element table, LCELLV, etc. were generated allowing the POLAR conjugate gradient routines to be tested. The results are shown graphically in Figures 5.3, 5.4, and 5.5. Comparison with results for the same object using the NASCAP code confirm that the routines written so far are operating successfully.

5.6 ELECTRON BEAM OPERATIONS AND ELECTRON COLLECTION BY A POSITIVELY CHARGED SPACECRAFT

The theoretical and numerical model described in the preceding sections is limited to ion collection (e.g., negative spacecraft ground) or weakly positive potentials, that is, potentials much less than the ambient plasma temperature. When the vehicle becomes electron attracting, the picture of charged particles streaming across a collisionless sheath fails drastically. While rocket experiments have demonstrated that voltages of several hundred to a thousand volts are required to draw a hundred microamperes of ion current to a rocket,[38] the voltages required to neutralize equivalent electron currents (accounting for the square root of the mass ratio) are down by over an order of magnitude. Indeed, almost all of the over 25 rocket launches with electron beam experiments developed positive potentials that are very small compared to those predicted by space charge limited theories.[40] Only the recent SCATHA experiments at very high altitudes have driven the spacecraft ground to beam potentials.[39] Unlike the case of the ion collecting sheath, the theoretical basis for constructing a computational model of an electron collecting sheath is much weaker. Below we present a description of what a model must contain and how we expect to approach the problem. An intensive theoretical study will be performed before the final electron beam emission-electron sheath collection computer model is constructed.

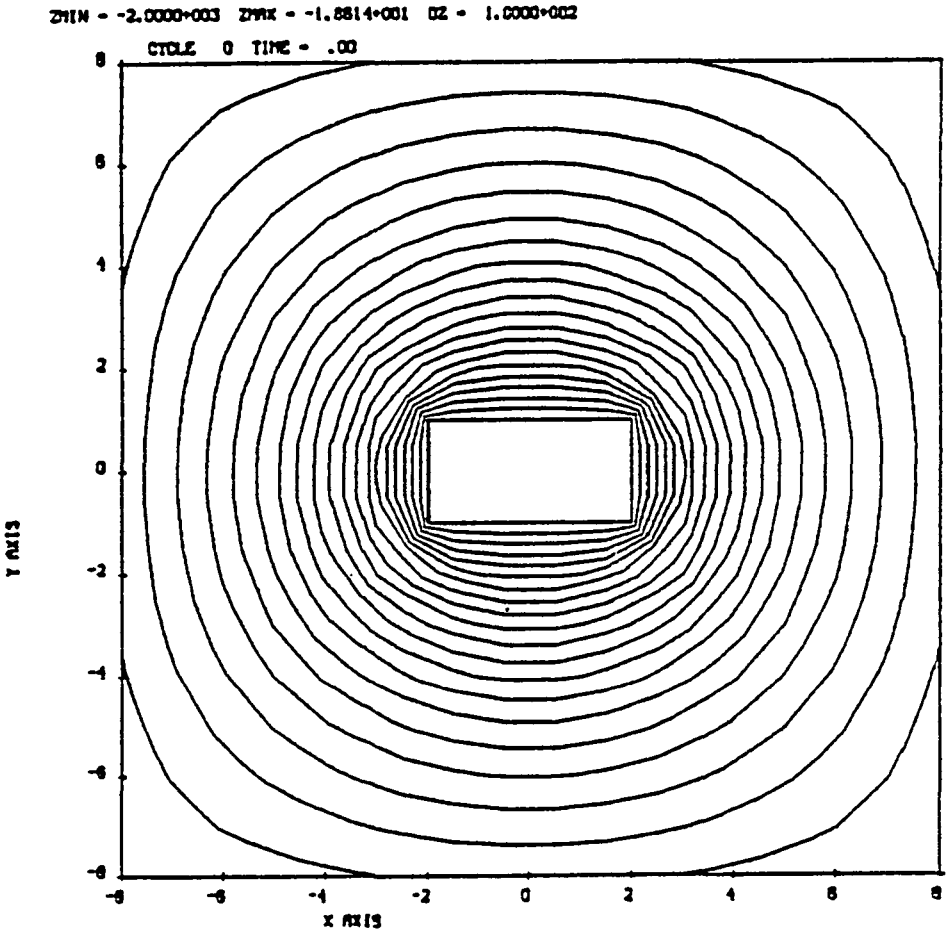

Figure 5.3. Potential contours in the X-Y plane of a 3 x 2 x 4 cuboid object.

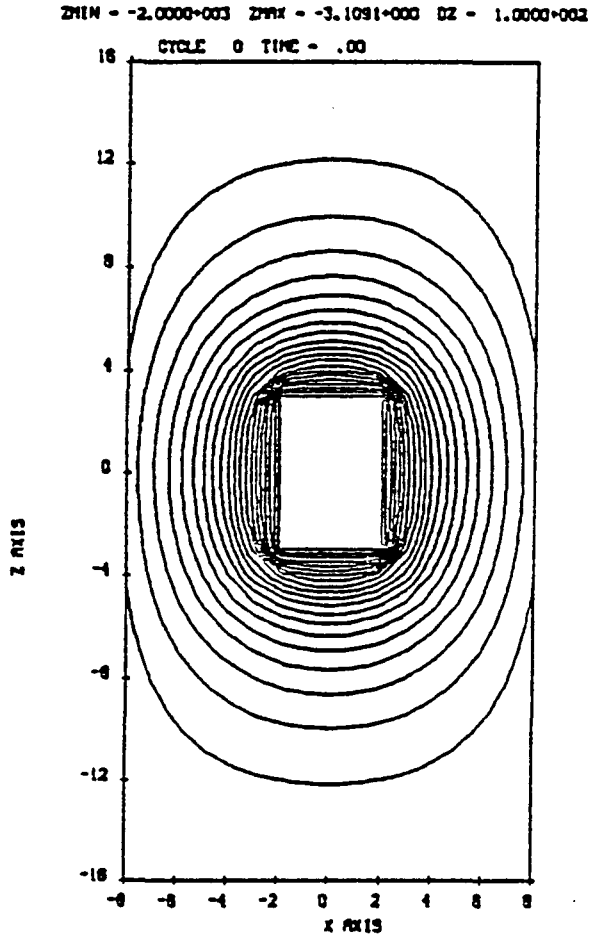

Figure 5.4. Potential contours in the X-Z plane of a 3 x 2 x 4 cuboid object.

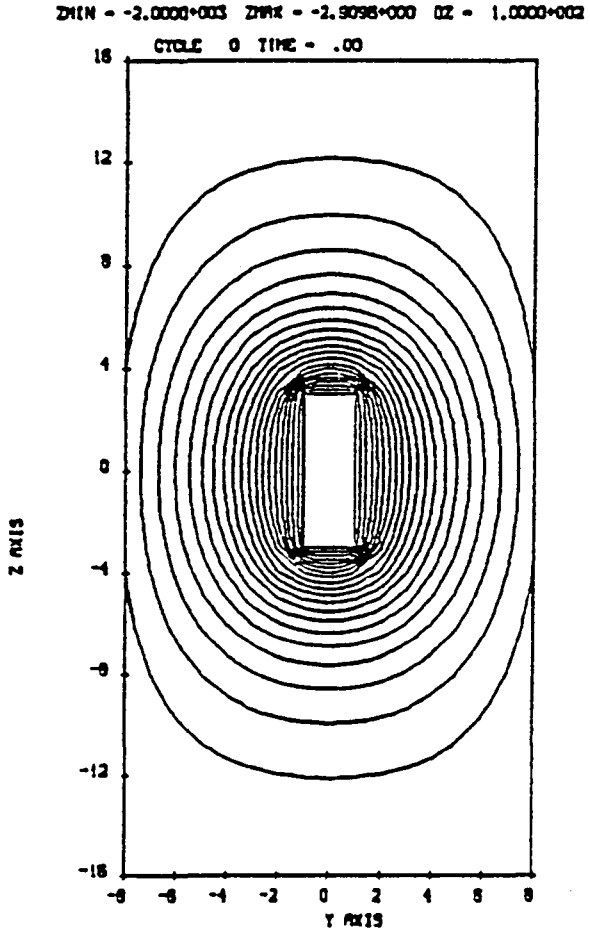

Figure 5.5. Potential contours in the Y-Z plane of a 3 x 2 x 4 cuboid object.

The most striking piece of data from rocket experiments, aside from the small values of the potentials, is that when collecting electron current even an order of magnitude larger than the ambient thermal current, there was no apparent energy cutoff or discontinuity in the collected electron flux as has been seen for ions. This indicates that the turbulence in the sheath region is enough to swamp any collisionless electron streams. Thus, locally, the electron gas may be well described as a fluid. A fluid-like treatment developed at S-Cubed has been extremely successful in describing the electron collecting sheath outside an ion thruster beam.[58] This description is in terms of electron continuity, momentum, and energy equations, and thus takes into account heating processes within the sheath.

Observations of radio emissions have shown that the local plasma densities during beam emission and ion collection are enhanced substantially over ambient conditions.[59] To account for this, the model must include ion generation both by the electron beam and in the sheath region. The primary beam-ambient plasma interactions include secondary electron generation, backscatter, and plasma heating through beam-wave interactions. In the sheath region account must not only be taken of ion generation, but also ion loss by electric field acceleration away from the spacecraft, and by recombination with ambient electrons.

The incorporation of direct beam interaction and sheath ionization into the electron fluid description will result in a comprehensive model which will fit within the POLAR code framework. Combined with the previously discussed surface physics models, not only will spacecraft potential be predicted but also other features of experimental interest including near vehicle plasma temperatures, thermal decay times, and the effect of neutral gases on the returning electron current.

6. CONCLUSIONS

From this work we conclude that NASCAP predictions and the observed SCATHA charging response are in good agreement. Furthermore, the overwhelming body of evidence suggests that NASCAP embodies the physical mechanisms essential for predicting spacecraft charging in geosynchronous orbit, and is able to represent them adequately. NASCAP has shown itself to be an extremely useful tool in understanding and predicting spacecraft charging; NASCAP was designed to calculate surface potentials of objects exposed to the plasma environment of geosynchronous earth orbit.

The three-dimensional nature of the NASCAP code, and its ability to take into account the suppression of low energy surface emission (e.g., photoemission and secondary emission) by fields due to neighboring charged surfaces, has been shown to be essential to the understanding of charging of the SCATHA spacecraft in sunlit environments, in moderate, eclipsed environments, and during beam emission experiments.

In summary the NASCAP model, which was based on knowledge obtained from laboratory charging experiments, has been demonstrated to successfully reproduce results observed in space, under a wide range of conditions, and has through such simulations extended the level of understanding of spacecraft charging.

The charging of large objects in polar earth orbit has been examined, and the potential solving machinery for a code modeling this phenomenon has been established and tested.

APPENDIX

FITS FOR DAYS 114, 98, AND 272

FITS FOR DAY 114

TIME=25944. NORMALIZATION FACTOR= .58
ELECTRONS AT 25944. N1= 2.0+005 T1=10000. N2= 4.1+005 T2=11000.
IONS AT 25944. N1= 5.6+003 T1= 400. N2= 3.8+005 T2=29000.

TIME=25960. NORMALIZATION FACTOR= .56
ELECTRONS AT 25960. N1= 5.6+004 T1= 3000. N2= 6.8+005 T2=12000.
IONS AT 25960. N1= 1.6+004 T1= 1100. N2= 4.4+005 T2=32000.

TIME=25976. NORMALIZATION FACTOR= .49
ELECTRONS AT 25976. N1= 3.7+005 T1=11000. N2= 1.7+005 T2=12000.
IONS AT 25976. N1= 8.1+004 T1= 2700. N2= 2.6+005 T2=50000.

TIME=25992. NORMALIZATION FACTOR= .59
ELECTRONS AT 25992. N1= 5.6+005 T1=12103. N2= 6.9+004 T2= 3103.
IONS AT 25992. N1= 1.6+005 T1= 1900. N2= 2.3+005 T2=50000.

TIME=26008. NORMALIZATION FACTOR= .39
ELECTRONS AT 26008. N1= 1.3+005 T1= 3000. N2= 3.4+005 T2=10000.
IONS AT 26008. N1= 9.3+004 T1= 3100. N2= 2.0+005 T2=29000.

TIME=26024. NORMALIZATION FACTOR= .55
ELECTRONS AT 26024. N1= 1.6+005 T1=13000. N2= 4.5+005 T2=12000.
IONS AT 26024. N1= 1.1+005 T1= 2500. N2= 2.7+005 T2=38000.

TIME=26040. NORMALIZATION FACTOR= .48
ELECTRONS AT 26040. N1= 3.2+005 T1= 8000. N2= 1.6+005 T2= 9000.
IONS AT 26040. N1= .0 T1= 0. N2= 3.1+005 T2= 7000.

TIME=26056. NORMALIZATION FACTOR= .46
ELECTRONS AT 26056. N1= 4.1+005 T1=13000. N2= 1.9+005 T2=12000.
IONS AT 26056. N1= 1.5+004 T1= 700. N2= 3.6+005 T2=27000.

TIME=26072. NORMALIZATION FACTOR= .57
ELECTRONS AT 26072. N1= 7.4+005 T1=11000. N2= 2.5+004 T2=10000.
IONS AT 26072. N1= 1.6+004 T1= 600. N2= 4.6+005 T2=31000.

TIME=26088. NORMALIZATION FACTOR= .54
ELECTRONS AT 26088. N1= 3.0+005 T1=10000. N2= 3.2+005 T2=11000.
IONS AT 26088. N1= 2.4+004 T1= 800. N2= 3.6+005 T2=30000.

TIME=26104. NORMALIZATION FACTOR= .49
ELECTRONS AT 26104. N1= 4.4+005 T1=11000. N2= 2.1+005 T2=12000.
IONS AT 26104. N1= 2.8+004 T1= 500. N2= 3.8+005 T2=22000.

TIME=26120. NORMALIZATION FACTOR= .43
ELECTRONS AT 26120. N1= 3.1+004 T1= 9000. N2= 4.3+005 T2=10000.
IONS AT 26120. N1= 3.5+004 T1= 3300. N2= 2.5+005 T2=35000.

FITS FOR DAY 114 (Continued)

```
 TIME=26136. NORMALIZATION FACTOR=     .69
 ELECTRONS AT 26136. N1=   6.5+005 T1=11000. N2=   8.2+004 T2= 3000.
 IONS      AT 26136. N1=   1.5+005 T1= 2900. N2=   3.1+005 T2=50000.

 TIME=26152. NORMALIZATION FACTOR=     .44
 ELECTRONS AT 26152. N1=   5.0+003 T1= 3000. N2=   4.0+005 T2= 9000.
 IONS      AT 26152. N1=   5.1+004 T1= 2600. N2=   1.9+005 T2=26000.

 TIME=26168. NORMALIZATION FACTOR=     .46
 ELECTRONS AT 26168. N1=   5.2+005 T1=12000. N2=   3.0+004 T2=13000.
 IONS      AT 26168. N1=   2.3+004 T1=  800. N2=   3.8+005 T2=29000.

 TIME=26184. NORMALIZATION FACTOR=     .48
 ELECTRONS AT 26184. N1=   5.5+003 T1= 3000. N2=   3.8+005 T2= 9000.
 IONS      AT 26184. N1=   5.4+004 T1= 2500. N2=   1.9+005 T2=28000.

 TIME=26200. NORMALIZATION FACTOR=     .71
 ELECTRONS AT 26200. N1=   4.4+005 T1=13000. N2=   4.9+005 T2=12000.
 IONS      AT 26200. N1=   5.8+004 T1=  600. N2=   5.1+005 T2=28000.

 TIME=26216. NORMALIZATION FACTOR=     .76
 ELECTRONS AT 26216. N1=   5.8+005 T1=11000. N2=   2.7+005 T2=12000.
 IONS      AT 26216. N1=   2.4+005 T1= 1300. N2=   3.0+005 T2=33000.

 TIME=26232. NORMALIZATION FACTOR=     .55
 ELECTRONS AT 26232. N1=   5.1+005 T1=11000. N2=   1.0+005 T2=10000.
 IONS      AT 26232. N1=   6.0+004 T1=  400. N2=   3.3+005 T2=29000.

 TIME=26248. NORMALIZATION FACTOR=     .52
 ELECTRONS AT 26248. N1=   9.9+004 T1= 3000. N2=   5.6+005 T2=11000.
 IONS      AT 26248. N1=   3.4+004 T1= 1400. N2=   3.7+005 T2=31000.

 TIME=26264. NORMALIZATION FACTOR=     .55
 ELECTRONS AT 26264. N1=   3.2+004 T1= 3000. N2=   6.7+005 T2=10000.
 IONS      AT 26264. N1=   2.6+004 T1=  800. N2=   4.1+005 T2=29000.

 TIME=26280. NORMALIZATION FACTOR=     .54
 ELECTRONS AT 26280. N1=   4.4+005 T1=11000. N2=   2.0+005 T2=12000.
 IONS      AT 26280. N1=   3.6+004 T1=  600. N2=   3.6+005 T2=31000.

 TIME=26296. NORMALIZATION FACTOR=     .49
 ELECTRONS AT 26296. N1=   2.5+005 T1= 9000. N2=   7.2+005 T2=10000.
 IONS      AT 26296. N1=   9.9+004 T1= 2000. N2=   2.6+005 T2=31000.

 TIME=26312. NORMALIZATION FACTOR=     .72
 ELECTRONS AT 26312. N1=   7.0+005 T1=12000. N2=   2.5+005 T2=13000.
 IONS      AT 26312. N1=   1.1+005 T1=  900. N2=   4.9+005 T2=36000.
```

FITS FOR DAY 114 (Concluded)

TIME=26328. NORMALIZATION FACTOR= .72

ELECTRONS	AT 26328.	N1=	6.2+004	T1= 3000.	N2=	5.5+005	T2=10000.
IONS	AT 26328.	N1=	1.5+005	T1= 2600.	N2=	2.3+005	T2=31000.

TIME=26344. NORMALIZATION FACTOR= .80

ELECTRONS	AT 26344.	N1=	5.1+005	T1=10000.	N2=	1.4+005	T2=11000.
IONS	AT 26344.	N1=	6.9+004	T1= 4500.	N2=	3.4+005	T2=50000.

TIME=26360. NORMALIZATION FACTOR= .89

ELECTRONS	AT 26360.	N1=	1.3+005	T1= 3000.	N2=	8.6+005	T2=10000.
IONS	AT 26360.	N1=	3.3+005	T1= 2200.	N2=	2.8+005	T2=36000.

TIME=26376. NORMALIZATION FACTOR= .41

ELECTRONS	AT 26376.	N1=	2.9+005	T1= 9000.	N2=	2.2+005	T2=10000.
IONS	AT 26376.	N1=	5.3+004	T1= 3200.	N2=	2.6+005	T2=39000.

FITS FOR DAY 98

```
TIME=44858. NORMALIZATION FACTOR=   1.19
ELECTRONS AT 44858. N1=   9.6+005 T1= 3900. N2=   1.1+004 T2=24800.
IONS      AT 44858. N1=   5.3+004 T1= 1700. N2=   4.1+005 T2=18500.

TIME=44878. NORMALIZATION FACTOR=   1.22
ELECTRONS AT 44878. N1=   9.9+005 T1= 3900. N2=   1.2+004 T2=21800.
IONS      AT 44878. N1=   5.5+004 T1= 1700. N2=   4.2+005 T2=18500.

TIME=44898. NORMALIZATION FACTOR=   1.03
ELECTRONS AT 44898. N1=   8.3+005 T1= 4100. N2=   9.1+003 T2=24800.
IONS      AT 44898. N1=   6.8+004 T1= 2600. N2=   3.3+005 T2=18500.

TIME=44918. NORMALIZATION FACTOR=   1.10
ELECTRONS AT 44918. N1=   9.0+005 T1= 4000. N2=   1.1+004 T2=21800.
IONS      AT 44918. N1=   6.8+004 T1= 2500. N2=   3.6+005 T2=18500.

TIME=44938. NORMALIZATION FACTOR=   1.15
ELECTRONS AT 44938. N1=   8.7+005 T1= 3800. N2=   1.4+004 T2=20800.
IONS      AT 44938. N1=   8.8+004 T1= 2900. N2=   3.3+005 T2=18500.

TIME=44958. NORMALIZATION FACTOR=   1.00
ELECTRONS AT 44958. N1=   8.3+005 T1= 4100. N2=   9.9+003 T2=22800.
IONS      AT 44958. N1=   5.5+004 T1= 2000. N2=   3.4+005 T2=18500.

TIME=44978. NORMALIZATION FACTOR=   1.24
ELECTRONS AT 44978. N1=   9.8+005 T1= 4200. N2=   1.2+004 T2=23800.
IONS      AT 44978. N1=   3.2+004 T1= 1000. N2=   4.4+005 T2=18500.

TIME=44998. NORMALIZATION FACTOR=   1.13
ELECTRONS AT 44998. N1=   9.6+005 T1= 4300. N2=   7.8+003 T2=23800.
IONS      AT 44998. N1=   4.6+004 T1= 1600. N2=   4.1+005 T2=19500.

TIME=45018. NORMALIZATION FACTOR=   1.21
ELECTRONS AT 45018. N1=   9.8+005 T1= 4100. N2=   1.0+004 T2=27800.
IONS      AT 45018. N1=   4.3+004 T1=  900. N2=   4.3+005 T2=19500.

TIME=45038. NORMALIZATION FACTOR=   1.24
ELECTRONS AT 45038. N1=   9.8+005 T1= 4000. N2=   1.2+004 T2=23800.
IONS      AT 45038. N1=   2.8+004 T1=  900. N2=   4.4+005 T2=18500.

TIME=45058. NORMALIZATION FACTOR=   1.12
ELECTRONS AT 45058. N1=   8.8+005 T1= 4200. N2=   5.5+003 T2=29800.
IONS      AT 45058. N1=   5.1+004 T1= 2300. N2=   3.7+005 T2=18500.

TIME=45078. NORMALIZATION FACTOR=   1.12
ELECTRONS AT 45078. N1=   8.5+005 T1= 4100. N2=   8.2+003 T2=26800.
IONS      AT 45078. N1=   6.3+004 T1= 2100. N2=   3.4+005 T2=18500.
```

FITS FOR DAY 98 (Continued)

```
TIME=45098. NORMALIZATION FACTOR=   1.18
ELECTRONS AT 45098. N1=   9.3+005 T1= 4000. N2=   1.0+004 T2=24800.
IONS      AT 45098. N1=   3.5+004 T1= 1700. N2=   4.1+005 T2=17500.

TIME=45118. NORMALIZATION FACTOR=   1.06
ELECTRONS AT 45118. N1=   8.3+005 T1= 4100. N2=   9.0+003 T2=25800.
IONS      AT 45118. N1=   3.7+004 T1= 1600. N2=   3.6+005 T2=18500.

TIME=45138. NORMALIZATION FACTOR=   1.08
ELECTRONS AT 45138. N1=   8.3+005 T1= 4000. N2=   8.4+003 T2=24800.
IONS      AT 45138. N1=   9.3+004 T1= 2700. N2=   3.1+005 T2=18500.

TIME=45158. NORMALIZATION FACTOR=    .91
ELECTRONS AT 45158. N1=   7.1+005 T1= 3700. N2=   1.1+004 T2=19800.
IONS      AT 45158. N1=   8.4+004 T1= 2700. N2=   2.6+005 T2=20500.

TIME=45178. NORMALIZATION FACTOR=    .86
ELECTRONS AT 45178. N1=   6.4+005 T1= 4000. N2=   6.5+003 T2=28800.
IONS      AT 45178. N1=   7.5+004 T1= 2500. N2=   2.3+005 T2=17500.

TIME=45198. NORMALIZATION FACTOR=   1.20
ELECTRONS AT 45198. N1=   8.4+005 T1= 3700. N2=   1.3+004 T2=21800.
IONS      AT 45198. N1=   5.5+004 T1= 2300. N2=   3.5+005 T2=19500.

TIME=45218. NORMALIZATION FACTOR=   1.03
ELECTRONS AT 45218. N1=   7.5+005 T1= 4000. N2=   8.7+003 T2=26800.
IONS      AT 45218. N1=   5.2+004 T1= 2000. N2=   3.1+005 T2=18500.

TIME=45238. NORMALIZATION FACTOR=   1.01
ELECTRONS AT 45238. N1=   7.9+005 T1= 4100. N2=   7.2+003 T2=28800.
IONS      AT 45238. N1=   7.8+004 T1= 2500. N2=   3.0+005 T2=18500.

TIME=45258. NORMALIZATION FACTOR=   1.00
ELECTRONS AT 45258. N1=   8.1+005 T1= 4200. N2=   7.3+003 T2=26800.
IONS      AT 45258. N1=   9.0+004 T1= 2500. N2=   3.0+005 T2=18500.

TIME=45278. NORMALIZATION FACTOR=   1.05
ELECTRONS AT 45278. N1=   7.9+005 T1= 4000. N2=   8.3+003 T2=29800.
IONS      AT 45278. N1=   6.3+004 T1= 1800. N2=   3.2+005 T2=19500.

TIME=45298. NORMALIZATION FACTOR=   1.17
ELECTRONS AT 45298. N1=   9.1+005 T1= 4200. N2=   1.0+004 T2=26800.
IONS      AT 45298. N1=   3.6+004 T1= 1400. N2=   4.0+005 T2=17500.

TIME=45318. NORMALIZATION FACTOR=   1.22
ELECTRONS AT 45318. N1=   9.2+005 T1= 4200. N2=   1.1+004 T2=27800.
IONS      AT 45318. N1=   3.6+004 T1= 1700. N2=   4.1+005 T2=18500.

TIME=45338. NORMALIZATION FACTOR=   1.04
ELECTRONS AT 45338. N1=   8.2+005 T1= 4200. N2=   8.0+003 T2=29800.
IONS      AT 45338. N1=   7.3+004 T1= 2700. N2=   3.2+005 T2=19500.
```

FITS FOR DAY 98 (Concluded)

```
TIME=45358. NORMALIZATION FACTOR=   1.02
ELECTRONS AT 45358. N1=   7.6+005 T1= 4300. N2=   8.3+003 T2=26800.
IONS      AT 45358. N1=   6.9+004 T1= 2400. N2=   2.9+005 T2=18500.

TIME=45378. NORMALIZATION FACTOR=   1.20
ELECTRONS AT 45378. N1=   8.8+005 T1= 4000. N2=   1.4+004 T2=21800.
IONS      AT 45378. N1=   2.8+004 T1= 1100. N2=   3.9+005 T2=19500.

TIME=45398. NORMALIZATION FACTOR=   1.10
ELECTRONS AT 45398. N1=   8.4+005 T1= 4300. N2=   7.0+003 T2=29800.
IONS      AT 45398. N1=   5.0+004 T1= 1900. N2=   3.5+005 T2=19500.

TIME=45418. NORMALIZATION FACTOR=   1.13
ELECTRONS AT 45418. N1=   9.1+005 T1= 4200. N2=   1.4+004 T2=18800.
IONS      AT 45418. N1=   3.8+004 T1= 2600. N2=   4.0+005 T2=18500.

TIME=45438. NORMALIZATION FACTOR=   1.12
ELECTRONS AT 45438. N1=   8.7+005 T1= 4100. N2=   8.6+003 T2=27800.
IONS      AT 45438. N1=   6.5+004 T1= 2200. N2=   3.5+005 T2=18500.

TIME=45458. NORMALIZATION FACTOR=   1.24
ELECTRONS AT 45458. N1=   9.3+005 T1= 4100. N2=   1.0+004 T2=28800.
IONS      AT 45458. N1=   3.0+004 T1= 1200. N2=   4.2+005 T2=18500.

TIME=45478. NORMALIZATION FACTOR=   1.10
ELECTRONS AT 45478. N1=   8.3+005 T1= 4100. N2=   8.4+003 T2=25800.
IONS      AT 45478. N1=   7.7+004 T1= 2400. N2=   3.2+005 T2=19500.

TIME=45498. NORMALIZATION FACTOR=   1.38
ELECTRONS AT 45498. N1=   9.7+005 T1= 4000. N2=   1.0+004 T2=29800.
IONS      AT 45498. N1=   3.8+004 T1= 1500. N2=   4.3+005 T2=19500.

TIME=45518. NORMALIZATION FACTOR=   1.35
ELECTRONS AT 45518. N1=   1.0+006 T1= 4100. N2=   1.1+004 T2=28800.
IONS      AT 45518. N1=   8.1+004 T1= 2700. N2=   4.0+005 T2=19500.

TIME=45538. NORMALIZATION FACTOR=   1.46
ELECTRONS AT 45538. N1=   1.0+006 T1= 4100. N2=   1.1+004 T2=26800.
IONS      AT 45538. N1=   2.5+004 T1= 1500. N2=   4.7+005 T2=17500.

TIME=45558. NORMALIZATION FACTOR=   1.08
ELECTRONS AT 45558. N1=   8.3+005 T1= 4100. N2=   9.0+003 T2=27800.
IONS      AT 45558. N1=   7.5+004 T1= 2700. N2=   3.2+005 T2=18500.

TIME=45578. NORMALIZATION FACTOR=   1.02
ELECTRONS AT 45578. N1=   7.3+005 T1= 4000. N2=   8.7+003 T2=29800.
IONS      AT 45578. N1=   7.9+004 T1= 2200. N2=   2.7+005 T2=18500.

TIME=45598. NORMALIZATION FACTOR=    .80
ELECTRONS AT 45598. N1=   6.3+005 T1= 4000. N2=   8.6+003 T2=23800.
IONS      AT 45598. N1=   4.8+004 T1= 1700. N2=   2.6+005 T2=17500.
```

TIME=15586. NORMALIZATION FACTOR= 2.20
ELECTRONS AT 15586. N1= 2.2+006 T1= 1500. N2= 9.3+005 T2=10800.
IONS AT 15586. N1= 1.2+006 T1= 1000. N2= 2.8+005 T2=14500.

TIME=15603. NORMALIZATION FACTOR= .54
ELECTRONS AT 15603. N1= 4.8+005 T1= 1710. N2= 2.4+005 T2= 9910.
IONS AT 15603. N1= 4.7+004 T1= 600. N2= 3.0+005 T2=13500.

TIME=15620. NORMALIZATION FACTOR= 1.12
ELECTRONS AT 15620. N1= 9.5+005 T1= 1710. N2= 5.7+005 T2= 9910.
IONS AT 15620. N1= 4.4+005 T1= 1000. N2= 2.8+005 T2=15500.

TIME=15637. NORMALIZATION FACTOR= .90
ELECTRONS AT 15637. N1= 8.6+005 T1= 1943. N2= 2.9+005 T2=10043.
IONS AT 15637. N1= 3.3+005 T1= 2500. N2= 2.2+005 T2=13500.

TIME=15654. NORMALIZATION FACTOR= .46
ELECTRONS AT 15654. N1= 3.9+005 T1= 2043. N2= 2.3+005 T2=10043.
IONS AT 15654. N1= 6.2+004 T1= 1100. N2= 2.3+005 T2=14500.

TIME=15671. NORMALIZATION FACTOR= 1.30
ELECTRONS AT 15671. N1= 7.8+005 T1= 1543. N2= 5.8+005 T2=10043.
IONS AT 15671. N1= 4.1+005 T1= 1700. N2= 2.3+005 T2=13500.

TIME=15688. NORMALIZATION FACTOR= .56
ELECTRONS AT 15688. N1= 4.9+005 T1= 2143. N2= 2.6+005 T2=10043.
IONS AT 15688. N1= 7.0+004 T1= 1200. N2= 2.8+005 T2=13500.

TIME=15705. NORMALIZATION FACTOR= 1.42
ELECTRONS AT 15705. N1= 1.0+006 T1= 1910. N2= 6.6+005 T2= 9910.
IONS AT 15705. N1= 5.4+005 T1= 1100. N2= 2.5+005 T2=14500.

TIME=15722. NORMALIZATION FACTOR= .59
ELECTRONS AT 15722. N1= 5.8+005 T1= 1643. N2= 1.5+005 T2=10043.
IONS AT 15722. N1= 1.3+005 T1= 2100. N2= 2.1+005 T2=13500.

TIME=15739. NORMALIZATION FACTOR= .96
ELECTRONS AT 15739. N1= 8.0+005 T1= 2010. N2= 4.6+005 T2= 9910.
IONS AT 15739. N1= 3.7+005 T1= 900. N2= 2.3+005 T2=15500.

TIME=15756. NORMALIZATION FACTOR= 1.31
ELECTRONS AT 15756. N1= 1.2+006 T1= 1310. N2= 5.6+005 T2= 9910.
IONS AT 15756. N1= 5.1+005 T1= 1800. N2= 3.1+005 T2=12500.

TIME=15773. NORMALIZATION FACTOR= .56
ELECTRONS AT 15773. N1= 4.7+005 T1= 2243. N2= 2.5+005 T2=10043.
IONS AT 15773. N1= 6.1+004 T1= 900. N2= 2.8+005 T2=14500.

TIME=15790. NORMALIZATION FACTOR= 1.33
ELECTRONS AT 15790. N1= 8.1+005 T1= 1610. N2= 6.4+005 T2= 9910.
IONS AT 15790. N1= 4.2+005 T1= 1000. N2= 2.6+005 T2=13500.

```
 TIME=15807. NORMALIZATION FACTOR=     .73
 ELECTRONS AT 15807. N1=    6.1+005 T1= 1743. N2=    2.6+005 T2=10043.
 IONS      AT 15807. N1=    1.6+005 T1= 2200. N2=    2.6+005 T2=12500.

 TIME=15824. NORMALIZATION FACTOR=     .75
 ELECTRONS AT 15824. N1=    6.4+005 T1= 1910. N2=    3.3+005 T2=10910.
 IONS      AT 15824. N1=    1.8+005 T1=  900. N2=    2.7+005 T2=15500.

 TIME=15841. NORMALIZATION FACTOR=     .98
 ELECTRONS AT 15841. N1=    8.7+005 T1= 1443. N2=    2.8+005 T2=11043.
 IONS      AT 15841. N1=    2.9+005 T1= 1900. N2=    2.5+005 T2=13500.

 TIME=15858. NORMALIZATION FACTOR=     .54
 ELECTRONS AT 15858. N1=    3.9+005 T1= 2043. N2=    2.5+005 T2=10043.
 IONS      AT 15858. N1=    9.1+004 T1= 1100. N2=    2.1+005 T2=14500.

 TIME=15875. NORMALIZATION FACTOR=    6.49
 ELECTRONS AT 15875. N1=    4.2+006 T1= 1810. N2=    2.9+006 T2= 9910.
 IONS      AT 15875. N1=    3.1+006 T1= 1200. N2=    2.8+005 T2=14500.

 TIME=15892. NORMALIZATION FACTOR=     .71
 ELECTRONS AT 15892. N1=    5.5+005 T1= 1643. N2=    3.0+005 T2= 9043.
 IONS      AT 15892. N1=    1.1+005 T1= 1300. N2=    2.9+005 T2=12500.

 TIME=15909. NORMALIZATION FACTOR=     .75
 ELECTRONS AT 15909. N1=    5.0+005 T1= 1910. N2=    3.7+005 T2= 9910.
 IONS      AT 15909. N1=    2.1+005 T1= 1000. N2=    2.0+005 T2=15500.

 TIME=15926. NORMALIZATION FACTOR=     .88
 ELECTRONS AT 15926. N1=    6.7+005 T1= 1410. N2=    2.9+005 T2= 9910.
 IONS      AT 15926. N1=    2.0+005 T1= 2600. N2=    2.6+005 T2=13500.

 TIME=15943. NORMALIZATION FACTOR=     .67
 ELECTRONS AT 15943. N1=    5.6+005 T1= 2343. N2=    3.8+005 T2=10043.
 IONS      AT 15943. N1=    8.4+004 T1=  900. N2=    3.6+005 T2=15500.

 TIME=15960. NORMALIZATION FACTOR=    2.44
 ELECTRONS AT 15960. N1=    9.7+005 T1= 1610. N2=    1.1+006 T2= 9910.
 IONS      AT 15960. N1=    5.7+005 T1= 1400. N2=    4.0+005 T2=13500.

 TIME=15977. NORMALIZATION FACTOR=     .80
 ELECTRONS AT 15977. N1=    5.7+005 T1= 1743. N2=    3.5+005 T2= 9043.
 IONS      AT 15977. N1=    8.9+004 T1=  900. N2=    3.5+005 T2=13500.

 TIME=15994. NORMALIZATION FACTOR=     .99
 ELECTRONS AT 15994. N1=    5.8+005 T1= 2010. N2=    4.4+005 T2= 9910.
 IONS      AT 15994. N1=    1.3+005 T1=  800. N2=    3.5+005 T2=16500.
```

```
 TIME=16011. NORMALIZATION FACTOR=   1.14
 ELECTRONS AT 16011. N1=   6.6+005 T1= 1810. N2=   2.6+005 T2=10910.
 IONS      AT 16011. N1=   2.8+005 T1= 2400. N2=   1.6+005 T2=17500.

 TIME=16028. NORMALIZATION FACTOR=    .92
 ELECTRONS AT 16028. N1=   6.2+005 T1= 2110. N2=   4.0+005 T2= 9910.
 IONS      AT 16028. N1=   1.1+005 T1=  600. N2=   3.7+005 T2=16500.

 TIME=16045. NORMALIZATION FACTOR=   1.42
 ELECTRONS AT 16045. N1=   7.9+005 T1= 1610. N2=   5.5+005 T2=10910.
 IONS      AT 16045. N1=   3.3+005 T1= 1500. N2=   3.1+005 T2=13500.

 TIME=16062. NORMALIZATION FACTOR=    .70
 ELECTRONS AT 16062. N1=   4.4+005 T1= 2110. N2=   2.7+005 T2= 9910.
 IONS      AT 16062. N1=   6.7+004 T1=  700. N2=   2.7+005 T2=13500.

 TIME=16079. NORMALIZATION FACTOR=   1.15
 ELECTRONS AT 16079. N1=   6.3+005 T1= 2310. N2=   4.6+005 T2= 9910.
 IONS      AT 16079. N1=   2.1+005 T1=  800. N2=   3.0+005 T2=14500.

 TIME=16096. NORMALIZATION FACTOR=   1.08
 ELECTRONS AT 16096. N1=   6.4+005 T1= 1910. N2=   3.2+005 T2= 9910.
 IONS      AT 16096. N1=   1.9+005 T1= 2500. N2=   2.6+005 T2=13500.

 TIME=16113. NORMALIZATION FACTOR=    .79
 ELECTRONS AT 16113. N1=   5.0+005 T1= 2110. N2=   3.1+005 T2= 9910.
 IONS      AT 16113. N1=   8.5+004 T1=  600. N2=   3.0+005 T2=14500.

 TIME=16130. NORMALIZATION FACTOR=   1.76
 ELECTRONS AT 16130. N1=   8.5+005 T1= 1510. N2=   6.0+005 T2= 9910.
 IONS      AT 16130. N1=   4.2+005 T1= 1500. N2=   2.6+005 T2=13500.

 TIME=16147. NORMALIZATION FACTOR=    .70
 ELECTRONS AT 16147. N1=   4.6+005 T1= 2010. N2=   2.5+005 T2= 9910.
 IONS      AT 16147. N1=   9.4+004 T1=  500. N2=   2.5+005 T2=13500.

 TIME=16164. NORMALIZATION FACTOR=    .53
 ELECTRONS AT 16164. N1=   5.3+005 T1= 1971. N2=   2.5+005 T2= 9571.
 IONS      AT 16164. N1=   7.4+004 T1=  800. N2=   3.0+005 T2=19500.

 TIME=16181. NORMALIZATION FACTOR=   1.04
 ELECTRONS AT 16181. N1=   5.0+005 T1= 2000. N2=   2.9+005 T2= 8800.
 IONS      AT 16181. N1=   1.2+005 T1= 1700. N2=   2.5+005 T2=11500.

 TIME=16198. NORMALIZATION FACTOR=   2.98
 ELECTRONS AT 16198. N1=   1.4+006 T1= 2500. N2=   1.2+006 T2= 9800.
 IONS      AT 16198. N1=   9.3+005 T1= 3200. N2=   3.0+005 T2=17500.
```

```
TIME=16215. NORMALIZATION FACTOR=   9.45
ELECTRONS AT 16215. N1=   3.3+006 T1= 1700. N2=   3.2+006 T2= 9800.
IONS      AT 16215. N1=   3.1+006 T1= 4200. N2=   7.0+004 T2=36500.

TIME=16232. NORMALIZATION FACTOR=   1.26
ELECTRONS AT 16232. N1=   6.3+005 T1= 2000. N2=   5.2+005 T2= 9800.
IONS      AT 16232. N1=   3.9+005 T1= 2800. N2=   1.5+005 T2=18500.

TIME=16249. NORMALIZATION FACTOR=   2.51
ELECTRONS AT 16249. N1=   9.3+005 T1= 1800. N2=   1.1+006 T2= 9800.
IONS      AT 16249. N1=   7.4+005 T1= 1500. N2=   2.3+005 T2=14500.

TIME=16266. NORMALIZATION FACTOR=   2.69
ELECTRONS AT 16266. N1=   1.5+006 T1= 1500. N2=   1.2+006 T2= 8800.
IONS      AT 16266. N1=   1.1+006 T1= 3700. N2=   1.5+005 T2=17500.

TIME=16283. NORMALIZATION FACTOR=   1.15
ELECTRONS AT 16283. N1=   5.8+005 T1= 2100. N2=   5.3+005 T2= 9800.
IONS      AT 16283. N1=   3.3+005 T1= 2000. N2=   1.9+005 T2=16500.

TIME=16300. NORMALIZATION FACTOR=  12.80
ELECTRONS AT 16300. N1=   5.7+006 T1= 1300. N2=   4.4+006 T2= 8800.
IONS      AT 16300. N1=   4.7+006 T1= 3700. N2=   7.8+004 T2=49500.
```

REFERENCES

1. Katz, I., et al., "A Three Dimensional Dynamic Study of Electrostatic Charging in Materials," NASA CR-135256, August 1977.

2. Katz, I., J. J. Cassidy, M. J. Mandell, G. W. Schnuelle, P. G. Steen, D. E. Parks, M. Rotenberg and J. H. Alexander, "Extension, Validation, and Application of the NASCAP Code," NASA CR-159595, January 1979.

3. Cassidy, J. J., "NASCAP User's Manual - 1978," NASA CR-159417, August 1978.

4. Katz, I., J. J. Cassidy, M. J. Mandell, G. W. Schnuelle, P. G. Steen and J. C. Roche, "The Capabilities of the NASA Charging Analyzer Program," Spacecraft Charging Technology-1978, NASA CP-2071, AFGL-TR-79-0082, p. 101, 1979.

5. Schnuelle, G. W., D. E. Parks, I. Katz, M. J. Mandell, P. G. Steen, J. J. Cassidy and A. Rubin, "Charging Analysis of the SCATHA Satellite," Spacecraft Charging Technology-1978, NASA CP-2071, AFGL-TR-79-0082, p. 123, 1979.

6. Stannard, P. R., et al., "Analysis of the Charging of the SCATHA (P78-2) Satellite," NASA CR-165348, December 1980.

7. Laframboise, J. G. and L. W. Parker, "Probe Design for Orbit-Limited Current Collection," Physics of Fluids, 16, p. 629, 1973.

8. Roche, J. C. and C. K. Purvis, "Comparison of NASCAP Predictions with Experimental Data," Spacecraft Charging Technology-1978, NASA CP-2071, AFGL-TR-79-0082, p. 144, 1979.

9. Stevens, N. J., "Computer and Laboratory Simulation of Interactions Between Spacecraft Surfaces and Charged-Particle Environments," NASA TM 79219, 1979.

10. Whipple, E. C., private communication.

11. Kaye, S., et al., SC8 data, private communication.

12. Mandell, M. J., I. Katz, G. W. Schnuelle and P. G. Steen, "The Decrease in Effective Photocurrents Due to Saddle Points in Electrostatic Potentials Near Differentially Charged Spacecraft," IEEE Transactions on Nuclear Science, NS-25, p. 1313, 1978.

13. Aggson, T., private communication.

14. Laframboise, J. G., private communication.

15. Purvis, C. K. and J. V. Staskus, "SSPM Charging Response: Comparison of Ground Test and Flight Data to NASCAP Predictions for Eclipse Conditions," Spacecraft Charging Technology-1980, NASA CP-2182, AFGL-TR-81-0270, p. 592, 1981.

16. Stannard, P. R., I. Katz and D. E. Parks, "Bootstrap Charging of Surfaces Composed of Multiple Materials," IEEE Transactions on Nuclear Science, NS-28, p. 4563, 1981.

17. Mizera, P. F., M. S. Leung and H. K. A. Kan, "Laboratory and Space Results from the SSPM Experiment," The Aerospace Corporation, Report No. TOR-0080(5505-02)-2.

18. Nightingale, R. W., J. B. Reagan, W. L. Imhof and E. E. Gaines, "SCATHA SC-3 Special Event Data," LMSC/D766804, 1980.

19. Mizera, P. F., private communication.

20. Kellogg, P. J., "Measurements of Potential of a Cylindrical Monopole Antenna on a Rotating Spacecraft," Journal of Geophysical Research, 85, p. 5157, 1980.

21. Stevens, N. J., J. V. Staskus and J. C. Roche, "Initial Comparison of SSPM Ground Test Results and Flight Data to NASCAP Simulations," NASA TM 81394, 1980.

22. Staskus, J. V. and J. C. Roche, "Testing of a Spacecraft Model in a Combined Environment Simulator," IEEE Transactions on Nuclear Science, NS-28, p. 4509, 1981.

23. Mandell, M. J., I. Katz and D. E. Parks, "NASCAP Simulation of Laboratory Spacecraft Charging Tests Using Multiple Electron Guns," IEEE Transactions on Nuclear Science, NS-28, p. 4568, 1981.

24. Stevens, N. J., "Voltage Gradients in Solar Array Cavities as Possible Breakdown Sites in Spacecraft-Charging Induced Discharges," IEEE Transactions on Nuclear Science, NS-28, p. 4558, 1981.

25. Olsen, R. C., C. E. McIlwain and E. C. Whipple, Jr., "Observations of Differential Charging Effects on ATS-6," Journal of Geophysical Research, 86, p. 6809, 1981.

26. Schnuelle, G. W., P. R. Stannard, I. Katz and M. J. Mandell, "Simulation of Charging Response of SCATHA (P78-2) Satellite," Spacecraft Charging Technology-1980, NASA CP-2182, AFGL-TR-81-0270, p. 580, 1981.

27. Saflekos, N. A., M. F. Tautz, A. G. Rubin, D. A. Hardy, P. M. Mizera and J. Feynman, "Three Dimensional Analysis of Charging Events on Days 87 and 114, 1979 from SCATHA," Spacecraft Charging Technology-1980, NASA CP-2182, AFGL-TR-81-0270, p. 608, 1981.

28. Rubin, A. G., H. A. Cohen, D. A. Hardy, M. F. Tautz and N. A. Saflekos, "Computer Simulation of Spacecraft Charging on SCATHA," Spacecraft Charging Technology-1980, NASA CP-2182, AFGL-TR-81-0270, p. 632, 1981.

29. See Chapter 2.

30. Marshall Space Flight Center, Solar Electric Propulsion Stage Description, March 1979.

31. Woodcock, G. R., "Solar Satellites - Space Key to Our Power Future," Astronautics and Aeronautics, 15, p. 30, July/August 1977.

32. Glaser, P. E., "Solar Power from Satellites," Physics Today, 30, p. 30, February 1977.

33. Parker, L. W., "Plasma Sheath Effects and Voltage Distributions of Large High Power Satellite Solar Arrays," in Spacecraft Charging Technology-1978, edited by R. C. Finke and C. P. Pike, NASA CP-2071/AFGL-TR-79-0082, p. 341, 1979.

34. Parker, L. W., "Plasmasheath-Photosheath Theory for Large High-Voltage Space Structures," in Space Systems and Their Interactions with Earth's Space Environment, edited by H. B. Garrett and C. P. Pike, AIAA Press, New York, p. 477, 1980.

35. Kennerud, K. L., "High Voltage Solar Array Experiments," The Boeing Company, Seattle, WA, NASA CR-121280, March 1974.

36. Stevens, N. J., "Review of Biased Solar Array-Plasma Interaction Studies," AIAA Paper No. 81-0738, NASA TM-82693, 1981.

37. McCoy, J. E., A. Konradi and O. K. Garriott, "Current Leakage for Low Altitude Satellites," in Space Systems and Their Interactions with Earth's Space Environment, edited by H. B. Garrett and C. P. Pike, AIAA Press, New York, p. 523, 1980.

38. Cohen, H. A., C. Sherman and E. A. Mullen, "Spacecraft Charging Due to Positive Ion Emission: An Experimental Study," Geophysical Research Letters, 6, p. 515, 1981.

39. Cohen, H. A., et al., "P78-2 Satellite and Payload Responses to Electron Beam Operations on March 30, 1979," Spacecraft Charging Technology-1980, NASA CP-2182, AFGL-TR-81-0270, p. 509, 1981.

40. Winckler, J. R., "The Application of Artificial Electron Beams to Magnetospheric Research," Rev. Geophysical Space Physics, 18, p. 659, 1980.

41. Beard, D. B. and F. S. Johnson, "Ionospheric Limitations on Attainable Satellite Potential," Journal of Geophysical Research, 66, p. 4113, 1961.

42. Linson, L. M., "Current-Voltage Characteristics of an Electron-Emitting Satellite in the Ionosphere," Journal of Geophysical Research, 74, p. 2368, 1969.

43. Parker, L. W. and B. L. Murphy, "Potential Buildup on an Electron-Emitting Ionospheric Satellite," Journal of Geophysical Research, 72, p. 1631, 1967.

44. McPherson, D. A., D. P. Cauffman and W. R. Schober, "Spacecraft Charging at High Altitudes: SCATHA Satellite Program," Journal of Spacecraft and Rockets, 12, p. 621, 1975.

45. Stevens, J. R. and A. L. Vampola, "Description of the Space Test Program P78-2 Spacecraft and Payloads," SAMSO TR-78-24, 1974.

46. Mizera, P. F., "Natural and Artificial Charging: Results from the Satellite Surface Potential Monitor Flown on P78-2," AIAA Paper No. 80-0334, 1980.

47. DeForest, S. E., "Spacecraft Charging at Synchronous Orbit," Journal of Geophysical Research, 77, p. 651, 1972.

48. Whipple, E. C., Jr., "The Equilibrium Electric Potential of a Body in the Upper Atmosphere," NASA X-615-65-296, 1965.

49. Laframboise, J. G., Theory of Spherical and Cylindrical Probes in a Collisionless Maxwellian Plasma At Rest, UTIAS Report No. 100, June 1966.

50. Grard, R. J. L. and J. R. E. Tunaley, "Photoelectron Sheath Near a Plasma Probe in Interplanetary Space," Journal of Geophysical Research, 76, p. 2498, 1971.

51. Fahleson, U., "Plasma-Vehicle Interactions in Space - Some Aspects on Present Knowledge and Future Development," Photon and Particle Interactions with Surfaces in Space, R. J. L. Grard, Editor, D. Reidel Publishing Company, Dordrecht, Holland, p. 563, 1973.

52. Whipple, E. C., Jr., "Theory of the Spherically Symmetric Photoelectron Sheath: A Thick Sheath Approximation and Comparison with the ATS-6 Observations of a Potential Barrier," Journal of Geophysical Research, 81, p. 601, 1976.

53. Chaky, R. C., J. H. Nonnast and J. Enoch, "A Numerical Simulation of Plasma-Insulator Interactions in the Spacecraft Environment," Journal of Applied Physics, 52, p. 7092, 1981.

54. Prokopenko, S. M. L. and J. G. Laframboise, "Prediction of Large Negative Shaded-Side Spacecraft Potentials," Proceedings of the Spacecraft Charging Technology Conference, AFGL-TR-77-0051, NASA TMX-73537, p. 369, 1977.

55. Besse, A. L., "Unstable Potential of Geosynchronous Spacecraft," Journal of Geophysical Research, 86, p. 2443, 1981.

56. Parks, D. E. and I. Katz, "Charging of a Large Object in Low Polar Earth Orbit," Spacecraft Charging Technology-1980, NASA CP-2182, AFGL-TR-81-0270, p. 979, 1981.

57. Katz, I. and M. J. Mandell, "Parasitic Current Losses Due to Solar Electric Propulsion Generated Plasmas," Journal of Spacecraft and Rockets, 19, p. 129, 1982.

58. Parks, D. E., M. J. Mandell and I. Katz, "Fluid Model of Neutralized Ion Beams," AIAA-81-0141, AIAA 19th Aerospace Sciences Meeting, St. Louis, MO, 1981.

59. Izhovkina, N. I. and Yu. Ya. Ruzhin, "Rate of Plasma Production by Electron Pulses in the Immediate Vicinity of the Rocket and HF Radioemission in "ARAKS" and "ZARNITZA" Experiments," Ann. Geophys., 36, p. 411, 1980.

DISTRIBUTION LIST

National Aeronautics and Space Administration Washington, D. C. 20546	
Attn: W. R. Hudson/Code RP	1 copy
D. P. Williams, III/Code RS-5	1 copy
National Aeronautics and Space Administration Ames Research Center Moffett Field, CA 94035	
Attn: H. Lum, Jr./M.S. 244-7	1 copy
National Aeronautics and Space Administration Goddard Space Flight Center Greenbelt, MD 20771	
Attn: R. O. Bartlett/Code 408.0	1 copy
A. Kampinsky/Code 727.0	1 copy
E. G. Stassinopoulos/Code 601.0	1 copy
R. S. Bever/Code 405.0	1 copy
Jet Propulsion Laboratory 4800 Oak Grove Drive Pasadena, CA 91103	
Attn: Ray Goldstein	1 copy
H. Garrett	1 copy
E. V. Pawlik	1 copy
Paul Robinson	1 copy
National Aeronautics and Space Administration Lyndon B. Johnson Space Center Houston, TX 77058	
Attn: J. E. McCoy/Code SN3	1 copy
A. Konradi/Code SN3	1 copy
National Aeronautics and Space Administration Langley Research Center Hampton, VA 23665	
Attn: J. W. Goslee/M.C. 364	2 copies
National Aeronautics and Space Administration Lewis Research Center 21000 Brookpark Road Cleveland, OH 44135	
Attn: Head, Mechanics, Fuels and Physics Section/ M.S. 501-11	1 copy
Technology Utilization Office/M.S. 7-3	1 copy
Report Control Office/M.S. 5-5	1 copy
Office of Reliability and Quality Assurance/ M.S. 500-211	1 copy
AFSC Liaison Office/M.S. 501-3	2 copies
Library/M.S. 60-3	2 copies
J. C. Roche/M.S. 77-4	24 copies
Patent Counsel/M.S. 500-318	1 copy

National Aeronautics and Space Administration
George C. Marshall Space Flight Center
Marshall Space Flight Center, AL 35812
Attn: C. R. Chappell/ES 51 — 1 copy
J. H. Harlow/PF 13 — 1 copy
M. R. Carruth/PF 13 — 1 copy
R. N. Seitz/EF 31 — 1 copy

National Aeronautics and Space Administration
Scientific and Technical Information Facility
P. O. Box 8757
Baltimore/Washington International Airport
Maryland 21240
Attn: Accessioning Department — 10 copies

Air Force Geophysics Laboratory
Hanscom Air Force Base, MA 01731
Attn: PH/C. P. Pike — 1 copy
PHG/A. G. Rubin — 1 copy

Air Force Materials Laboratory
Wright-Patterson Air Force Base, OH 45433
Attn: MBE/W. Lehn — 1 copy

Air Force Office of Scientific Research
Bolling Air Force Base
Washington, D. C. 20332
Attn: H. R. Radoski/NP — 1 copy

Air Force Weapons Laboratory
Kirtland Air Force Base, NM 87117
Attn: Capt. W. G. Kuller — 1 copy
Capt. D. Hanifen — 1 copy

Headquarters Space Division (AFSC)
Los Angeles AF Station
P. O. Box 92960
Worldway Postal Center
Los Angeles, CA 90009
Attn: YLVS/Lt. R. Weidenheimer — 1 copy

Defense Nuclear Agency Headquarters
Washington, D. C. 20305
Attn: RAEV/Maj. H. Joonsar — 1 copy

Department of Electrical Engineering
Pennsylvania State University
121 Electrical Engineering
East Building
University Park, PA 16801
Attn: J. Robinson — 1 copy

Department of Physics
University of California at San Diego
P. O. Box 109
La Jolla, CA 92037
Attn: E. C. Whipple — 1 copy

Aerojet Electrosystems Company
1100 West Hollyvale Street
Azusa, CA 91720
Attn: C. Fischer/Dept. 6751 — 1 copy

Aerospace Corporation
P. O. Box 92957
Los Angeles, CA 90009
Attn: J. R. Stevens — 1 copy
R. M. Broussard — 1 copy
J. F. Fennell — 1 copy

Beers Associates, Inc.
P. O. Box 2549
Reston, VA 22090
Attn: Dr. Brian Beers — 1 copy

Boeing Aerospace Company
P. O. Box 3999
Seattle, WA 98124
Attn: H. Liemohn/M.S. 8C-23 — 1 copy
D. Tingey/M.S. 8C-23 — 1 copy

Communications Satellite Corporation
Comsat Laboratories
Clarksburg, MD 20734
Attn: A. Meulenberg, Jr. — 1 copy

European Space Agency
ESTEC
Zwartweg, Noordwijk
Netherlands
Attn: John Reddy, P.B. TTM, 1719 8 2883 — 1 copy

Ford Aerospace and Communications Corporation
Western Development Laboratories Division
3939 Fabian Way
Palo Alto, CA 94303
Attn: D. M. Newell/M.S. G-80 — 1 copy
J. Pherson/M.S. N-01 — 1 copy

General Dynamics Convair
Kearny Mesa Plant
P. O. Box 80847
San Diego, CA 92138
Attn: J. I. Valerio/Mail Zone 42-6210 — 1 copy

General Electric Company
Valley Forge Space Center
P. O. Box 8555
Philadelphia, PA 19101
Attn: V. Belanger/U-2439 — 1 copy
A. Eagles — 1 copy

Grumman Aerospace
Bethpage, NY 11714
Attn: M. Stauber — 1 copy

Hughes Aircraft Company
P. O. Box 92919
Los Angeles, CA 90009
Attn: E. Smith/M.S. A620 — 1 copy
A. H. Narevsky — 1 copy

Hughes Research Laboratories
3011 Malibu Canyon Road
Malibu, CA 90265
Attn: Dr. Jay Hyman — 1 copy

IRT Corporation
P. O. Box 80817
San Diego, CA 92138
Attn: J. Wilkenfeld — 1 copy

JAYCOR
P. O. Box 85154
San Diego, CA 92138
Attn: E. P. Wenaas — 1 copy

Kaman Science
1500 Garden of the Gods Road
Colorado Springs, CO 80907
Attn: F. Rich — 1 copy

Lee W. Parker, Inc.
252 Lexington Road
Concord, MA 01742
Attn: L. Parker — 1 copy

Lockheed Palo Alto Research Laboratory
3251 Hanover Street
Palo Alto, CA 94303
Attn: J. B. Reagan/Bldg. 205, Dept. 52-12 — 1 copy
D. P. Cauffman — 1 copy

Martin Marietta Corporation
P. O. Box 179
Denver, CO 80201
Attn: D. E. Hobbs/M.S. D8350 — 1 copy
K. Killian/M.S. D8350 — 1 copy

DISTRIBUTION LIST (Continued)

Massachusetts Institute of Technology
Lincoln Laboratory
P. O. Box 73
Lexington, MA 02173
Attn: F. G. Walther — 1 copy

McDonnell Douglas Astronautics Company
5301 Bolsa Avenue
Huntington Beach, CA 92647
Attn: W. P. Olson — 1 copy

Mission Research Corporation
5434 Ruffin Road
San Diego, CA 92123
Attn: V. van Lint — 1 copy

RCA Astroelectronics Division
P. O. Box 800
Princeton, NJ 08540
Attn: H. Strickberger/M.S. 91 — 1 copy
W. Franklin — 1 copy

Science Applications, Inc.
101 Continental Building
Suite 310
El Segundo, CA 90245
Attn: D. McPherson — 1 copy

Science Applications, Inc.
2860 South Circle Drive
Colorado Springs, CO 80906
Attn: E. E. O'Donnell — 1 copy

Simulation Physics, Inc.
41 B Street
Burlington, MA 01803
Attn: R. G. Little — 1 copy

SRI International
333 Ravenswood Avenue
Menlo Park, CA 90425
Attn: J. Nanevicz — 1 copy

TRW Systems
One Space Park
Redondo Beach, CA 90278
Attn: G. T. Inouye/Bldg. R-5, Rm. 2011 — 1 copy

Lockheed Missile and Space Company
P. O. Box 504
Sunnyvale, CA 94086
Attn: G. Pack — 1 copy

End of Document